

COMPREHENSIVE MODELLING OF GAS CONDENSATE RELATIVE
PERMEABILITY AND ITS INFLUENCE ON FIELD PERFORMANCE

A THESIS SUBMITTED TO
THE GRADUATE SCHOOL OF NATURAL AND APPLIED SCIENCES
OF
MIDDLE EAST TECHNICAL UNIVERSITY

BY

HÜSEYİN ÇALIŞGAN

IN PARTIAL FULFILLMENT OF THE REQUIREMENTS
FOR
THE DEGREE OF DOCTORATE OF PHILOSOPHY
IN
PETROLEUM AND NATURAL GAS ENGINEERING

SEPTEMBER 2005

Approval of the Graduate School of Natural and Applied Sciences.

Prof. Dr. Canan Özgen
Director

I certify that this thesis satisfies all the requirements as a thesis for the degree of Philosophy of Doctorate.

Prof. Dr. Birol Demiral
Head of Department

This is to certify that we have read this thesis and that in our opinion it is fully adequate, in scope and quality, as a thesis for the degree of Philosophy of Doctorate.

Prof. Dr. Birol Demiral
Co-Supervisor

Assoc. Prof. Dr. Serhat Akın
Supervisor

Examining Committee Members

Prof. Dr. Mahmut Parlaktuna	(METU, PETE)	_____
Assoc. Prof. Dr. Serhat Akın	(METU, PETE)	_____
Prof. Dr. Birol Demiral	(METU, PETE)	_____
Asst. Prof. Dr. Hasan Ö. Yıldız	(İTÜ, PETE)	_____
Prof. Dr. Nurkan Karahanoğlu	(METU, GEOE)	_____

I hereby declare that all information in this document has been obtained and presented in accordance with academic rules and ethical conduct. I also declare that, as required by these rules and conduct, I have fully cited and referenced all material and results that are not original to this work.

Name, Last name: Hüseyin Çalışgan

Signature :

ABSTRACT

COMPREHENSIVE MODELLING OF GAS CONDENSATE RELATIVE PERMEABILITY AND ITS INFLUENCE ON FIELD PERFORMANCE

ÇALIŞGAN, Hüseyin

Ph.D., Department of Petroleum and Natural Gas Engineering

Supervisor: Assoc. Prof. Dr. Serhat Akın

Co-Supervisor: Prof. Dr. Birol Demiral

September 2005, 139 pages

The productivity of most gas condensate wells is reduced significantly due to condensate banking when the bottom hole pressure falls below the dew point. The liquid drop-out in these very high rate gas wells may lead to low recovery problems. The most important parameter for determining condensate well productivity is the effective gas permeability in the near wellbore region, where very high velocities can occur. An understanding of the characteristics of the high-velocity gas-condensate flow and relative permeability data is necessary for accurate forecast of well productivity.

In order to tackle this goal, a series of two-phase drainage relative permeability measurements on a moderate permeability North Marmara –1 gas well carbonate core plug sample, using a simple synthetic binary retrograde condensate fluid sample were conducted under reservoir conditions which corresponded to near miscible conditions. As a fluid system, the model of methanol/n-hexane system was used as a binary model that exhibits a critical point at ambient conditions. The interfacial tension by means of temperature and the flow rate were varied in the laboratory measurements. The laboratory

experiments were repeated for the same conditions of interfacial tension and flow rate at immobile water saturation to observe the influence of brine saturation in gas condensate systems.

The laboratory experiment results show a clear trend from the immiscible relative permeability to miscible relative permeability lines with decreasing interfacial tension and increasing velocity. So that, if the interfacial tension is high and the flow velocity is low, the relative permeability functions clearly curved, whereas the relative permeability curves straighten as a linear at lower values of the interfacial tension and higher values of the flow velocity. The presence of the immobile brine saturation in the porous medium shows the same shape of behavior for relative permeability curves with a small difference that is the initial wetting phase saturations in the relative permeability curve shifts to the left in the presence of immobile water saturation.

A simple new mathematical model is developed to compute the gas and condensate relative permeabilities as a function of the three-parameter. It is called as condensate number; N_K so that the new model is more sensitivity to temperature that represents implicitly the effect of interfacial tension. The new model generated the results were in good agreement with the literature data and the laboratory test results. Additionally, the end point relative permeability data and residual saturations satisfactorily correlate with literature data. The proposed model has fairly good fitness results for the condensate relative permeability curves compared to that of gas case. This model, with typical parameters for gas condensates, can be used to describe the relative permeability behavior and to run a compositional simulation study of a single well to better understand the productivity of the field.

Keywords: Gas Condensate, Relative Permeability, Interfacial Tension, Capillary Number, Bond Number, Condensate Number, Immobile Water Saturation, Near Critical Pressure

ÖZ

GÖZENEKLİ ORTAMDA GAZ KONDENSATIN GÖRELİ GEÇİRGENLİK ETKİSİNİN MODELLENMESİ VE SAHA PERFORMANSINA ETKİSİ

ÇALIŞGAN, Hüseyin

Doktora, Petrol ve Doğal Gaz Mühendisliği Bölümü

Tez Yöneticisi: Doç. Dr. Serhat Akın

Ortak Tez Yöneticisi: Prof. Dr. Birol Demiral

Eylül 2005, 139 sayfa

Gaz Kondensat kuyularının çoğundaki üretim ile birlikte kuyudibi basıncının çiylenme noktası (dew point) basıncının altına düşmesi sonucunda oluşan kondensat yoğuşmasının olumsuz etkisi nedeniyle önemli miktarda kuyu üretimi azalır. Gaz kondensat kuyularından yapılan üretimi etkileyen en önemli parametre kuyuya yakın noktalarda çok yüksek akış hızlarının oluşması nedeniyle kuyuya yakın noktalarındaki etkin gaz geçirgenliğidir. İleriye dönük doğru bir kuyu üretim tahmini yapabilmek için kuyu cidarındaki yüksek hızdaki gaz kondensat akış karakterini anlamak gereklidir.

Bu amacı hedefleyebilmek için, orta geçirgenlik değerine sahip Kuzey Marmara-1 gaz kuyusu karbonat karotlarına ait tapa örneği üzerinde, yalın sentetik iki bileşenli gaz kondensat akışkan örneği kullanılarak kritik nokta basınç yakınına uygun olarak rezervuar koşullarında bir dizi iki fazlı drenaj görelî geçirgenlik ölçümleri yapılmıştır. Akışkan sistemi olarak, çevre koşullarında kritik nokta özelliği gösteren iki bileşenli metanol / hekzan

systemi model olarak kullanılmıştır. Sıcaklığın sayesinde yüzey gerilim katsayısı ve akış debisi değiştirilerek laboratuvar testleri yapılmıştır. Formasyon suyu doymuşluğun gaz kondensat sistemlerine etkisini gözlemleyebilmek için kalıcı su doymuşluğunda, laboratuvar testleri aynı yüzey gerilim ve akış debileri için tekrarlanmıştır.

Laboratuvar testlerinin sonuçları yüzey geriliminin azalımı ve akış hızının artışı ile birlikte karışmayan görelî geçirgenlik eğrisinin davranışından karışabilir çizgisine doğru net bir eğilim gösterir. Öyle ki, yüzey gerilimin yüksek ve akış hızı düşük ise görelî geçirgenlik fonksiyonu açıkça kavis alırken düşük yüzey gerilim ve yüksek akış hızlarında doğrusal düz çizgi şeklini alır. Gözenekli ortamda kalıcı su doymuşluğunun bulunması görelî geçirgenlik eğrilerinin ılatımlı faz doymuşluğunun sola kayması dışında aynı şekilde davranış gösterir.

Üç parametrelî kondensat sayısının fonksiyonu olarak gaz ve kondensat görelî geçirgenlik verilerinin elde edilmesi için yeni sade bir matematiksel model geliştirilmiştir. Kondensat sayısı olarak adlandırılan yeni model yüzey gerilimin etkisine sıcaklığın değişimi dolayısıyla daha fazla hassasiyet göstermektedir. Yeni model daha önce yayınlanmış yayınlarla ve laboratuvar test sonuçlarıyla uyumlu veriler üretmiştir. İlave olarak, uç noktası görelî geçirgenlik ve kalıcı doymuşluk verilerinin yayınlamış çalışmalarla uyum içindedir. Söz konusu önerilen model gaz görelî geçirgenliğine kıyasla kondensat görelî geçirgenliği için oldukça yüksek uygunluk değerleri vermiştir. Bu model; görelî geçirgenlik sisteminin tanımlanmasında ve bir sahanın üretim kapasitesinin daha iyi anlamak için yapılan bileşenli simülasyon çalışmasında gaz kondensatlara özgü tipik parametrelerle kullanılabilir.

Anahtar Kelimeler: Gaz Kondensat, Görelî Geçirgenlik, Yüzey Gerilimi, Kapiler Sayısı, Bond Sayısı, Kondensat Sayısı, Kalıcı Su Doymuşluğu, Kritik Nokta Basınç Yakını

This Dissertation is dedicated:

To my mother and father;

Yeter and Halil Çalışgan,
who helped me grow into the person I am today and who have been "with me"
in every sense in all phases of this Ph.D. journey,
and

to my wife and my lovely daughters;

Cemile, Sıla Deniz and Aslı Derya Çalışgan
who had inexhaustible patience during this rigorous and long study.

ACKNOWLEDGEMENTS

First, and foremost, I would like to thank Assoc. Prof. Dr. Serhat Akin, my research advisor and "mentor," for his excellent guidance and encouragement throughout my research, and for his friendship during my years as a graduate student. His high standards of scholarship and intellectual integrity, as well as his openness and flexibility, contributed substantially to the understanding of the implementation of near miscible analogy to gas condensate systems and mathematical modeling of fluid flow, which is presented in this dissertation. I was extremely fortunate to work under his supervision for my Ph.D.

I want to express my sincere gratitude to my co-supervisor Prof. Dr. Birol Demiral for his guidance and insight throughout the thesis study.

I am also grateful to the other members of my qualifying examination and dissertation committees: Mahmut Parlaktuna, Hasan Özgür Yıldız, and Nurkan Karahanoğlu who provided me valuable guidance, suggestions and comments on this dissertation.

I also want to sincerely thank all the members, old and new, of Core and PVT Laboratory at the Research Center, which provided a home with a friendly and helpful research environment, greatly strengthening the outcome and quality of this work.

Last but not least, my friends and colleagues: namely Erşan Alpay, Uğur Karabakal and our technician Adem Çuhadar deserve my special thanks for helping me to conduct laboratory tests and to overcome many obstacles along the way.

I would like to express my special gratitude appreciations to my beloved wife, Cemile, and my lovely daughters; Sila Deniz and Aslı Derya, for their inexhaustible patience especially during the last year of my Ph.D. studies.

Furthermore, my deep appreciation to my beloved wife, Cemile, to my lovely sister, Filiz, to my brothers, Rıza and İsmail and to my brothers' wives, Lale and Nihal, who specifically offered strong moral support, their encouragements and sacrifices over the many years devoted to all my rigorous and long studies.

Finally, I would like to thank TPAO Administration for permission to perform the study of this thesis by using the core laboratory facilities, and especially thank to Dr. Oğuz Ertürk, Osman Gündüz and A. H. Ersun.

TABLE OF CONTENTS

PLAGIARISM.....	iii
ABSTRACT	iv
ÖZ.....	vi
DEDICATION	viii
ACKNOWLEDGEMENTS	ix
TABLE OF CONTENTS	xi
LIST OF TABLES	xv
LIST OF FIGURES.....	xvii
LIST OF SYMBOLS.....	xx
LIST OF ABBREVIATIONS.....	xxii

CHAPTER 1

INTRODUCTION	1
1.1 Flow in Porous Media.....	1
1.1.1 Relative Permeability	2
1.1.2 Near Miscible Fluids	3
1.2 Problem Description	4
1.3 Importance of the Study	8
1.3.1 Applications of near-miscible flow	9
1.4 Objective and Methodology of the Study	9
1.5 Outline.....	10

CHAPTER 2

THEORY AND BASIC CONCEPTS	12
---------------------------------	----

2.1 Relative Permeability	12
2.1.1 Fluid distribution on the pore scale	12
2.1.1.1 Interfacial tension	13
2.1.1.2 Wettability	13
2.1.1.3 Capillarity	14
2.1.1.4 Capillary forces in porous media.....	15
2.1.2 Flow of immiscible fluids	16
2.1.2.1 Relative Permeability to immiscible fluids	18
2.1.3 Flow outside the capillary-dominated regime.....	19
2.1.3.1 Capillary Number	20
2.1.3.2 Viscosity Ratio	21
2.1.3.3 Bond Number	21
2.2 Near Miscible Fluids.....	22
CHAPTER 3	
LITERATURE SURVEY	24
CHAPTER 4	
STATEMENT OF THE PROBLEM	29
CHAPTER 5	
LABORATORY TEST SYSTEM	31
5.1 Introduction.....	31
5.2 Core Properties	32
5.3 Test Set-up System	34
5.4 Test Fluid Selection	36
5.5 Laboratory Test Procedures	42
5.5.1 Displacement Procedures	43

CHAPTER 6

LABORATORY TEST RESULTS	46
6.1 Introduction	46
6.2 Experimental Results	46
6.3 Reproducibility of the Test Results	47
6.4 Relative Permeability Tests without immobile water saturation	48
6.4.1 Flow rate effect on relative permeability	49
6.4.2 Effect of interfacial tension on relative permeability	54
6.5 Relative Permeability Tests at immobile water saturation (Swi)....	59
6.5.1 Flow rate effect on relative permeability curves at Swi	64
6.5.2 Effect of interfacial tension on relative permeability curves at Swi	66
6.6 Influence of Immobile Water Saturation on Relative Permeability	69
6.6.1 Effect of Flow Rate on Relative Permeability at Swi	70
6.6.2 Effect of Interfacial Tension on Relative Permeability at Swi	72
6.7 Test Assumptions and Source of Errors	74

CHAPTER 7

MATHEMATICAL MODELLING	78
7.1 Introduction	78
7.2 Mathematical Model Description	79
7.3 Comparison of Mathematical Model with Laboratory Tests	82
7.4 Discussion of the Mathematical Model and Laboratory Test Results	91

CHAPTER 8

CONCLUSIONS	97
-------------------	----

CHAPTER 9

RECOMMENDATIONS	100
-----------------------	-----

REFERENCES	101
------------------	-----

APPENDICES	115
------------------	-----

A. Measured Data on the Fluid System	115
--	-----

B. Measured Data of the Flood Tests.....	117
--	-----

C. Results of the Relative Permeability Tests.....	128
--	-----

D. Methanol Solubility in Water.....	134
--------------------------------------	-----

E. Curriculum Vitae	138
---------------------------	-----

LIST OF TABLES

TABLES

Table 2.1: Literature Survey on Capillary Number.....	21
Table 5.1: Testing Fluid and Core Data Properties.....	32
Table 6.1: The List of Relative Permeability Tests.....	47
Table 7.1: Condensate Parameters for Tests at 50 cc/hr	83
Table 7.2: Condensate Parameters for Tests at 100 cc/hr	84
Table 7.3: Condensate Parameters at 50 cc/hr at Swi	90
Table 7.4: Condensate Parameters at 100 cc/hr at Swi	90
Table A.1: Measured Density and Viscosity Data for Hexane	115
Table A.2: Measured Density and Viscosity Data for Methanol	115
Table A.3: Measured Interfacial Tension for Methanol/Hexane	116
Table B.1: Laboratory Measured Test Data for 100 cc/hr at 32.8 °C.....	117
Table B.2: Laboratory Measured Test Data for 50 cc/hr at 32.8 °C.....	118
Table B.3: Laboratory Measured Test Data for 100 cc/hr at 30.1 °C.....	119
Table B.4: Laboratory Measured Test Data for 50 cc/hr at 30.1 °C.....	120
Table B.5: Laboratory Measured Test Data for 100 cc/hr at 18 °C.....	121
Table B.6: Laboratory Measured Test Data for 75 cc/hr at 32.8 °C.....	122
Table B.7: Laboratory Measured Test Data for 50 cc/hr at 18 °C.....	123
Table B.8: Laboratory Measured Test Data for 50 cc/hr at 18 °C for Swi.....	124
Table B.9: Laboratory Measured Test Data for 100 cc/hr at 18 °C for Swi...	125
Table B.10: Laboratory Measured Test Data for 100 cc/hr at 32.8 °C for Swi	126
Table B.11: Laboratory Measured Test Data for 50 cc/hr at 32.8 °C for Swi	127

Table C.1: Result of Relative Permeability Test for 100 cc/hr at 32.8 °C	128
Table C.2: Result of Relative Permeability Test for 50 cc/hr at 32.8 °C	129
Table C.3: Result of Relative Permeability Test for 100 cc/hr at 30.1 °C	129
Table C.4: Result of Relative Permeability Test for 50 cc/hr at 30.1 °C	130
Table C.5: Result of Relative Permeability Test for 100 cc/hr at 18 °C	130
Table C.6: Result of Relative Permeability Test for 75 cc/hr at 32.8 °C	131
Table C.7: Result of Relative Permeability Test for 50 cc/hr at 18 °C	131
Table C.8: Result of Relative Permeability Test for 100 cc/hr at 18 °C at Swi	132
Table C.9: Result of Relative Permeability Test for 50 cc/hr at 18 °C at Swi	132
Table C.10: Result of Relative Permeability Test for 100 cc/hr at 32.8 °C at Swi	133
Table C.11: Result of Relative Permeability Test for 50 cc/hr at 32.8 °C at Swi	133

LIST OF FIGURES

FIGURES

Figure 1.1: Relative permeability measured by Wyckoff and Botset (1936).	3
Figure 1.2: Relative Permeability to Fully Miscible Phases	6
Figure 2.1: The Contact Angle Between a Solid and a Fluid-Fluid Interface	14
Figure 2.2: The Graph for the Zero Contact Angle	14
Figure 2.3: Capillary Rise in a Tube	15
Figure 2.4: A Typical Relative Permeability Curve.....	19
Figure 3.1: Relative Permeability Dependence on IFT	28
Figure 5.1: Vertically CT Scanned Cross-sectional Image of N.Marmara-1 Core Plug Sample	33
Figure 5.2: Cross-sectional CT Scans of the Plug Sample	34
Figure 5.3: Laboratory Test Set-up.	35
Figure 5.4 Co-existence Curve of Methanol-Hexane.....	37
Figure 5.5: Measured Density along the Co-existence Curve.....	39
Figure 5.6: Viscosity of the Co-existing Phases.....	39
Figure 5.7: Interfacial Tension of the Fluid System.....	40
Figure 5.8: Interfacial Tension as a Function of the Reduced System.....	40
Figure 6.1: Cumulative Produced Volume of Methanol (Condensate) Rich Phase versus Time	49
Figure 6.2: Measured Pressure Drop across the Porous Medium in Time.....	50
Figure 6.3: Flow Rate Effect on Relative Permeability at °18 C	51
Figure 6.4: Flow Rate Effect on Relative Permeability at °18 C by Blom 2000	52

Figure 6.5: Flow Rate Effect on Relative Permeability at 32.8 °C	53
Figure 6.6: Flow Rate Effect on Relative Permeability at 32.8 °C by Blom 2000	54
Figure 6.7: Relative Permeability at Different Interfacial Tension at 50 cc/hr	55
Figure 6.8: Relative Permeability at Different Interfacial Tension at 100 cc/hr	56
Figure 6.9: Relative Permeability Curve at Different Interfacial Tensions by Blom et al 2000.	57
Figure 6.10: Flow Rate and Temperature Effect on Relative Permeability ..	58
Figure 6.11: Cumulative Produced Volume of Condensate Phase in Time at Swi	60
Figure 6.12: Pressure Drop across the Porous Medium in Time at Swi	62
Figure 6.13: Flow Rate Effect on Relative Permeability at 18 °C at Swi	64
Figure 6.14: Flow Rate Effect on Relative Permeability at 32.8 °C at Swi	65
Figure 6.15 Relative Permeability at Different Interfacial Tension at 50 cc/hr at Swi	66
Figure 6.16 Relative Permeability at Different Interfacial Tension at 100 cc/hr at Swi	67
Figure 6.17: Flow Rate and Interfacial Tension Effect on Relative Permeability Curves at Swi	68
Figure 6.18: Influence of Immobile Water Saturation on Relative Permeability at 18 °C at 50 cc/hr	69
Figure 6.19: Influence of Immobile Water Saturation on Relative Permeability at 18 °C at 100 cc/hr	69
Figure 6.20: Influence of Immobile Water Saturation on Relative Permeability at 32.8 °C at 50 cc/hr	69
Figure 6.21: Influence of Immobile Water Saturation on Relative Permeability at 32.8 °C at 100 cc/hr	69
Figure 6.22: Influence of Immobile Water Saturation with Flow Rate	

Change on Relative Permeability at 18 °C	70
Figure 6.23: Influence of Immobile Water Saturation with Flow Rate	
Change on Relative Permeability at 32.8 °C	71
Figure 6.24: Influence of Immobile Water Saturation with Interfacial	
Tension Change on Relative Permeability at 50 cc/hr	72
Figure 6.25: Influence of Immobile Water Saturation with Interfacial	
Tension Change on Relative Permeability at 100 cc/hr	73
Figure 7.1: Gas Relative Permeability versus Gas Saturation.....	85
Figure 7.2: Condensate Relative Permeability versus Condensate	
Saturation.....	85
Figure 7.3: End Point Relative Permeability versus Condensate Number.....	86
Figure 7.4: Effect of various Condensate Parameters on the End Point	
Relative Permeability and Condensate Number	87
Figure 7.5: Normalized Residual Saturations versus Condensate Number....	88
Figure 7.6: Effect of various Condensate Parameters on the Normalized	
Residual Saturations and Condensate Number	89
Figure 7.7: Relative Permeability Data from Mathematical Model	
for various IFT at 50 cc/hr.....	93
Figure 7.8: Relative Permeability Data from Mathematical Model	
for 75 cc/hr	93
Figure 7.9: Relative Permeability Data from Mathematical Model	
for various IFT at 100 cc/hr.....	94
Figure 7.10: Relative Permeability Data from Mathematical Model	
for various IFT at 50 cc/hr at Swi.....	95
Figure 7.11: Relative Permeability Data from Mathematical Model	
for various IFT at 100 cc/hr at Swi.....	95
Figure C.1: Phase Segregation	136

LIST OF SYMBOLS

Latin

k	Permeability	L^2, m^2
u	Fluid Velocity	$L/t, cm / sec$
r	Radius of the Pipe	L, mm
q	Flow Rate	$L^3/t, cm^3 / sec$
P	Pressure	$m/(Lt^2), Pa$
T	Temperature	$T, ^\circ C$
S	Saturation	$L^3/L^3, Fraction$
f	Fraction	
g	Gravitational Acceleration	$L/t^2, m/s^2$
h	Column Height	L, mm
k_r	Relative permeability	
Re	Reynolds number	
\vec{k}	Permeability tensor	L^2, m^2
k_{rd}	Relative permeability of phase d	
k_{rd}^0	Endpoint relative permeability of phase d	
k_{rd}^{0high}	Phase d endpoint relative permeability at high trapping number	
k_{rd}^{0low}	Phase d endpoint relative permeability at low trapping number	
S_{dr}	Residual Saturation of phase d, $L^3/L^3, PV$	
S_{dr}^{high}	Residual saturation of phase d at high N_K	
S_{dr}^{low}	Residual saturation of phase d at high N_K	
N_c	Capillary number	

N_B	Bond number	
N_K	Condensate number	
X	Mole fraction	
$J(S)$	Leverett function	Dimensionless
a	Trapping parameter for phase d	
b	Trapping model parameter for phase d	
c	Trapping parameter for phase d	
n	Number of the phases	

Greek

σ	Interfacial Tension	m/t^2 , mN/m
μ	Dynamic Viscosity	m/(Lt) , Pa.s
ϕ	Porosity	L^3/L^3 , PV
θ	Contact angle	
$\sigma_{dd'}$	Interfacial tension of phases d and d'	m/t^2 , mN/m
$\vec{\nabla}\Phi_d$	Flow potential gradient	$\text{mL}^{-1}\text{t}^{-2}$, Pa
ρ_d	Density of phase d	mL^{-3} , g/cm^3
Φ_d	Potential of phase d	$\text{mL}^{-1}\text{t}^{-2}$, Pa

Subscripts

ω	Phase indicator
Ω	Phase indicator
nw	non-wetting phase
w	wetting phase
d	Displaced phase
d'	Displacing phase

r	Residual
-----	----------

Superscripts

high	high trapping number
low	low trapping number
0	end point

LIST OF ABBREVIATIONS

IFT	Interfacial Tension
JBN	Johnson-Bossler-Naumann

CHAPTER 1

INTRODUCTION

1.1 Flow in Porous Media

Porous rocks are fluid-permeated, containing oil, gas, or water as a standing point of reservoir engineering aspects. Gravitational and capillary forces largely control the distribution of these fluids in petroleum accumulations. The porous medium's storage capacity is denoted by porosity, i.e., the void fraction of the volume available for the fluids. The ability of the porous medium to transmit the fluid pass through its pore spaces is specified by the quantity of permeability. The concept of conductivity that is known as permeability was introduced by Darcy (1856) [1]. The dimension of permeability is the square of length.

Apart from the properties of the porous medium, we also need to specify the properties of the fluid that is flowing. Some fluids are easy to flow through porous medium. The fluid property that accounts for the differences of flow is due to viscosity, a measure of internal friction within the fluid. The density of the fluid is an important factor in porous medium to characterize the flow behavior.

Whenever all these parameters are determined, it can be easily predicted how fast the fluid will flow at a given differential pressure difference.

1.1.1 Relative Permeability

Two fluid phases that flow simultaneously through a porous medium will generally impede each other. To account for this aspect of two-phase flow in porous media, Muskat and Meres (1936) introduced the concept of relative permeability [2]. Relative permeability will depend on which fraction of pore volume is occupied by a phase, called the saturation. At unit phase saturation, the phase in question occupies all pores, so that the apparent permeability is exactly equal to the single-phase absolute permeability.

At a given saturation, the actual value of relative permeability depends on the shape of the pores and on the fluid distribution in the pore space. This is due to the preference of the porous material for being covered (or wet) by one of the phases, known as the wetting phase. The interaction between the fluid phases and the pore wall gives rise to capillary forces that influence the distribution in the medium. The wetting phase is preferentially present in the small pores, thus maximizing contact with the pore wall. On the other hand, the non-wetting phase (e.g., the oil phase) tends to occupy the space in the middle of the larger pores, which minimizes contact surface with wall.

The difference in fluid distribution can be seen in relative permeability to the wetting phase and non-wetting phase. This may be seen in Figure 1.1, which was showed by Wyckoff and Botset (1936) [3], i.e., who got the earliest relative permeability measurement results on simultaneous flow of water and carbon dioxide gas through sand columns. One may see in Figure 1.1 that when the sand pack is equally filled with both fluids (i.e., saturation has a value of 0.5) the wetting phase (water) relative permeability is much lower than the non-wetting (gas) relative permeability.

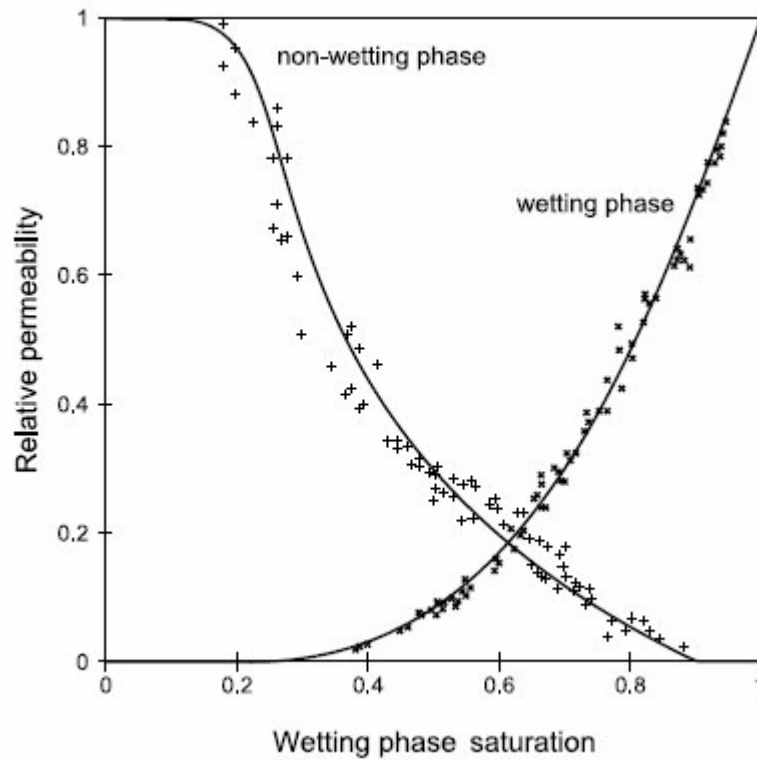


Figure 1.1: Relative permeability measured
by Wyckoff and Botset (1936) [3]

The reason is that the wetting phase encounters more friction from the pore walls than the non-wetting phase, because wetting phase tends to flow in channels that connect the smaller pores and contact with wall in small pores, on the other hand the non-wetting phase mostly flows through connecting the larger pores. Therefore, the non-wetting phase flows more easily through out the porous medium than the wetting phase.

1.1.2 Near Miscible Fluids

Some fluids are miscible, and they always form a single, homogeneous, phase, and no interface i.e., among them no any interface (boundary) can be observed.

Some of the other fluids are mutually immiscible in that case no matter how much effort is applied into mixing them; two distinct phases will emerge together. In between, there are partially miscible fluids in that case fluids do mix in each other, but not all proportions. The degree to which partially miscible fluids mix depends on chemical composition, temperature, and the pressure.

The combination of pressure and temperature at which the difference between phases vanishes is called the critical point. Just below the critical point, fluids become near miscible.

Since near-miscible fluids mix almost entirely, the two phases are very much alike. There is still an interface between the phases, but it can be easily deformed, because the interfacial tension is low. The interfacial tensions a measure of the force that is needed to deform the interface among the phases. At the critical point, the interfacial tension and the difference in attraction (adhesion) within the two phases vanishes. In the remaining part of this thesis, the term near-miscibility will be reserved for a situation in which the interfacial tension is low due to very similar chemical composition of the fluids.

1.2 Problem Description

In general, relative permeability is used to model the flow of two immiscible phases in a porous medium. When the interfacial tension between the two phases is high, porous medium preference for one of the phase will contribute a great effect on fluid distribution inside the pore spaces. Therefore, this distribution is drastically influenced by an increase in flow velocity. Thus, capillary forces relative to viscous forces on the micro pore scale dominate immiscible multi-phase flow. Consequently, macroscopic flow quantities like relative permeability may be considered to be independent of flow velocity and

interfacial tension. Under these conditions, relative permeability functions only depend on fluid saturation, saturation history, and properties of the porous medium.

It was shown in many experimental studies that relative permeability of low interfacial tension fluids is much higher than that of high interfacial tension (Bardon and Langeron, 1980 [4]; Ameafule and Handy, 1982 [5]; Harbert, 1983 [6]; Asar and Handy [7], 1988; Haniff and Ali, 1990 [8]; Schechter and Haynes, 1992 [9]; Jerauld, 1997 [10]; Morel et al. 1996 [11]) [4-11]. The relative permeability curves are affected because the capillary forces weaken with decreasing interfacial tension. Considering the zero interfacial tension that corresponds to single-phase flow can see the reason for this behavior that causes an increase in relative permeability.

The single phase is splitted into two identical phases, by putting a hypothetical label on part of the fluid particles. As the phases do not differ in each other for their wetting properties, there will be no preference for one of the phases to take the faster path way.

Single-phase relative permeability with hypothetical unit-slope straight lines is shown in Figure 1.2. If the interfacial tension between two phases is sufficiently low, the capillary forces are so weak that they can be neglected with regard to the viscous forces that are caused by friction within the flowing fluids. Consequently, the ratio of viscous forces to capillary forces on pore scale results in a change in flow regime so that the relative permeability curves come close to the lines Figure 1.2. For the main part of the saturation interval, relative permeability amounts have a slight increase compared to conventional relative permeability curve presented in Figure 1.1.

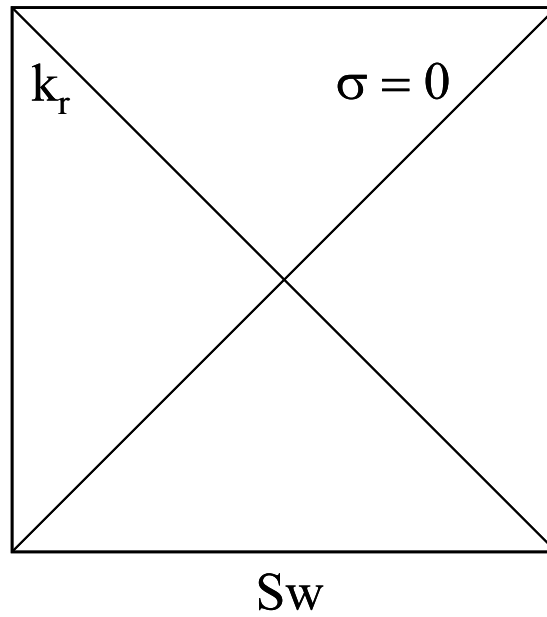


Figure 1.2: Relative Permeability to Fully Miscible Phases

As a second cause of relative permeability changes at near miscible conditions may be a change in wetting state. If the interfacial tension is below a certain value, a new layer of the wetting phase is formed in between the phases. The transition in the wetting state was predicted by Cahn (1977) [12]. The wetting transition will have influence on the relative permeability curve up to a certain value of the interfacial tension, rather than at a certain ratio of viscous forces to capillary forces on pore scale.

When a review of the literature is done it can be easily seen that there is no consensus on how near-miscibility affect relative permeability curves and which parameters are controlling this change. Some investigators have found that relative permeability to the non-wetting phase is affected more easily (Ameafule and Handy, 1982 [5]; Harbert, 1983 [6]; Henderson et al., 1996 [13]), whereas others observed a greater increase of the relative permeability to the wetting phase compared with the relative permeability to the non wetting phase (Asar and Handy, 1988 [7]; Schechter and Haynes, 1992 [9]). Other

authors did not find an effect on interfacial tension at all (Delclaud et al., 1987 [14]; Kalaydjian et al., 1996 [15]).

For the effect of flow velocity on near-miscible relative permeability, some investigators find no effect (Fulcher et al., 1985 [16]; Schechter, 1988 [17]), on the other hand other researchers reported the effect (Harbert, 1983 [6]; Boom et al., 1995 [18]). In addition, Henderson et al. (1996) [13] have reported that the flow velocity only affects relative permeability if the fluids enter the porous medium as a single, homogenous phase, and subsequently are allowed to separate into two phases inside the pores.

It appears to be two conflicting views on which mechanism controls the increase in relative permeability. Whereas, the wetting transition is held responsible (Teletzke et al., 1981 [19]; Schechter, 1988 [17]; Haniff and Ali, 1990 [8]), on the other hand, several investigators claim that the controlling parameter is the strength of the viscous forces relative to that of capillary forces on the pore scale (Leverett, 1939 [20]; Bardon and Langeron, 1980 [4]; Ameafule and Handy, 1982 [5]; Harbert, 1983 [6]; Boom et al., 1995 [18]; Henderson et al., 1996 [13]; Kalaydjian et al., 1996 [15]; Jerauld, 1997 [10]; Pope et al., 1998 [21]).

The main important question in this thesis is therefore: If relative permeability is used to model the flow of two near miscible fluids through a porous medium with and without introducing immobile water saturation, how is relative permeability affected by interfacial tension and by flow velocity?

1.3 Importance of the Study

This study was carried out to model the problem of well impairment in gas condensate reservoirs. These reservoirs are natural gas fields in which condensation of a liquid phase occurs when the reservoir pressure decreases due to the depletion. Mostly, those reservoirs have a phase behavior of near its critical points, so that the interfacial tension between the gas phase and the condensate phase is low.

Gas condensate fields contribute an important percent of the hydrocarbon reserves of the world. They are all over the major oil fields found including the North Sea, Russia, Kazakhstan, the Middle East, Canada, Texas, and Gulf of Mexico.

The production and development of gas condensate reservoirs is quite difficult. Wells that have been drilled into such reservoirs perform badly because of the condensing oil or liquid banking inside the pore spaces. The pressure in the vicinity of well bore decreases when the gas has been started to deplete. Whenever it reaches a certain point, condensation starts and liquid phase builds up which results to have the gas flow impeded by the condensate phase.

Well impairment by condensate drop out is more complicated multi-phase flow problem in which we may expect an effect of near miscibility on the relative permeability curves. A realistic estimate of well impairment is highly important to enable decisions on the number of wells that will be drilled in the reservoir.

1.3.1 Applications of near-miscible flow

Near-miscible flow in porous media may have different other applications within the oil industry. First of all, reservoir fluids in volatile oil reservoirs may be near miscible. Just like gas condensate fields, these reservoirs are found at pressures and temperatures near the critical point of the reservoir fluid. In volatile oil reservoirs, if the pressure is lowered, gas will be formed out of the liquid phase. Whenever the interfacial tension between the volatile oil and gas is low, the near-miscible relative permeability functions should be used to describe the flow of oil and gas present in the porous medium.

Also, near-miscible flow conditions can be observed when a gas injected into a gas condensate reservoir or into a volatile oil reservoir. This gas injection process is done to maintain the pressure at high values to prevent phase separation.

Another application of modeling near miscible flow that may be at the stage of enhanced oil recovery treatment of pumping water with surfactant through hydrocarbon reservoirs. The surfactant lowers the interfacial tension between oil and water, which reduces the residual oil saturation. The relative permeability representations in this thesis can be used to find a functional representation of relative permeability to oil in the presence of water with surfactant to model the flow and the phase behavior of the fluids present in porous medium.

1.4 Objectives and Methodology of the Study

To investigate the effect of interfacial tension and flow velocity on relative permeability, a series of flood test were conducted by using a well-defined porous medium, N. Marmara –1 gas field and a near miscible binary liquid

system. As a result of these injection tests, a series of near miscible relative permeability curves at different interfacial tension and flow velocity for with/without immobile brine saturation were first determined

Secondly, a mathematical model for the representation of near miscible relative permeability is developed to describe flow of condensate reservoir. The developed mathematical model was compared with literature data. The laboratory test results have been used in this mathematical model to compare with literature results.

The third objective is to demonstrate how near-miscible relative permeability affects the impairment of gas condensate producing wells.

1.5 Outline

This thesis is divided into 9 chapters. The various symbols used in this work can be found in the Nomenclature at the beginning of this dissertation. The references have been presented in the References section at the end of this thesis.

Chapter 1 gives an introduction for essential concepts of relative permeability and near miscible fluid system for the flow in porous media.

In Chapter 2, the theory and basic concept on the two-phase flow was reviewed. The effect of interfacial tension and wettability on the distribution of immiscible fluids in the pore space is presented.

Chapter 3 gives the literature surveys for the phase behavior of fluids near a critical point, relative permeability survey, and the critical phenomena that are relevant to this study.

In Chapter 4, the statement of the problem was described for the experimental part of this study for the near-miscible fluid system.

Chapter 5 gives information on the laboratory test system. The test set-up and the testing procedure used in the flood tests were described. The laboratory test results of the density and viscosity of the coexisting phases, and the interfacial tension as a function of temperature were presented.

In Chapter 6, the laboratory test results to measure near-miscible relative permeability were shown. As a result of these injection tests, the near miscible relative permeability curves as a function of interfacial tension and flow rate were presented with/without immobile water saturation.

In Chapter 7, a mathematical model was developed to describe the near-miscible relative permeability. These mathematical model results based on the laboratory experiments were compared with literature.

Chapters 8 and finally 9 are the last chapters that present the main conclusions of this thesis along with recommendations for further research.

CHAPTER 2

THEORY AND BASIC CONCEPTS

2.1 Relative Permeability

The concept of relative permeability is used to model the resistance to the flow of a fluid through a porous medium that contains a second fluid. That's why, the relative permeability presents the complex interaction between the fluids and the porous medium. The objective of this chapter is to introduce the concept of relative permeability. For this reason, how capillary forces act upon the fluid distribution in the static condition where there is no flow is introduced. Next, the flow of immiscible fluids under capillary-dominated conditions and concept of relative permeability conditions were reviewed. Then, how viscous and gravitational forces may affect relative permeability if the flow is outside the capillary-dominated regime is described.

2.1.1 Fluid distribution on the pore scale

Two fluids inside a porous medium are not randomly distributed over the pores. The distribution is strongly influenced by capillary forces, which is a result of the interaction between the porous medium and the two fluids by wettability in combination with the cohesion within the fluids that is interfacial tension.

2.1.1.1 Interfacial tension

Boundaries between two immiscible phases exhibit a contractile tendency that is observed in the form of an interfacial tension. It can be defined as an amount of energy that is required to create a unit area of interface. Also, it can be seen as the force per unit length acting along an arbitrary line on the interface.

Laplace (1806) derived [22] that the pressure difference over a curved interface of principal radii R_1 and R_2 is derived as:

$$P_{\Omega} - P_{\omega} = \sigma_{\Omega,\omega} \left(\frac{1}{R_1} + \frac{1}{R_2} \right) \quad (2.1)$$

Where P_{Ω} and P_{ω} are the pressures in the two immiscible phases, respectively, and $\sigma_{\Omega,\omega}$ is the interfacial tension between phases.

2.1.1.2 Wettability

What happens at the point where a fluid-fluid interface comes into contact with the solid phase that forms the porous medium. In general, the attraction of a solid to a specific fluid phase will differ from that to another fluid phase so that it is the preference of the fluids in solid porous medium among of fluids, which will wet the surface, is described by wettability.

The wetting phase is pulled and wide spreads towards the solid surface. The angle between the interface and the solid is generally smaller than 90 degrees. Figure 2.1 illustrates the angle for a droplet of the wetting phase (w) that is surrounded by a second phase (o).

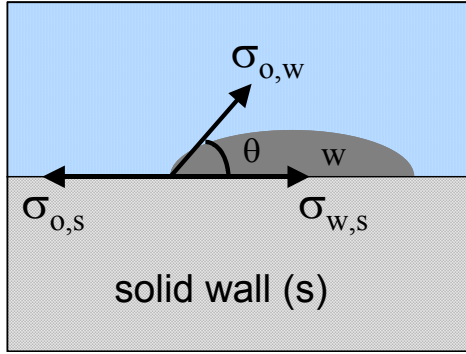


Figure 2.1: The contact angle between solid/fluid/fluid system

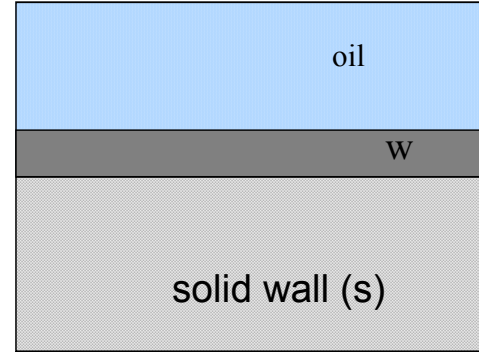


Figure 2.2: Graph for the zero contact (water spreading)

The angle between a solid and a fluid-fluid interface is called as a contact angle and can be used to quantify wettability.

$$\cos \theta = \frac{\sigma_{oil,solid} - \sigma_{water,solid}}{\sigma_{oil,water}} \quad (2.2)$$

where θ is the contact angle, measured through the denser liquid phase and ranges from 0 to 180°. Whenever the contact angle between phases is closer to zero value as shown in Figure 2.2 that is considered as completely wetting (spreading) the solid surface by the phase (w).

2.1.1.3 Capillarity

The interaction of the wetting state and the fluid-fluid interfacial tension results in a specific fluid configuration that is maintained by capillary forces as shown in Figure 2.3. Capillarity promotes the capillary flow of the wetting phase into the medium as imbibition process, whereas it opposes the flow of the wetting phase out of the porous medium as drainage.

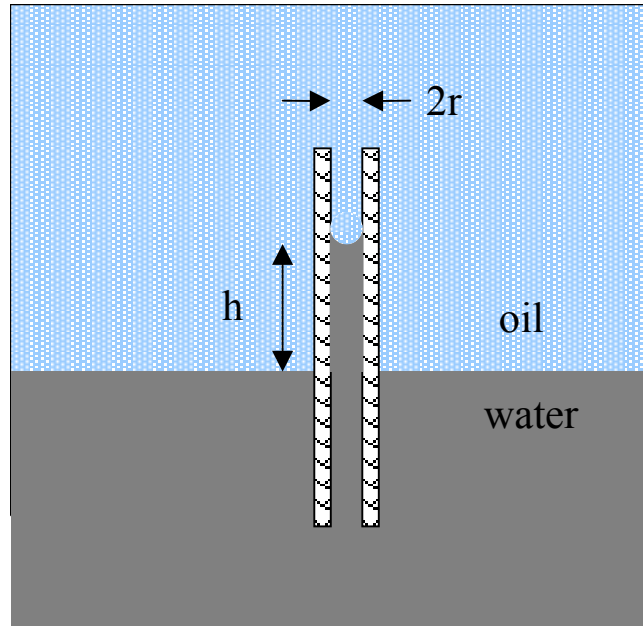


Figure 2.3: Capillary Rise in a Capillary Tube

$$P_c = (\rho_{water} - \rho_{oil})gh = \frac{2\sigma \cos \theta}{r} \quad (2.3)$$

where ρ is the mass density of the phase, and h is the height of the interface in the tube with regard to the interface outside the tube, as indicated in Figure 2.3. In this equation, r is the inner radius of the capillary tube.

2.1.1.4 Capillary forces in porous media

If a preferentially wetting phase is brought into contact with a porous medium, it will be pulled close to the pore walls, and it will have a curvature of the interface will cause the fluid to flow into porous medium. On the other hand, if a porous medium is fully saturated with a preferentially wetting phase, a non-wetting phase will only enter into the medium if the pressure in the non-

wetting phase exceeds the pressure in the wetting phase by a certain amount (i.e. threshold pressure). When a pressure difference between the two phases is applied, the existing interfaces will deform and move until capillary forces balanced the distribution of the phases. The pressure difference between the non-wetting phase and the wetting phase that remains when a steady state is reached is called capillary pressure.

The pressure difference between a non-wetting phase and a wetting phase in a porous medium depends on how much of the non-wetting phase has been forced into the medium. Leverett (1941) measured [23] the capillary pressure as a function of saturation for different combinations of fluids and porous media, and he concluded that the capillary pressure can be written in terms of the interfacial tension and the properties of the porous medium, as follows:

$$P_c = P_{nw} - P_w = \sigma \sqrt{\frac{\phi}{k}} J(S) \quad (2.4)$$

where nw and w refer to the non-wetting and wetting phase, respectively, ϕ is the porosity of the porous medium, k is the permeability of the medium, and $J(S)$ is a dimensionless capillary pressure, called the Leverett function.

2.1.2 Flow of immiscible fluids

The relative permeability concept is the extension of the permeability. The property of porous medium is first defined by Darcy's equation (1856), which states [1] that the flow velocity of homogeneous fluid in a porous medium depends linearly on the gradient in the flow potential of the fluid, written as:

$$\vec{u} = -\frac{k}{\mu} (\vec{\nabla}P + \rho \vec{g}) \quad (2.5)$$

In this equation, u , superficial Darcy velocity, is the volumetric flux per unit cross-sectional flow area, k is the permeability of the medium, and μ is the viscosity of the fluid.

The definition of permeability is questioned due to term of “specific to the porous medium”. It can be correlated to the pore geometry, like porosity as a ratio of pore volume to total volume, tortuosity defined by the ratio of the actual path length to the effective distance, and specific surface area (Kozeny, 1927 [24]; Carman, 1937) [25]. These factors contribute to the resistance to flow.

Darcy’s equation, Equation 2.5 is valid for homogeneous, single phase, laminar flow of Newtonian fluids. Darcy’s equation ignores the pressure drops by changes in capillary flow direction and inertial effects, as the magnitude of the momentum of the fluid particles. Reynolds (1883) [26] defined the ratio of the inertial forces to viscous forces, known as the Reynolds number. For porous media, the characteristic pore scale length, which may be estimated by the square root of permeability over porosity mentioned in the Leverett’s capillary pressure equation, Equation 2.4, give this size. The expression for the Reynolds number of the form (Collins, 1961) is derived as [27]:

$$Re = \frac{\rho \|u\|}{\mu} \sqrt{\frac{k}{\phi}} \quad (2.6)$$

Tests conducted to check for the validity of Darcy’s equation showed the deviations of the Reynolds number values that they are greater than 0.1 to 75 (Scheidegger, 1974) [28]. Ergun (1952) showed [29] that critical Reynolds number could be used for unconsolidated porous media with satisfactorily. His analysis along with various literature works indicated the approximate critical

value of 10. At higher critical Reynolds number, the relationship between pressure drop and flow velocity becomes non-linear.

2.1.2.1 Relative Permeability to immiscible fluids

If there are two immiscible fluids, such as oil and water, flowing simultaneously through a porous medium, then each fluid has its own, so called, effective permeability. These permeabilities are dependent on the saturations of each fluid, and the sum of the effective permeabilities is always less than the absolute permeability.

Darcy's equation can be modified to describe two-phase flow (Muskat and Meres, 1936) [2] as:

$$u_o = -\frac{kk_{ro}}{\mu_o}(\nabla P_o + \rho_o g) \quad (2.7)$$

Where k_{ro} is the o -phase relative permeability, defined as the fractional reduction in the absolute permeability to the phase o due to presence of the second phase.

Relative permeability is a function of saturation as S_w , wetting phase and S_{nw} , non-wetting phase saturation ($S_{nw} = 1 - S_w$), a typical relative permeability curve is given in Figure 2.4.

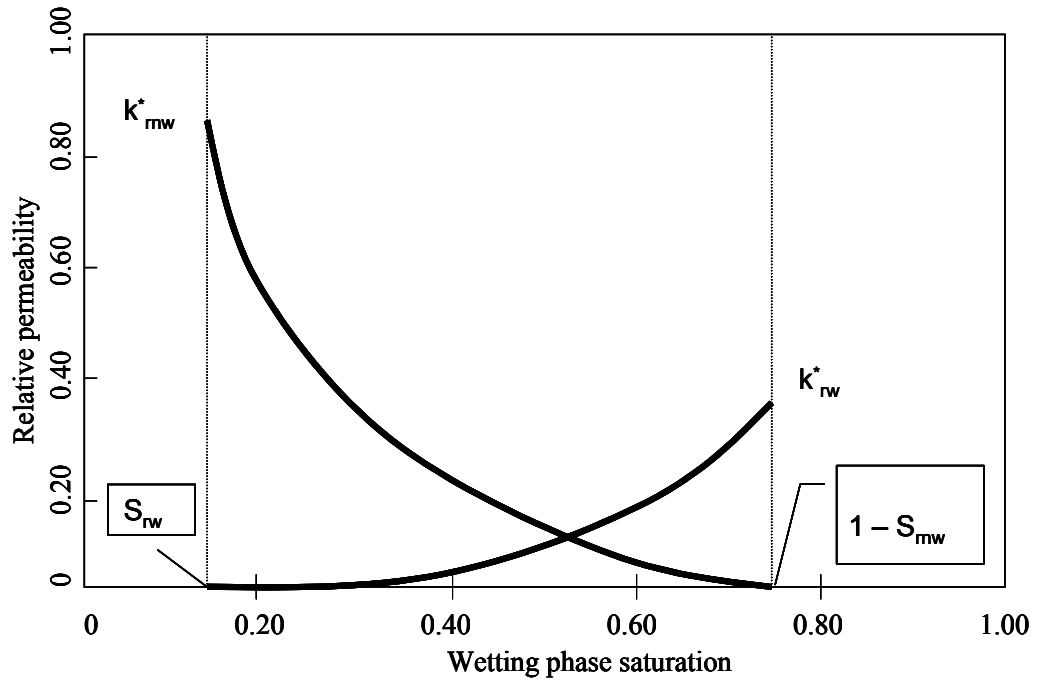


Figure 2.4: A Typical Relative Permeability Curve

The relative permeability curves in Figure 2.4 could only be plotted for the saturation interval where both phases are mobile. In Figure 2.4, S_{rw} is the saturation where wetting phase does not have mobility in that case only non-wetting phase flows through pore spaces. For the left side of the curve (where $S_w < S_{rw}$) wetting phase saturation is trapped. For the right side of the curve, the non-wetting phase is not connected to any flow path (if $S_w > 1 - S_{rnw}$).

2.1.3 Flow outside the capillary-dominated regime

Relative permeability test results will give the same shape of curves regardless of tests conditions if the capillary forces have an effect on the fluid distribution. Whenever viscous forces or gravitational forces have some effect, then the shape of the relative permeability curve will change.

The researcher, Lefebvre du Prey (1973) [30] concluded that relative permeability may depend on fluid viscosity ratios, on the ratio of the viscous forces to capillary forces on the pore scale, and this dimensionless ratio is called as capillary number, N_c . Also, relative permeability can be affected by the ratio of gravitational forces to capillary forces on the pore scale, and this dimensionless ratio is called as the Bond number, N_B . This dimensionless term was originally defined by Bond and Newton (1928) [98]. In generally, relative permeability of two fluids is a function of saturation (S), wetting properties, pore geometry, and saturation history. Also, outside the capillary dominated region, the relative permeability depends on viscosity ratio (μ_o/μ_w), the capillary number (N_C), and the Bond number (N_B).

2.1.3.1 Capillary Number

Many researchers have worked on the ratio of the viscous forces to capillary forces to show the effect for fluid distribution in pore spaces. The effect of capillary number on the residual saturation has been widely studied during the surfactant injection as an enhanced oil recovery study (Stegemeier, 1977) [31]. It was found that the residual saturation decreases when the viscous forces increase compared to the capillary forces.

There is no a unique agreement on how to define capillary Number N_C , which is defined as the ratio of viscous forces to capillary forces (Taber, 1981 [32]; Larson et al. 1981 [33]). The various definitions proposed in the literature are presented in Table 2.1. In the definitions, the most important factor is in how viscous forces are expressed as the measurable quantities. The first four definitions point out the viscous pressure gradient. The last three definitions are expressed in terms of the product of the viscosity and the velocity. An increase in the capillary number improves the relative permeability to both phases.

Table 2.1: Literature [43] Survey on Capillary Number

Leverett (1939)	$N_c = \sqrt{\frac{k}{\phi} \frac{\ \nabla p\ }{p_c}}$
Brownell and Katz (1947)	$N_c = \frac{k \ \nabla p + \rho \mathbf{g}\ }{\sigma \cos \theta}$
Ehrlich <i>et al.</i> (1974)	$N_c = \frac{k \ \nabla p\ }{\phi \sigma}$
Larson <i>et al.</i> (1981)	$N_c = \frac{k \ \nabla p\ }{\sigma}$
Moore and Slobod (1956)	$N_c = \frac{\mu \ \mathbf{u}\ }{\sigma \cos \theta}$
Saffman and Taylor (1958)	$N_c = \frac{\mu \ \mathbf{u}\ }{\sigma}$
Foster (1973)	$N_c = \frac{\mu \ \mathbf{u}\ }{\phi \sigma}$

2.1.3.2 Viscosity Ratio

Viscosity ratio of the fluid pair may influence the relative permeability if the capillary number is high. When a highly viscous phase is displaced by a less viscous phase, a channeling may be seen rather than the equilibrium conditions of capillary forces. The relative permeability to the highly viscous phase is observed to decrease, and the relative permeability of less viscous phase is observed to increase with increasing viscosity contrast (Peters and Khataniar, 1987) [34].

2.1.3.3 Bond Number

The dimensionless term is the ratio of gravitational forces to capillary forces on the pore scale is defined as Bond Number, N_B as shown in Equation 2.8 below.

This is the case where we have one of the fluids is much denser than the other so that capillary rise is negligible since it is too low, interfacial tension is low and pore size is large. If the Bond number is high, segregation due to gravity will happen. This means that the heavier fluid flows in the lower part of the pores, and the lighter fluid flows in the upper parts so it affects the fluid distribution. Relative permeability curves will have the same shape of Figure 1.2 by approaching to the straight lines.

$$N_B = \frac{k\Delta\rho\|g\|}{\phi\sigma} \quad (2.8)$$

2.2 Near Miscible Fluids

This thesis basically focuses on near-miscible fluids. Near miscible fluids are found at conditions that are very close to a critical point of the fluid system. The most important factor for the critical point is that it has very low interfacial tension. The important effect of low interfacial tension is to diminish the capillary forces that basically control the distribution of the phases.

Near-miscible systems can be found in two types of fluid. It can be either in gas and liquid as gas/liquid system or two liquid phases, called as a liquid/liquid system. The equilibrium conditions of the phases for miscibility are determined by pressure, temperature, and the composition of the components.

The behavior of interfacial tension near the vicinity of critical point is almost same for gas/liquid systems and liquid/liquid systems. Because in both cases the near –miscible phases become increasingly similar. Although a theory on the critical point was initially developed for a pure gas/liquid system (Van der

Waals, 1873) [35] more specific properties were identified for many systems by Griffiths and Wheeler (1970) [36].

CHAPTER 3

LITERATURE SURVEY

In a gas condensate reservoir, there are many important differences between the flow regimes in the regions close to and far from the well. These different flow regimes are reflected in the requirements for relative permeability data for the deep reservoir and near well regions. Far from the well, flow rates are low, and liquid mobility is usually less important, except in reservoirs containing very rich light components fluids. In the near well region, both liquid and gas phases are mobile, flow rates are high, and the liquid mobility is important.

At initial reservoir conditions the hydrocarbon fluids are mostly present at near-critical conditions. Consequently, the physical properties of the oil phase are very similar, and the interfacial tension between oil and gas is very low. During the production phase of gas condensate reservoir multi phase fluid problem becomes important below dew point pressure. One of the important multi-phase fluid flow problems at near critical conditions is condensate drop out in the vicinity of wells in gas condensate reservoirs. This drop out causes an apparent skin resistance at the well bore that impairs the production capacity of well.

Along with Fevang and Whitson (1996) [38], Afidick *et al.* (1994) [39] and Barnum *et al.* (1995) [40] have reported field data which show that under some conditions a significant loss of well productivity can occur in gas wells due to near wellbore condensate accumulation.

As pointed out by Boom *et al.*, (1996) [41, 62, 63, 64, 65, 68] even for lean fluids with low condensate dropout, high condensate saturations may build up as many pore volumes of gas pass through the near wellbore region. As the condensate saturation increases, the gas relative permeability decreases, and thus the productivity of the well decreases. The gas relative permeability is a function of the interfacial tension (IFT) between the gas and condensate among other variables. For this reason, several laboratory studies [41-49] have been reported on the measurement of relative permeability data of gas-condensate fluids as a function of interfacial tension. These studies show a significant increase in the relative permeability of the gas as the interfacial tension between the gas and condensate decreases.

The relative permeability data of the gas and condensate can be modeled by an empirical formula representing the interfacial tension [50]. But, it has been known since at least 1947 [51] that the relative permeability data in general actually depend on the ratio of forces on the trapped phase, which can be expressed as either a capillary number or Bond number. This has been recognized in recent years to be true for gas-condensate relative permeability data [18,13].

The important parameter to a gas-condensate relative permeability model is the dependence of the critical condensate saturation on the capillary number or its generalization called the trapping number. In the study conducted by Pope *et al.*, 1998 [21], a simple two-parameter capillary trapping model was developed. That model was a generalization of the approach first presented by Delshad *et al.* (1986) [52]. Then, a general scheme for computing the gas and condensate relative permeability data as a function of the trapping number was generated. The results of these cases for the low trapping numbers (high IFT) as input, had a reasonable output data in the literature Pope *et al.*, 1998 [21]. Such a model, with typical parameters for gas condensates, can be used in a compositional simulation study [60,61,76] of a single well to better understand the

productivity behavior of the wells and to evaluate the significance of condensate buildup.

Traditionally, multi phase flow in porous media is described by means of the concept of relative permeability functions, empirical relationships for decrease in effective permeability to flowing fluid phase as a function of the fluid saturation. At conditions far from the critical point, the capillary forces dominate multi-phase flow in porous media when the flow is compared with viscous and gravitational forces. Hence relative permeability functions may be considered to be constant that is independent of flow rate and interfacial tension. The constant functions are commonly referred as immiscible relative permeability functions. At the limit (i.e. zero interfacial tension) relative permeability curves reduce to linear functions of the fluid saturation.

The effect of near-criticality on the relative permeability is still an unsolved issue in reservoir engineering. Experimental studies published in the literature indicate a trend from immiscible to miscible relative permeability curves as the interfacial tension approaches zero.

A review of the literature [44] reveals that there is no consensus on how near miscibility changes relative permeability curves and which parameters are controlling this change. Some investigators have found that the relative permeability to the non-wetting phase is affected more easily, [5,6,13] whereas others observed a greater increase of the relative permeability to the wetting phase compared with the relative permeability to the non-wetting phase [7,9]. Other authors did not find an effect of interfacial tension at all [14-15]. Equally contradicting are the reports on the effect of flow velocity on near-miscible relative permeability. Some investigators find no effect [16,17], whereas others do [6,18]. In addition, Henderson et al. [13] have reported that relative permeability is only affected by the flow velocity if the fluids enter the porous

medium as a single, homogeneous phase, and subsequently, are allowed to separate into two phases inside the pores.

There appear to be two conflicting views on which mechanism controls the change in relative permeability. Many authors argue that a low interfacial tension affects relative permeability through the ratio between viscous forces and capillary forces, as denoted by the capillary number [4, 5, 6, 10, 13, 18, 20, 77, 78]. Most of these authors, however, suggest that there is a threshold interfacial tension below which the capillary-number dependence becomes important [4, 5, 6, 10, 13].

Other investigators interpret their relative permeability data in terms of the interfacial tension alone [7, 8, 9, 11, 45, 66]. In two cases, this was done in view of the fact that a transition from partial wetting to complete wetting, as predicted by Cahn, [12] may affect the mobility of both phases [8, 17]. The influence of such a transition cannot be described in terms of the capillary number, because it is directly induced by a change in the interfacial tension between the near-miscible phases.

According to current understanding of the flow behavior in gas condensate systems, two flow regimes may be considered: one corresponding to conditions away from the critical point, where IFT's are relatively high, and another to conditions near the critical point, where IFT's are very low [99]. The typical behavior of relative permeability curves as a function of IFT is shown schematically in Figure 3.1. Far from the critical point, the relative permeability curves show considerable curvature and appreciable residual saturations. Near the critical point, the IFT reaches very low values and the relative permeability curves become progressively straighter, with the residual saturations diminishing. In the limit of zero IFT, the curves become straight lines, the residual saturations vanish, and the sum of the relative permeabilities

is unity for all saturations. This scenario is supported by experimental studies [4, 37].

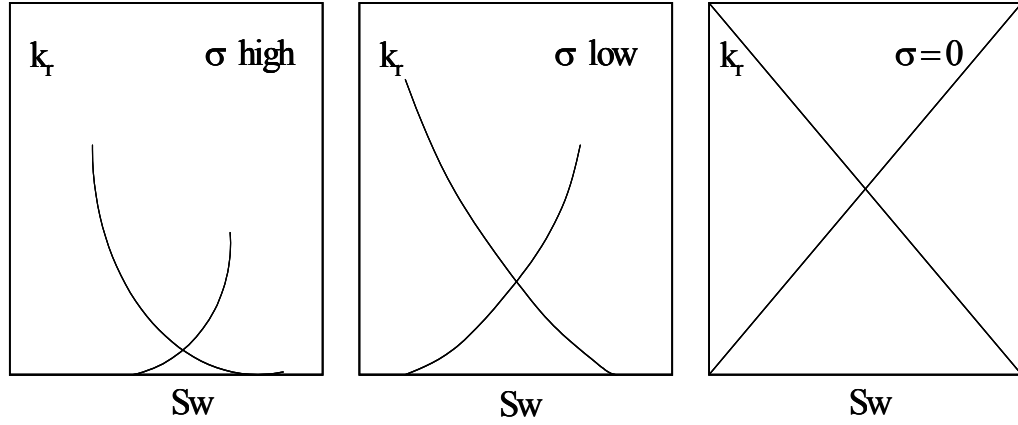


Figure –3.1: Relative Permeability Dependence on IFT

The relative permeability measurements show that the controlling parameter is the ratio of viscous forces to capillary forces on the pore scale, defined as capillary number, N_C . Similarly, relative permeability may be affected by the ratio of the gravitational forces to the capillary forces on the pore scale, expressed as Bond number, N_B . The calculations show that near-miscible relative permeability functions come into play in the vicinity of the well bore. For the mathematical modeling of two-phase flow, we have used the magnitude of flow rate and interfacial tension in addition to capillary and bond numbers, Fulcher (1983) [17], Henderson (1995) [13].

Coşkuner (1997) [67] has extended definition of N_c and Pope (1998) [21] defined trapping number N_t . Kalaydjian (1996) [15] combined N_B and N_c , however others like Bourbiaux (1995) accounted for inertial effects.

CHAPTER 4

STATEMENT OF THE PROBLEM

The main objectives of this work are described below. Firstly, we want to determine the shape of near critical relative permeability curves as a function of the ratio of viscous forces to capillary forces. For this purpose we have measured relative permeability curves of a near critical fluid system at varying interfacial tension and varying flow rates of non-wetting phase in the laboratory tests in which some of them were conducted at immobile water saturation. Secondly, we wanted to demonstrate the significance of using proper relative permeability curves for the evaluation of the effect of condensate drop out on the capacity of gas condensate wells.

The main application of this study, well impairment in gas condensate fields, concerns a gas/liquid system. Such systems become near-miscible only at very high pressures and temperatures (typically: critical pressure > 4.500 psi and critical temperature > 200 F). The high pressure and temperature complicates gas condensate laboratory experiments.

Initially, we tried to conduct a laboratory model with and without immobile water saturation both on unconsolidated and consolidated samples then we started to correlate a mathematical model that we developed for modeling of gas condensate flow behavior.

For the laboratory work, we have started by selecting a binary testing fluid system, which will be easier to handle, and representative of gas condensate behavior. For the reasons explained in detail in this study, methanol and n-hexane system has been selected as a synthetic testing binary fluid. Then, we have conducted unsteady state gas/condensate with and without immobile water saturation at different N_C , N_B and IFT to represent the different regions in phase behavior change. Relative permeability data was calculated by using JBN technique [74] to evaluate the K_r for viscous dominated region increasing condensate saturation.

The next stage of the work is to develop a mathematical model to represent gas condensate relative permeability behavior. The proposed new model is a combination of capillary and bond numbers accounting more sensitively the effect of temperature on the interfacial effect in gas condensate systems.

As a later stage, the mathematical model is to be compared with literature and the laboratory data to see the fitness or the deviation. In order to check the model, all the laboratory experiments has to be checked by using the Mean Square Error parameter to show the fitness degree.

The general equation aimed to develop for computing the gas and condensate relative permeabilities as a function of the Condensate number, N_K has to be more sensitivity to temperature that bare implicitly the effect of interfacial tension. This model, with typical parameters for gas condensates, can be used in a compositional simulation study of a single well to better understand the productivity of the field.

CHAPTER 5

LABORATORY TEST SYSTEM AND TEST PROCEDURE

5.1 Introduction

Measurements of gas condensate relative permeability can be carried out using reservoir fluid samples or with synthetic fluids in laboratory studies. Experiments with reservoir fluid samples are more realistic but expensive and time consuming. The advantages of using synthetic gas condensate fluids are easy to handle, better characterization, and no need to work at very high temperatures and pressures.

We have developed a test up for the measurement of near critical relative permeability by unsteady state displacement method. In this method relative permeability tests were conducted as a one dimensional immiscible displacement by measuring pressure drop across the core plug and recording the producing ends as a function of time by using Johnson, Bossler and Naumann method [74].

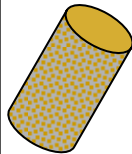
5.2 Core Properties.

Two types of porous medium were used in the tests. The first porous media consisted of sand particles with a diameter of 0.55 mm – 1.40 mm micrometer

that was packed in an aluminum core holder of 63 cm in length. The unconsolidated sample had a porosity of 0.38 ± 0.01 and a permeability of 8.0 ± 0.25 D. Then, we have used consolidated North Marmara plug sample in the relative permeability test run. The core used in this study to demonstrate the effect of high rate and interfacial tension was a carbonate core from a North Marmara Sea gas reservoir. The petro-physical properties of the plug sample are given in the Table 5.1

Table 5.1: Testing Fluid and Core Data Properties

Test Fluid		: Binary System	
		Methanol - n-Hexane	
• Binary:		: %56	- %44 Mole
• Methanol		: 0.80 g/cc,	Purity %95
• Hexane		: 0.66 g/cc,	Purity % 98
Core Sample		: Consolidated plug / Unconsolidated	
• Well		: N.Marmara –1	Crushed Limestone
• Plug Depth		: 1,155.10 m	
• Core Length		: 6.82 cm–	63 cm
• Diameter		: 1.5” (3.78 cm)	3.81 cm
• Pore Volume		: 20.52 cc	273 cc
• Kair / Porosity,%		: 18.56md/ 26,8	8±0.25d / 38±1
• Grain Density		: 2.70 gr/cc	2.71



North Marmara limestone core plug sample was exposed to CT for scanning in METU to identify porosity changes in 3-dimension. The core plug sample was viewed in Figures 5.1 and 5.2 by using a Philips Tomoscan TX 60 X-ray CT scanner in METU.

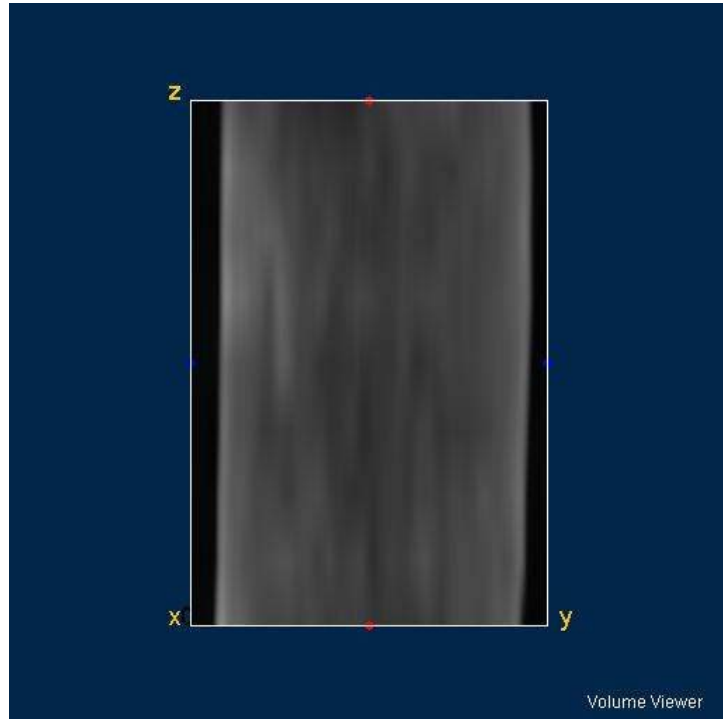


Figure 5.1: Vertically CT Scanned Cross-sectional Image of N. Marmara-1 Core Plug Sample

The sample studied, was a 1.5 in diameter N. Marmara-1 plug with 26.80 % He porosity and permeability of 18.56 md. The sample was initially scanned 3-D as x, y and z dimensions by CT and shown in Figure 5.1. The CT images shown in the Figure 5.1 has no fractures. The limestone core plug sample is relatively homogeneous except for small vugs as observed in the image.

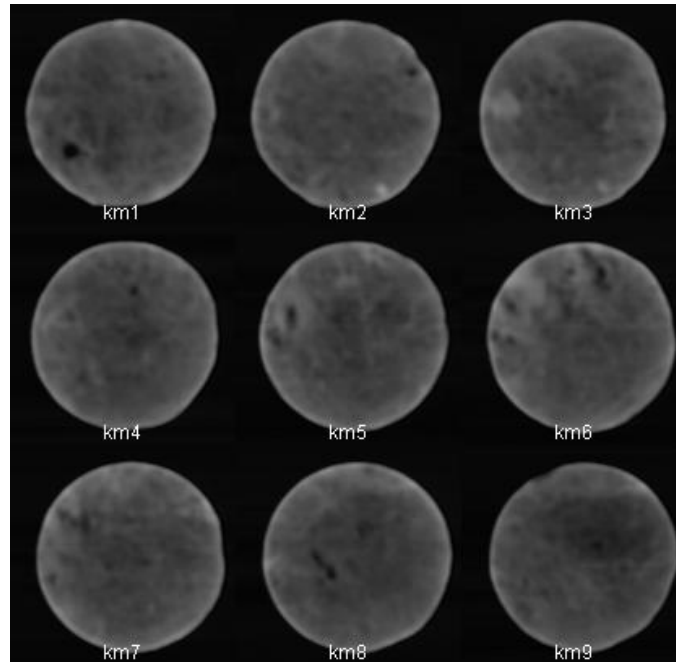


Figure 5.2: Cross-sectional CT Scans of the Plug Sample

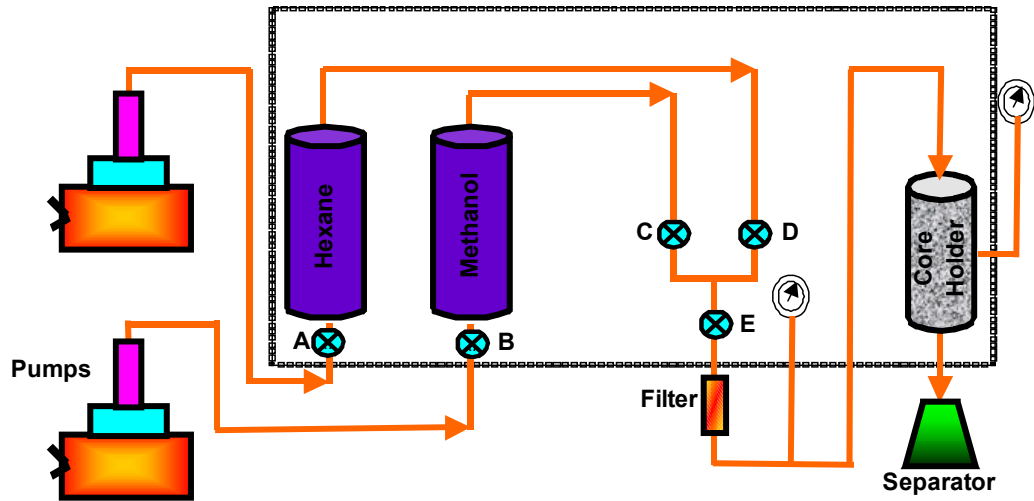
The sample was CT scanned using 1mm thick slices at 133 kV and 120 mA. As seen in the nine representative cross sections shown in Figure 5.2, the limestone core plug sample has a uniform porosity, except for a few mm-scale low porosity regions apparent both on CT and visually. Also, the sample CT images show relatively homogeneous view except some small vugs of low-density regions that can be identified as black colored region in the images.

5.3 Test Set-up System

The displacement test system is shown in Figure 5.3 for measuring near-miscible relative permeability. The Figure 5.3.a is used for consolidated sample in vertical position. On the other hand, the crushed limestone sample was positioned horizontally as shown in Figure 5.3.b. It consists of fluid storage

accumulators, constant flow rate injection pumps, core holder, pressure transducers, overburden pressure system, oven and PC with a data logger.

(a)



(b)

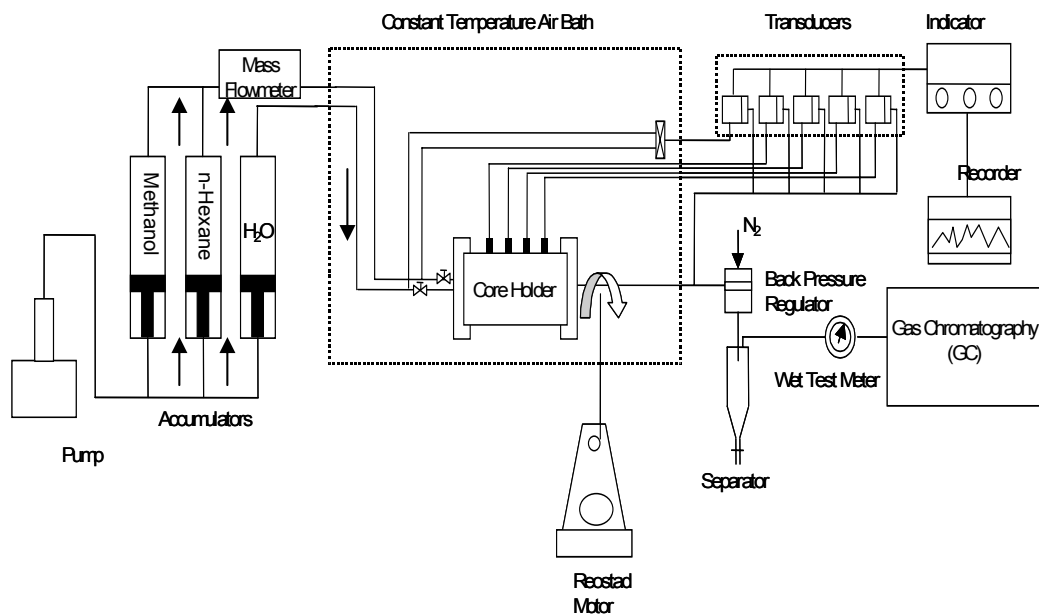


Figure 5.3. Laboratory Test Set-up (a): for Consolidated Core Plug Sample and (b: for Crushed Limestone Sample.

We have determined the relative permeability to near-miscible fluids using the Johnson-Bossler-Naumann (JBN) method [74] as generalized by Marle [75] to include gravitational forces. In this method, the relative permeability functions are derived from the characteristics of a displacement, notably the pressure drop across the porous medium in combination with the effluent volume of the displaced phase.

At the same time to ensure thermodynamic equilibrium, the two pumps for the core plug sample were set to work with such a rate that a mixture of methanol and hexane with a composition that was as close as possible to the critical methanol mole fraction of $X = 0.56$.

The injection pump was a gear pump that injected the hexane rich phase at a constant rate from the fluid storage vessel through the flow meter into the core plug.

5.4 Test Fluid Selection

Because of the universal behavior of near-critical thermodynamic quantities, [69] phenomena evoked by the vicinity of a critical point will occur both in gas/liquid equilibrium and in liquid/liquid equilibrium. Consequently, a near-miscible binary liquid system can be used as a model for a near-miscible gas/liquid system [41,44,78].

As a fluid system, we have selected the binary liquid mixture methanol/n-hexane as a model for a near-critical gas/condensate or gas/volatile oil system. The methanol/hexane system exhibits a critical solution temperature at atmospheric pressure, at a temperature of 33.5°C. Below this temperature, the

mixture may segregate into a methanol-rich liquid phase in equilibrium with a hexane-rich liquid phase [70].

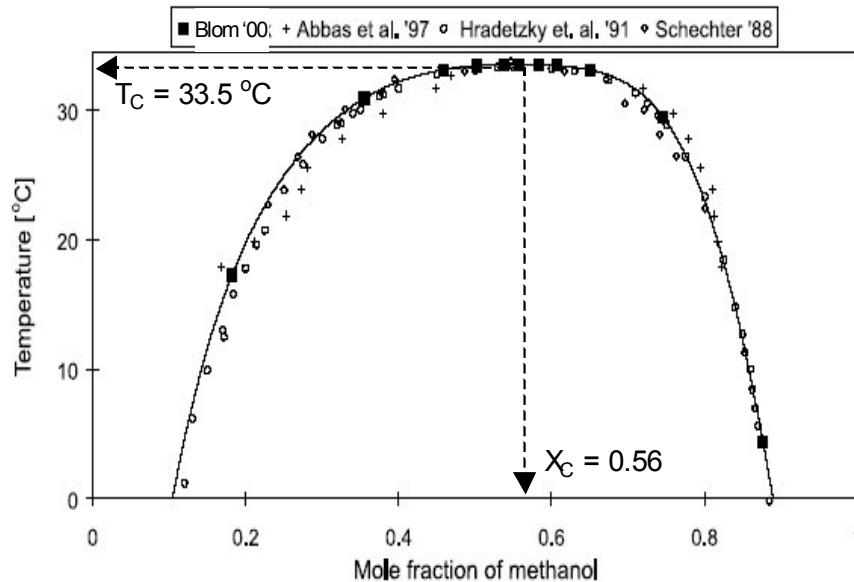


Figure 5.4 Co-existence Curve of Methanol-Hexane
(After Blom et al 2000)
($T_C = 33.5\text{ °C}$, $X_C = 0.56$ see references [17,43,71, 72]).

The main advantage of using a binary liquid system is that experiments can be performed at less extreme conditions, as the methanol/hexane system shows a critical point at atmospheric pressure and at a temperature of 33.5 °C . Another advantage is that the phase behavior of the binary liquid is not susceptible to the pressure changes. Therefore, methanol-rich phase acts as a liquid (condensate) and the hexane-rich phase plays the role of gaseous phase in the gas/condensate fluid. The experimental result of two – phase region of this fluid system along with the literature are shown in Figure 5.4.

A disadvantage of the methanol/hexane system is that its phase behavior is very sensitive to minor amounts of impurities, particularly water. This requires extra precautions in the handling of the fluids, to ensure the purity of the mixture. The methanol that we used was extra dried (maximum, 0.01% water), with an overall purity that was better than 99.5%. The purity of the n-hexane was better than 99.0% (maximum, 0.02% water).

To characterize the fluid system, the relevant properties of the coexisting phases as a function of the temperature were measured and the results of these experiments have been described in more detail [81, 82, 83]. The two-phase region of this fluid system was shown in Figure 5.4 along with literature data [17,43,71,72] and an analytical fit through our measurements. The good agreement of the measurements with recent literature data indicates that the precautions taken to prevent contamination with water and other components were sufficient. The critical solution point determined graphically from the measurements is given by $T_{cr} = 33.5 \pm 0.1^\circ\text{C}$ and $X_{cr} = 0.56 \pm 0.02$.

The methanol-rich phase is denser and more viscous than the hexane-rich phase [77, 79]. In addition, the methanol-rich phase is wetting the limestone core plug and the core crushed limestone. Therefore, it plays the same role as the liquid (condensate) in a gas/condensate fluid. Likewise, the hexane-rich phase plays the role of the gaseous phase.

The density of the coexisting phases was measured at several temperatures, by using an Anton Paar DMA 46 densitometer. The results were displayed in Figure 5.5, together with earlier measurements of the density along the coexistence curve of the methanol/hexane system [17,43,71,73].

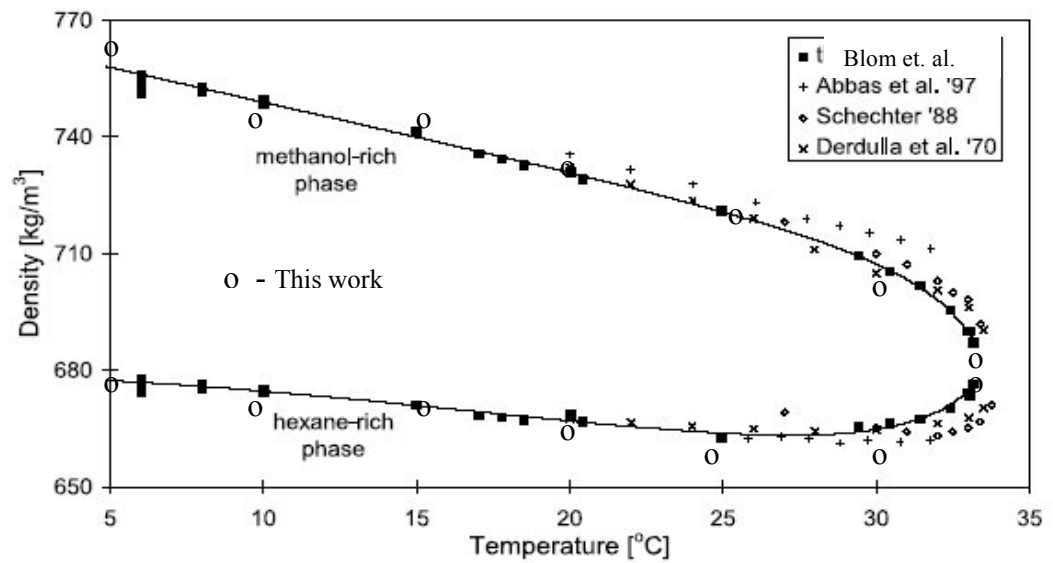


Figure 5.5: Measured Density along the Co-existence Curve.

(See Refs. 17, 43, 71, and 73.)

The viscosity of the coexisting phases was determined by using a Herzog HVM 472 full automatic viscometer with a vertical capillary tube. Figure 5.6 shows the resulting values of the dynamic viscosity. The only two literature data of methanol/hexane viscosity that we are aware of [17, 43] have been plotted in Figure 5.6.

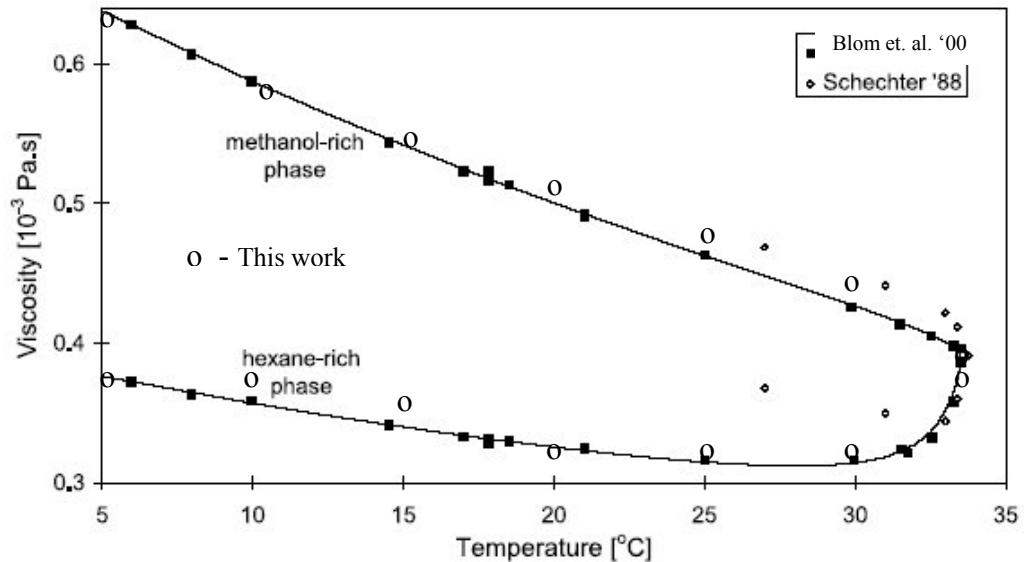


Figure 5.6: Viscosity of the Co-existing Phases. See Ref. [17,43]

Finally, the interfacial tension between the coexisting phases was measured by means of the pendant drop technique. Figure 5.7 and Figure 5.8 show how the results of our interfacial tension measurements compare with the literature data [17,43,71,73].

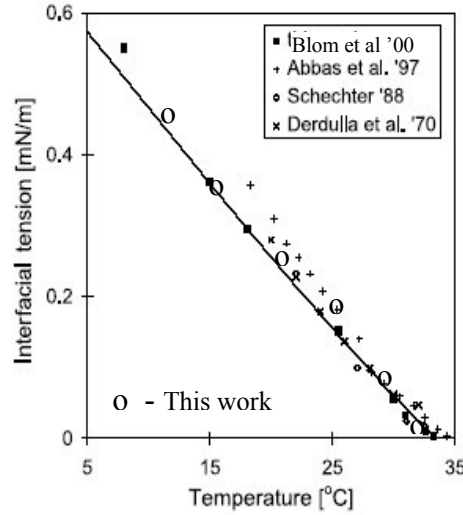


Figure 5.7: Interfacial Tension of the Fluid System

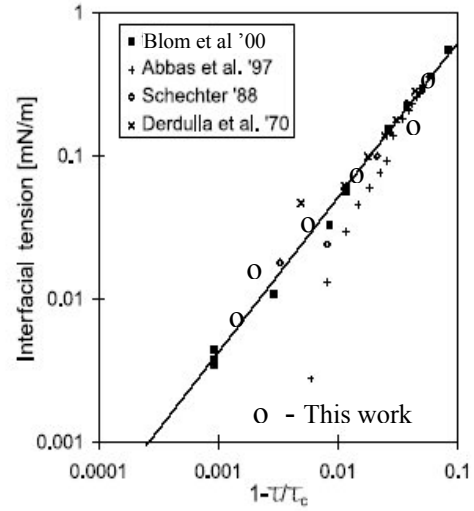


Figure 5.8: Interfacial Tension as a Function of the Reduced Temperature

The accuracy of the pendant drop technique has been reported to be better than 2 % (Huijgens, 1994) [90]. Since our density measurements were subjected to complications caused by the near-miscibility of the liquids so that the interfacial tension values may exhibit some errors. It is difficult to measure interfacial tension for the fluids when it is close to near-miscibility conditions.

The gas condensate fields deals with a gas/liquid system during depletion stage. Such a gas/liquid systems have a characteristics behavior of near-miscible at high pressure and temperatures, which gives hard time to conduct laboratory experiments by using bottom-hole sample.

As it is discussed in previous chapters, liquid/liquid systems are more suitable candidates for a model fluid than gas/liquid in a laboratory to run a displacement and phase behavior test because the phase behavior of liquid/liquid systems is hardly susceptible to changes in pressure. The interfacial tension of liquid/liquid systems varies much more strongly than that of gas/liquid systems, so that a smaller temperature range enables assessment of the influence of interfacial tension.

After the pointing out the importance of interfacial tension for selecting the test fluid used in the laboratory experiments, I want to emphasize the importance of near-miscible fluids in this study: Near-miscible fluids are special in a thermodynamic sense because they are found at conditions that are close to a critical point of the fluid system. The interfacial tension between near-miscible phases is low. Near-miscibility is found in two types of fluids systems as gas/liquid system i.e. gaseous and a liquid phase or as liquid/liquid system i.e. two liquid phases at specific pressure, temperature, and compositions.

The fluid system should satisfy two conditions: Firstly, the fluid system should be near-miscible under the conditions close to room temperature and atmospheric pressure. Secondly, the behavior of its physical properties as a function of the distance to the critical point should be analogous to that of a gas/condensate fluid. We selected the binary liquid mixture methanol/n-hexane as a near-miscible model throughout the all test runs.

The methanol - rich phase is wetting system in the model test system. The methanol is denser, heavier and more viscous phase, thus it plays the role of the liquid hydrocarbon phase. The hexane – rich phase in equilibrium with the methanol – rich phase represents the non-wetting phase.

The literature data on the critical points in the last 50 years are contradictory and indicates the following ranges:

$$33.2\text{ }^{\circ}\text{C} < T_c < 36.5\text{ }^{\circ}\text{C}$$

$$0.55 < \text{Methanol } X_C < 0.57$$

5.5 Laboratory Test Procedures

Before any injection experiment was started, the porous medium was flushed with under saturated methanol so that any residual hexane would dissolve. Then, the temperature of the thermostatic bath was chosen according to the desired interfacial tension, and the porous medium was fully saturated with the methanol-rich phase in equilibrium with hexane at this temperature. After the porous medium had been saturated with the wetting phase ($S_w = 1$), the single-phase permeability k was measured. Before we started the displacement, the accumulator was filled with the hexane-rich phase in equilibrium with the methanol-rich phase.

During the experiment, the wetting phase (methanol-rich phase) was displaced by the non-wetting phase (hexane-rich phase) at a constant flow rate. We recorded the pressure drop across the core plug along with the cumulative effluent volume of the wetting phase as functions of time.

The mathematical procedure that we have used for deriving the relative permeability functions from the displacement characteristics has been described by Marle [75]. This method is based on the assumptions that the displacement is strictly one-dimensional, and that the capillary pressure can be neglected on a macroscopic scale ($P_c = P_{nw} - P_w \cong 0$). The conditions of the experiments were examined for the assumptions underlying the measurement method are justifiable [44].

From the measured quantities (the overall pressure drop and the cumulative effluent volume of the wetting phase) we have calculated the pressure gradient, the fractional flow functions, and the saturation at the outlet of the core plug. Because the pressure drop and the effluent volume were not obtained at the same sampling frequency, the pressure drop was fitted as a function of time by an analytical function.

Following laboratory test steps were conducted in each temperature (i.e. interfacial tension and flow rate changes) as shown in the section 5.5.1.

5.5.1 Displacement Procedures

The laboratory experiments were conducted according to the following four main measurement stages:

I. Test Preparation Stage: Measurements

- Plug length, diameter, and mass data are measured.
- Porosity and absolute permeability were measured.
- n-Hexane and Methanol density and viscosity data were measured at:
 $T = 15\text{ }^{\circ}\text{C}, 20\text{ }^{\circ}\text{C}, 25\text{ }^{\circ}\text{C}, 30\text{ }^{\circ}\text{C}, 35\text{ }^{\circ}\text{C}$

II. n-Hexane Susceptibility Test at Room Temperature

- At different flow rates single phase n-Hexane permeability

III. Methanol Susceptibility Test at Room Temperature

- At different flow rates single-phase methanol permeability.

Note that n-hexane and methanol susceptibility experiments were conducted to check the reproducibility of the tests because the liquid permeability for both phases should be the same. Whenever I checked the results it was almost the same with the acceptable laboratory measurement limits.

IV. Hexane – Methanol Flood Tests

1. Stage: preparation of n-Hexane % 44 - Methanol % 56

- Plug length, diameter and dry mass determined.
- Placement of plug sample to core holder.
- Fill up of hexane and methanol to accumulator.
- Pump Methanol and n-Hexane at constant flow rates by maintaining % 44 n-hexane - % 56 methanol.

2. Stage: n-Hexane % 44 - Methanol % 56 Flood

- We let the system flow rate of % 44-mole n-hexane - % 56 moles methanol with line filter.
- Two phase flow about 10 - 20 pore volume

3. Stage: n-Hexane Flood for relative permeability

- Methanol valve is closed and n-hexane flood starts Data Record:
 - ✓ Output volumes of Methanol and n-Hexane,

- ✓ Pressure difference across the plug versus time, and
 - ✓ End point n-Hexane permeability
- were measured at the steady state stage by reaching irreducible methanol value. (i.e. no pressure change and no methanol amount produced at the end from the sample)

During the displacement stages, the net overburden pressure was set to be about 250 – 300 psi to confine the core sample. The pressure difference across the core sample was maximum 15 psi. The maximum overburden pressure was kept constant as 300 psi through out the sample.

CHAPTER 6

LABORATORY TEST RESULTS

6.1 Introduction

We measured drainage relative permeability curves at different temperatures and injection rates in 11 experiments; 4 of these tests were run under the conditions of immobile water saturation, as listed in Table 6.1. We conducted displacement experiments at three different temperatures; one of these three temperatures was very close to the critical point. In addition, we varied the injection rates with which the hexane-rich phase injected as the non-wetting phase. In the tests, at the lowest injection rate, the superficial velocity was 1.05 m/day and at the highest rate that we applied, the velocity was 2.10 m/day for the consolidated porous medium. When have reached the highest injection rate, the superficial velocity was 14.20 m/day for unconsolidated crushed limestone porous medium.

6.2 Experimental Results

The temperature and the injection rate were varied in the displacement experiments according to phase behavior of near miscible fluid (see Table 6.1). All experiments have been conducted at atmospheric pressure for the end point of the core plug sample. To reduce the effect of experimental errors, we

repeated several times the measurements at an interfacial tension of 0.01 mN/m and a superficial velocity of around 15 m/day.

Table 6.1: The List of Relative Permeability Tests

Tests	Temperature	I. Tension	q
No	(C)	(mN/m)	(cc/hr)
1*	32.8	0.010	100
2*	32.8	0.010	50
3*	18.0	0.290	100
4	18.0	0.290	75
5*	18.0	0.290	50
6	30.1	0.059	100
7	30.1	0.059	50

* Those tests were re-conducted with immobile water saturation

6.3 Checking and Reproducibility of the Test Results

To start with the same initial conditions, core samples were checked in every testing stage. The reproducibility of the results was very good matching with the previous test runs in all tests.

Methanol and n-hexane susceptibility experiments were conducted to check the reproducibility of the tests because the liquid permeability for both phases should be the same. Whenever I checked the experiment results for all the cases it was almost the same with the acceptable laboratory measurement limits.

In the case of higher interfacial tension the reproducibility of the experiments was very good. In the experiments at conditions closest to the critical temperature (low interfacial tension), reproducibility was less good. The almost same initial immobile brine saturation was maintained throughout the plug sample for the four tests conducted at immobile water saturation of %24.45 as the reproducibility data.

6.4 Relative Permeability Tests without immobile water saturation

The objective of the work presented in this section is to provide experimental test results for the effect of interfacial tension and flow velocity on near-miscible relative permeability.

To measure the relative permeability to near-miscible fluids, vertical displacement experiments on consolidated limestone core plug sample were conducted using the JBN-method (Johnson, Bossler, and Naumann; (1959) [74] as generalized by Marle (1981) [75] to include gravitational forces. A displacement procedure is an unsteady-state method, in which one phase was displaced by another immiscible phase. In this way, the saturation changes throughout the test. The relative permeability is calculated from the pressure drop across the porous medium, in combination with the effluent volume of displaced phase. With this method, the relative permeability data are obtained over a limited saturation range. By displacing the more viscous phase with the less viscous phase, saturation interval is maximized.

An unsteady-state method was used, because it is experimentally simpler and faster than a steady-state approach. The displacement tests were conducted at constant flow rate, and the pressure difference was measured during injection stages.

During the tests, the wetting phase was displaced from the porous medium by the non-wetting phase, so the drainage relative permeability curves were obtained. The fluid system that used was the binary liquid methanol-hexane, described in Chapter 5. It exhibits a critical point at atmospheric pressure, and at a temperature of $T_c = 33.5\text{ }^{\circ}\text{C}$ and a methanol mole fraction of $X_c = 0.56$. Because methanol/hexane/core system does not exhibit a wetting transition in the temperature range of the displacement experiments ($8\text{ }^{\circ}\text{C}$ to $33\text{ }^{\circ}\text{C}$)

In the different experiments, the interfacial tension between the fluids was controlled through adjustment of the temperature, whereas the flow velocity was regulated directly by adjusting the injection rate.

6.4.1 Flow Rate Effect on Relative Permeability

The first seven tests were run without introducing water in the core sample. Cumulative produced volume of methanol (condensate) rich phase versus time was shown in Figure 6.1.

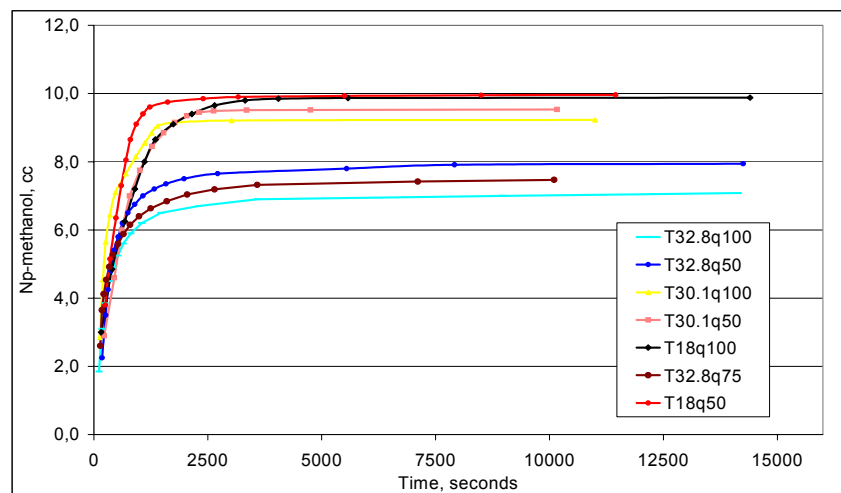


Figure 6.1: Cumulative Produced Volume of Methanol (Condensate)
Rich Phase versus Time

The measured pressure drop across the porous medium versus time for the first seven tests were run without introducing water in the core sample. was presented in Figure 6.2.

The abbreviations in the figures presented in this study were used to define the temperatures and flow rates at which the experiments were conducted. For example, the abbreviation “T18q50” in Figure 6.1 refers to the conditions at which the system temperature is 18 °C and the injection flow rate is 50 cc/hr.

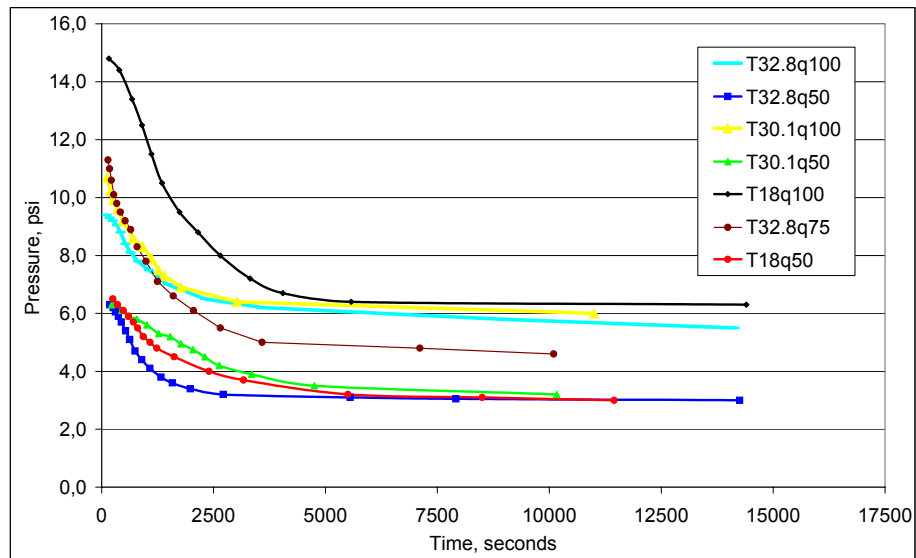


Figure 6.2: Measured Pressure Drop across the Porous Medium in Time

We have conducted two displacement tests at 18 °C, which is lower than critical point of the fluid. The n-hexane injection rate varied between 50 and 100 cc/hr. The interfacial tension was high (0.29 mN/m).

The relative permeability test results are shown in Figure 6.3. The figure shows that an increase of the flow velocity by a factor of 2 results in a slight increase of the relative permeability to the non-wetting phase. On the other hand, one may conclude that the wetting-phase relative permeability does not change.

Figure 6.3 shows the results of two experiments at a constant interfacial tension of 0.29 mN/m, at a superficial velocity of about 1 m/d (experiment 3 and 4) and 2 m/d (experiment 5). Figure 6.3 shows that an increase in the flow velocity by a factor of 2 results in a slight enhancement of the relative permeability to the non-wetting phase.

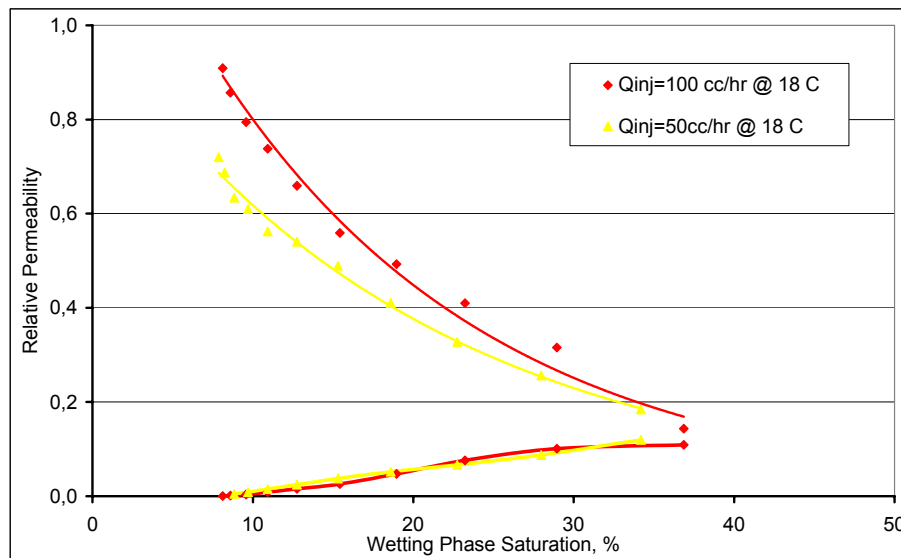


Figure 6.3: Flow Rate Effect on Relative Permeability at °18 C

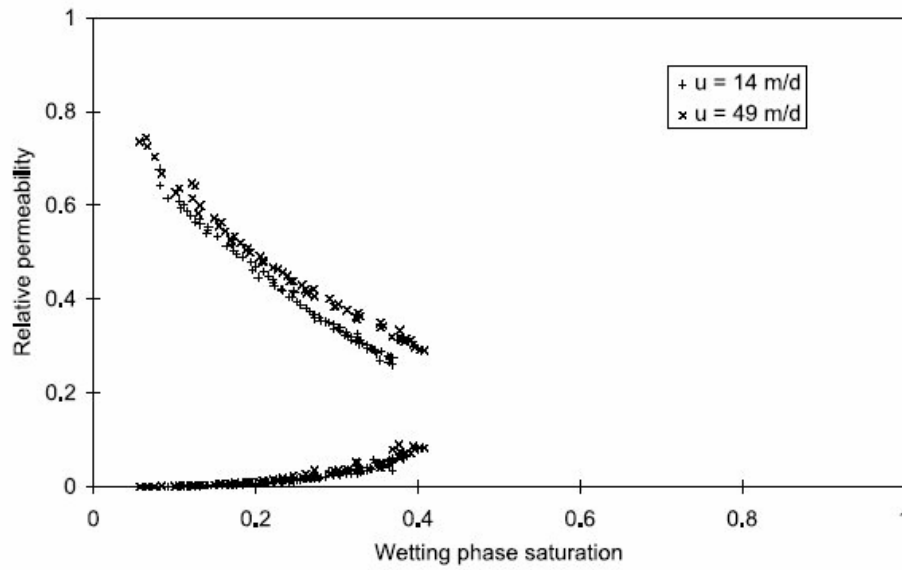


Figure 6.4: Flow Rate Effect on Relative Permeability at 18 °C by Blom 2000 [43] (i.e. at constant higher interfacial tension: $\sigma = 0.29$ mN/m.)

The test results match with literature study as given in Figure 6.4 for the case of relative permeability at varying flow velocity and constant higher interfacial tension of 0.29 mN/m.

To investigate the effect of flow rate near the critical point, we have conducted two displacement tests at 32.8 °C, which is very close to the critical point of the fluid. The n-hexane injection rates were 50 and 100 cc/hr, respectively. In these conditions the interfacial tension is very low (0.01 mN/m). The results of these relative permeability tests are shown in Figure 6.5 in the following page. The figure shows that a decrease of the flow velocity by a factor of 2 results in a slight lowering of the relative permeability to the non-wetting phase. We see that the wetting-phase relative permeability does not change within experimental error limits that can be seen during the pressure readings of gauges and the amounts of produced methanol and hexane volumes.

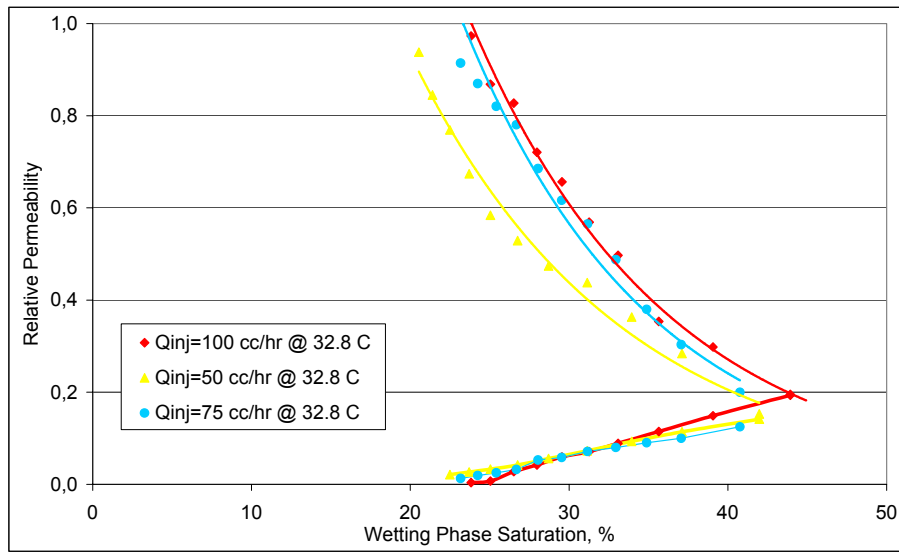


Figure 6.5: Flow Rate Effect on Relative Permeability @ 32.8 °C
(i.e. very close to critical point)

Figure 6.5 shows relative permeability data obtained at an interfacial tension of around 0.01 mN/m, and at values of the superficial velocity of 1 m/d (experiment 6) and 2 m/d (experiment 7).

At this interfacial tension level, the effect of increasing the superficial velocity by a factor of about 2 appears to be considerable. We see that increasing the flow velocity increases the relative permeability values to both phases. The fact that both a decrease in interfacial tension and an increase in flow velocity result in an increased relative permeability leads us to investigate whether our relative permeability data can be interpreted in terms of the balance between viscous forces and capillary forces.

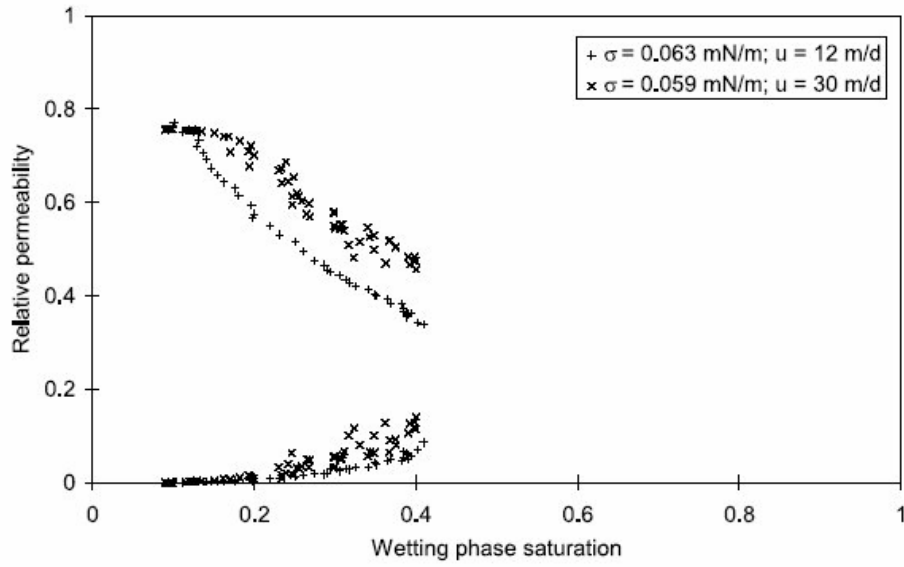


Figure 6.6: Flow Rate Effect on Relative Permeability at °32.8 C by Blom 1999 [44] (i.e. at constant lower interfacial tension: $\sigma = 0.06$ mN/m.)

The test results match with literature. Relative permeability at varying flow velocity and constant lower interfacial tension of about 0.06 mN/m as presented in Figure 6.6 show a similar behavior when compared to our results even though the tests were conducted using unconsolidated medium (Blom, 1999 [44]).

6.4.2 Effect of Interfacial Tension on Relative Permeability

Figure 6.7 shows the results of three measurements obtained at a flow rate of around 50 cc/hr, and at values of the interfacial tension of 0.29 mN/m (experiment 5), 0.059 mN/m (experiment 7), and 0.010 mN/m (experiment 2).

The laboratory tests conducted at higher temperature give relative permeability curves to the fluids with lower interfacial tension at constant flow rate. The

effect of changes of interfacial tension is summarized in Figures 6.7 and 6.8 at two different flow rates.

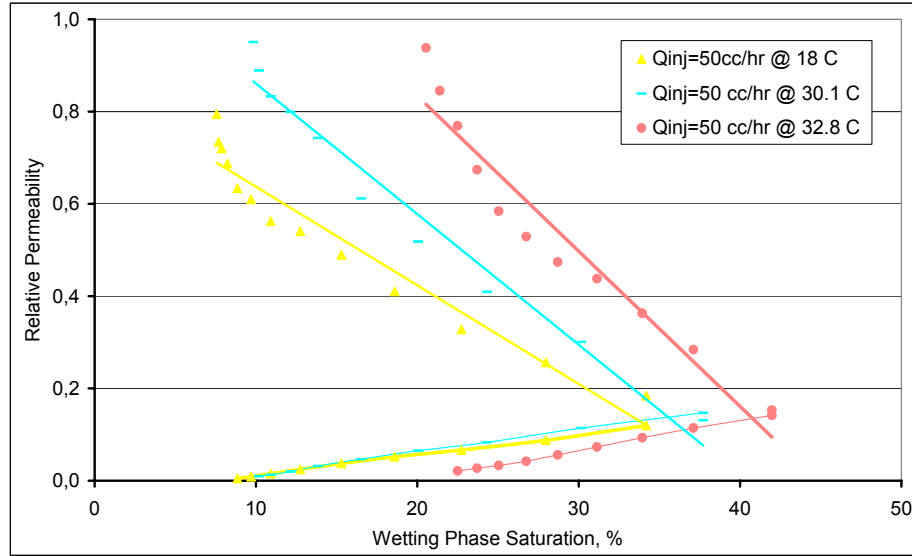


Figure 6.7: Relative Permeability at Different Interfacial Tension at 50 cc/hr.

The relative permeability curves in Figure 6.7 and 6.8 show a clear dependence on interfacial tension. The relative permeability to the non-wetting phase increases gradually when the interfacial tension decreases by a factor of 30. At very low interfacial tension, the non-wetting phase relative permeability approaches a unit-slope line for which the non-wetting relative permeability data approaches to the non-wetting phase saturation. The wetting phase relative permeability is not affected until the interfacial tension of the phases is decreased below 0.06 mN/m.

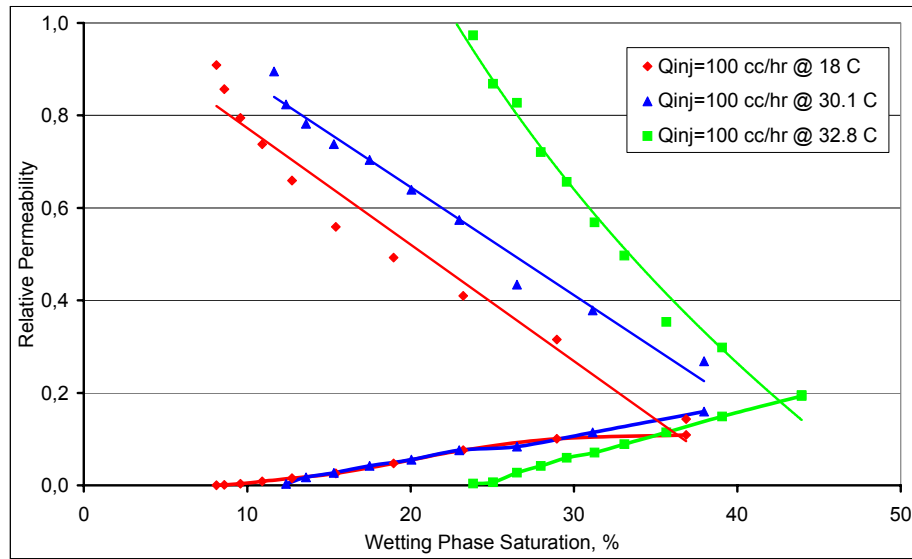


Figure 6.8: Relative Permeability at Different Interfacial Tension at 100 cc/hr.

The figures 6.7 and 6.8 show the results of three measurements at interfacial tension values of 0.29 mN/m, 0.06 mN/m and 0.01 mN/m. The non-wetting phase relative permeability gradually increases with decreasing interfacial tension i.e. raising the temperature.

The wetting phase relative permeability seems to be affected only at values of the interfacial tension below 0.06 mN/m. The measured wetting phase relative permeability is quite low, so it is difficult to point out differences the experiments.

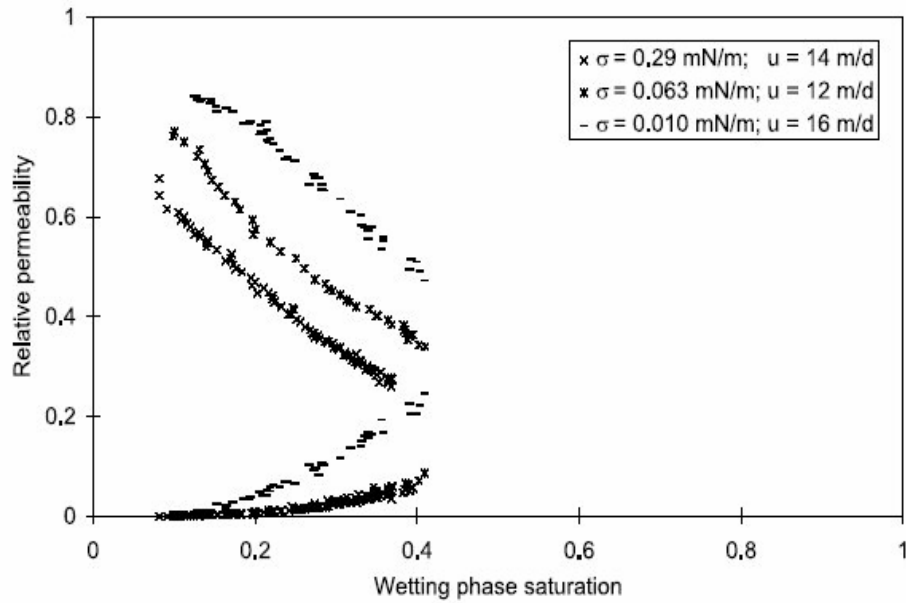


Figure 6.9: Relative Permeability Curve at Different Interfacial Tensions
Blom et al 2000 [43].

Relative permeability curves at different interfacial tensions at almost constant flow rate conducted by Blom et al 2000 [43] are presented in Figure 6.9 for the comparison with the test results shown in Figure 6.7 and 6.8.

The test results seen in our Figures have the similar behavior as the literature work done by the researchers (i.e. relative permeability to the wetting phase change is less than the non-wetting relative change).

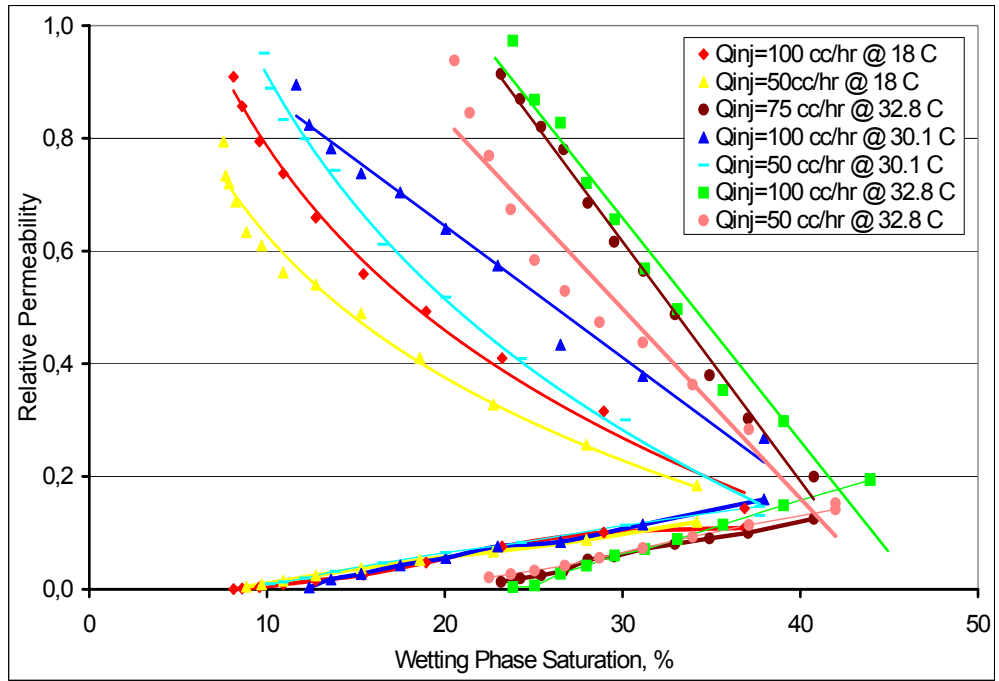


Figure 6.10: Flow Rate and Temperature Effect on Relative Permeability

Figure 6.10, in which we inserted all flow rate and interfacial tension curves on the same plot, shows clear relationship of relative permeability on the interfacial tension. As the interfacial tension decreases by increasing the temperature, the relative permeability to the non-wetting phase gradually increases. The wetting phase relative permeability seems to be affected at lower interfacial tensions. The measured wetting phase relative permeability is quite low, so that it is difficult to point out differences between experiments.

6.5 Relative Permeability Tests at Immobile Water Saturation (S_{wi})

The description of relative permeability for gas/condensate/water systems is becoming lately challenging topic in the literature. To investigate the influence of connate water and condensate saturation on inertial effects in gas/condensate reservoirs, a laboratory study has been performed with the aim to estimate the influence of pore structure and connate water saturation S_{wi} by a specific equipment built by IFP staff as Lombard, Longeron, and Kalaydjian (1999) [95]. Experiments were conducted on sand packs and sandstone core samples. Then, Kokal, Al-Dokhi and Sayegh (2003) [96] worked on the phase behavior of a gas-condensate/water system. They had an observation of the mass transfer of water into condensate phase. According to the authors, the effect of water/brine on the PVT properties of reservoir fluid was small. Lastly, Çınar and Orr (2005) [97] presented their work for an experimental investigation of the effects of variations in interfacial tension (IFT) on three-phase relative permeability. The combined Welge / JBN method was used to determine relative permeability data. As a result of Çınar and Orr [96] study, the measured three phase relative permeability data showed that the wetting phase (C_{16} -rich, water) relative permeability was not affected by the IFT variation between the non-wetting phases.

The same core plug sample of N. Marmara-1 well was run in the flood tests for relative permeability at the immobile water saturation. The plug sample was initially prepared with the same procedure followed for conditions of the first 7 experiment runs without any water introducing to the sample. To maintain immobile water saturation through out plug sample, the plug sample was completely saturated with % 100 water saturation under the compression of 1,500 psi for an overnight aging process. The N. Marmara-1 well had salinity

of 30,000 ppm so it is prepared in the lab. The fully brine saturated plug sample was then placed to the core flood test system into core holder.

The sample was then flushed by n-Hexane with a higher flow rate. The brine in the porous medium was displaced by n-Hexane, and then the amount of brine displaced was collected in the accumulator and used to measure immobile water saturation. The core sample has a pore volume of 20.52 cc, and 14.80 cc brine out of that pore volume was produced after n-hexane injected to the fully brine saturated (% 96.57) sample. The displacement process resulted to have an immobile saturation of 24.45 %. The relative permeability tests were conducted 4 more tests to check the effect of water presence in the core sample on the interfacial tension and flow rate changes.

The last four tests at immobile water saturation were run and their measured cumulative produced volume of methanol (condensate) rich phase in time at S_{wi} is shown in Figure 6.11 and measured pressure drop across the porous medium in time at S_{wi} is presented in Figure 6.12.

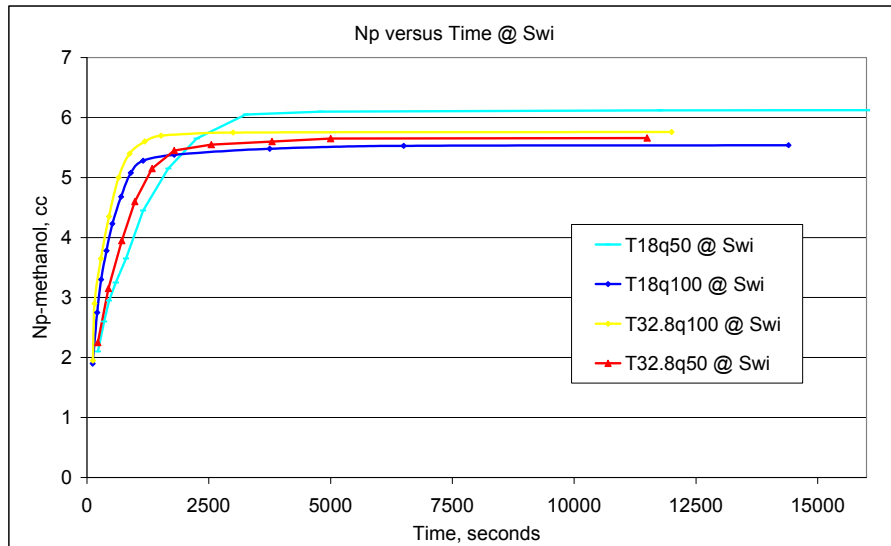


Figure 6.11: Cumulative Produced Volume of Condensate in Time at S_{wi}

The approach for measuring cumulative volume of the displaced phase introduces a time lag. This is the time between the moment a bubble of displacing phase leaves the core sample, and the moment it reaches the interface in the accumulators. In order to correct the measured data for this time lag, the breakthrough time for hexane rich phase and the moment at which the first hexane-rich blob reached the interface in the accumulator were recorded. In addition, the level of interface in the accumulator after the segregation completed was read. So the output data was corrected for extra time needed for segregation.

The data obtained in the first few seconds after arrival of the first hexane-rich phase drop cannot provide information on relative permeability. This is due to the fact that fluid particles flowing at a higher saturation catch up with particles at a lower saturation, because relative permeability is higher at higher saturation. As a result, the displacement front exhibits a saturation shock, in which the saturation jumps from the initial value to the shock value (Brinkman, 1948) [91].

Data that correspond to saturation below the shock saturation are not reliable. To determine which data should be discarded, the following procedure should be pursued. The shock saturation by means of the tangent construction of Welge (1952) [92] was determined. This method makes use of a plot of fractional flow of the injected phase against the saturation of the injected phase. The shock saturation is given by the saturation at which the tangent to the fractional flow curve crosses the point ($S = S_o$, $f = 0$), where S_o is the initial saturation.

The fractional flow of the injected phase is related to the time derivative of the measured cumulative output volume of the displaced phase. By drawing tangent to the fractional flow curve, the shock saturation was determined.

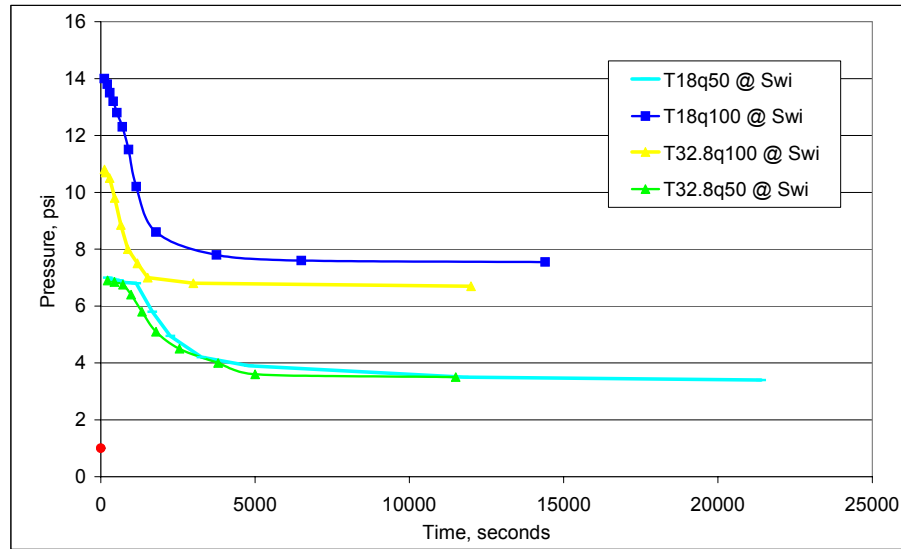


Figure 6.12: Pressure Drop across the Porous Medium in Time at S_{wi}

The pressure decline data is shown in Figure 6.12 for the four different test cases of two different flow rates and two different interfacial tension values. Two tests were performed at low constant flow velocity with high and low interfacial tensions, and the other two test were conducted at high flow velocity with also same interfacial tensions as high and low values.

Whenever the moment that injected hexane reached the outflow end of the porous medium, the pressure drop across the porous medium and the cumulative effluent volume of the displaced phase were recorded as a function of time.

In both experiments, the pressure difference increases until the first hexane-rich phase reaches the outlet of the core sample (i.e. breakthrough). After breakthrough, pressure difference across the core plug declines gradually. The reason for this is that more and more of the methanol-rich phase is displaced from the core sample, so that the flow characteristics become increasingly single-phase like.

Because of the sampling times of the pressure drop different from that of the output volume, the data were mostly not obtained at the same time. Therefore, the pressure difference as a function of time using a least-square fitting package. The package searches for a function that best fits the data set.

During the displacement experiments, the highest injection pressure through the core sample was observed in the case of the interfacial tension of 0.290 mN/m at a injection rate of 100 cc/hr.

The lowest pressure difference and injection pressure was seen when the experiment was run at a rate of 50 cc/hr and at a very low interfacial tension as 0.01 mN/m. The reason to have the lowest pressure resistant to flow is that the lowering the temperature makes the single phase fluid flow due to phase behavior where it comes closer to its critical conditions.

6.5.1 Flow Rate Effect on Relative Permeability Curves at S_{wi}

Figure 6.13 shows the results of two experiments at an interfacial tension of 0.29 mN/m, at the flow rates of 50 cc/hr and 100 cc/hr at the constant immobile water saturations of 24.45 %. In these two tests, the same amount of brine was produced to yield the same initial conditions prior to the displacement test for the relative permeability analysis.

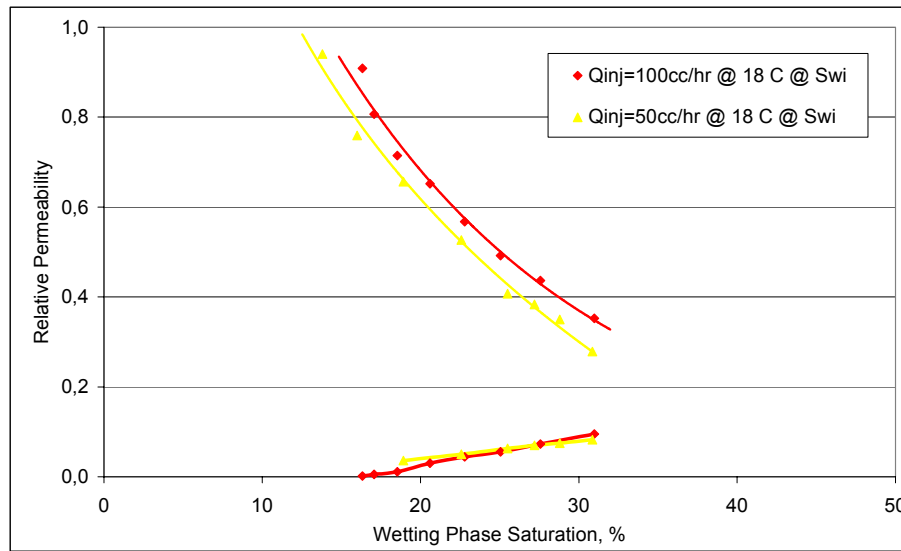


Figure 6.13: Flow Rate Effect on Relative Permeability at 18 °C
at S_{wi}

The effect of higher constant interfacial tension by changing the flow rate on relative permeability was shown in Figure 6.13 represents an increase in the flow velocity by a factor of about 2. This amount of relatively small ratio resulted in a slight improvement of the relative permeability data to the non-wetting phase as it can be clearly observed in Figure 6.13.

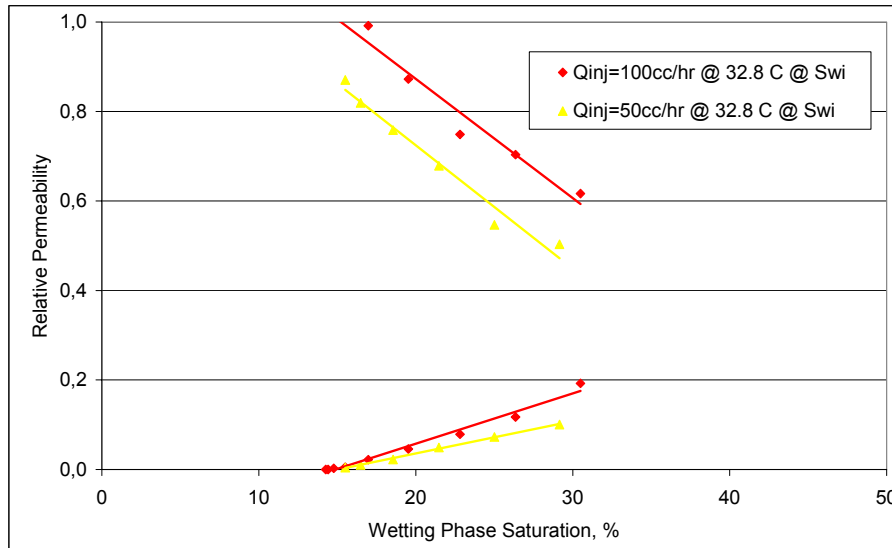


Figure 6.14: Flow Rate Effect on Relative Permeability @ 32.8 °C
at Swi

Figure 6.14 shows the results of two experiments at a lower interfacial tension value as 0.01 mN/m, with the hexane injection rates of 50 cc/hr and 100 cc/hr at the same constant immobile water saturations of 24.45 %. Also, the same amount of brine was collected during the displacement tests that gave the same initial conditions.

The lower interfacial tension has a clear effect on relative permeability data as it is observed in the Figure 6.14 that shows an increase in the flow velocity by a factor of about 2. That led to an obvious enhancement of the relative permeability data to the non-wetting phase as it can be clearly observed in Figure 6.14. If the figure is carefully examined, it can be noted that the wetting-phase relative permeability is increased as well.

6.5.2 Effect of Interfacial Tension on Relative Permeability Curves at S_{wi}

Figure 6.15 shows the results of two experiments at a flow rate of 50 cc/hr with the large interfacial tensions ranges of 0.29 mN/m and 0.010 mN/m at the constant immobile water saturations of 24.45 %. In these two tests, the same amount of brine was produced as an output to yield the same initial conditions prior to the displacement test for the relative permeability analysis. The interfacial tension among the phases was maintained by adjusting the applied temperature in the medium.

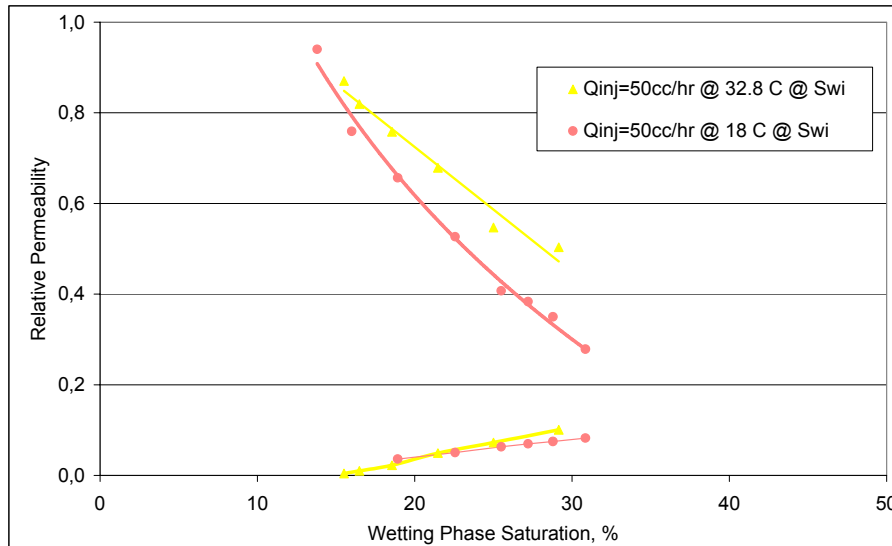


Figure 6.15 Relative Permeability at Different Interfacial Tension
at 50 cc/hr with S_{wi}

The effect of constant lower flow rate with the changes of interfacial tensions on relative permeability was shown in Figure 6.15 represents an increase in the interfacial tension by a factor of 29. This relatively high ratio gave a slight improvement of the relative permeability data to the non-wetting phase as it can be seen in Figure 6.15.

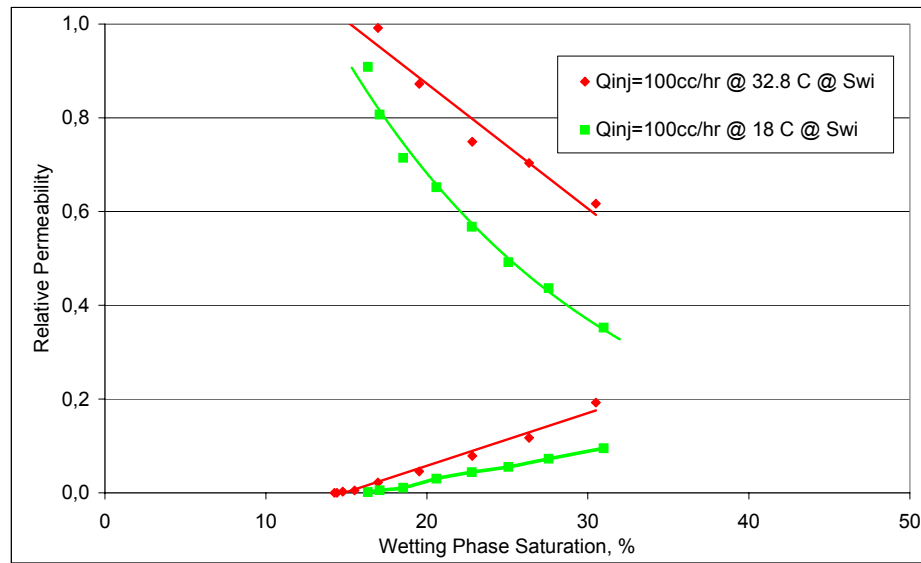


Figure 6.16 Relative Permeability at Different Interfacial Tension
at 100 cc/hr with S_{wi}

Figure 6.16 shows the results of two experiments at a doubling flow rate of previous figure as 100 cc/hr with the large interfacial tensions ranges of 0.29 mN/m and 0.010 mN/m at the same immobile water saturations of 24.45 %. The figure shows the same behavior with the Figure 6.15.

The experiments shown in Figures 6.15 and 6.16 performed at a low temperature (i.e. 18 °C) to give relative permeability curves to the fluids with a higher (i.e. 0.290 mN/m) interfacial tension, and performed at higher temperature (i.e. 32.8 °C) give relative permeability data with a lower (0.010 mN/m) interfacial tension.

The effect of varying the interfacial tension on relative permeability is summarized in Figure 6.17 where the effect of flow velocity on relative permeability curves is also presented.

Figure 6.17 shows clear dependence of relative permeability on interfacial tension. The relative permeability to non-wetting phase increases gradually when the interfacial tension decreases by a factor of 29. The wetting phase relative permeability seems to be affected increasingly only at the values of the interfacial tension that is closer to critical data as low as 0.01 mN/m.

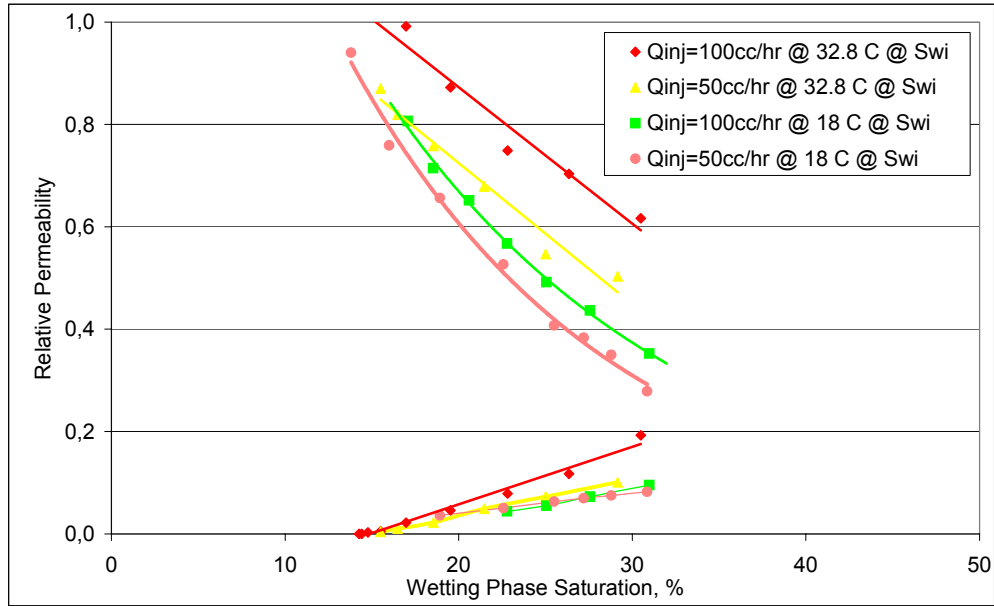


Figure 6.17: Flow Rate and Interfacial Tension Effect on Relative Permeability Curves at S_{wi}

It can be clearly seen that the effect of changing the flow velocity is much more noticed at lower values of the interfacial tension than at a higher values. In addition, it is noted that increasing the flow velocity increases the relative permeability to both phases as wetting phase and non-wetting phases. This is more clearly observed at lower interfacial tensions when fluids become closer to critical point. To verify the observation it has to be noted that even in Figure 6.8, it can be seen that the wetting phase relative permeability is not affected until the interfacial tension is decreased below 0.06 mN/m.

6.6 Influence of Immobile Water Saturation on Relative Permeability

The influence of immobile water saturation is presented in Figures from 6.18 through 6.20. All the experiments are compared to according to the same values of flow rates and interfacial tension values. In all four figures, flow rates and interfacial tensions are kept constant to be consistent. Figures 6.18 and 6.19 represent the data for high interfacial tension (i.e. 18 °C) at two different flow rates as 50 cc/hr and 100 cc/hr, respectively.

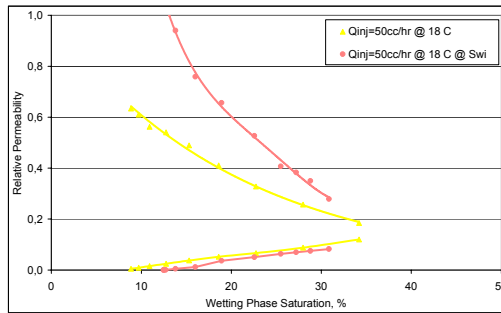


Figure 6.18: Influence of Immobile Water Saturation on Relative Permeability at 18 °C @ 50 cc/hr

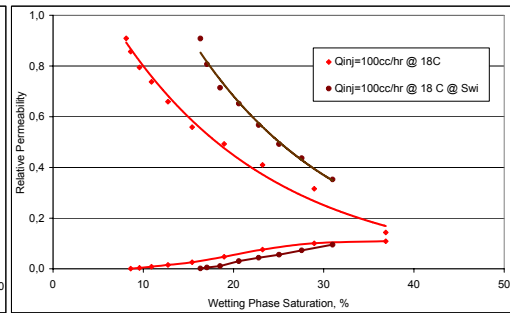


Figure 6.19: Influence of Immobile Water Saturation on Relative Permeability at 18 °C @ 100 cc/hr

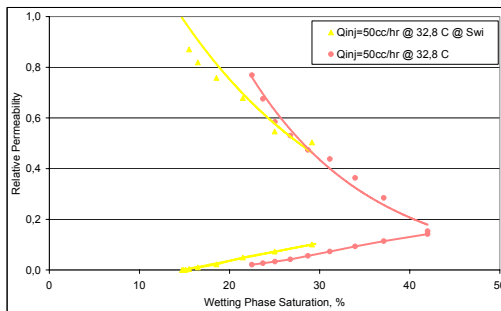


Figure 6.20: Influence of Immobile Water Saturation on Relative Permeability at 32.8 °C @ 50 cc/hr

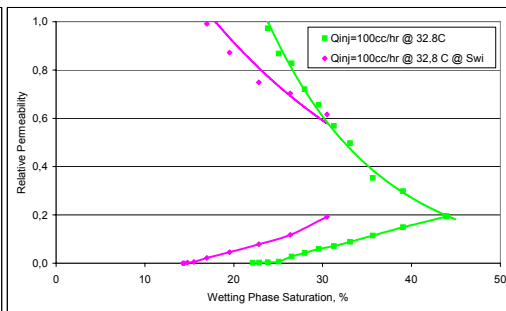


Figure 6.21: Influence of Immobile Water Saturation on Relative Permeability at 32.8 °C @ 100 cc/hr

6.6.1 Effect of Flow Rate on Relative Permeability at S_{wi}

The presence of immobile water saturation as 24.45 % makes the phase saturation lower than the compared the case of without water. The curve shifts to left when the brine presents in the system. Figure 6.22 shows the comparisons of four experiments at an interfacial tension of 0.29 mN/m, at the hexane injection rates of 50 cc/hr and 100 cc/hr with/out immobile water saturations of 24.45 %.

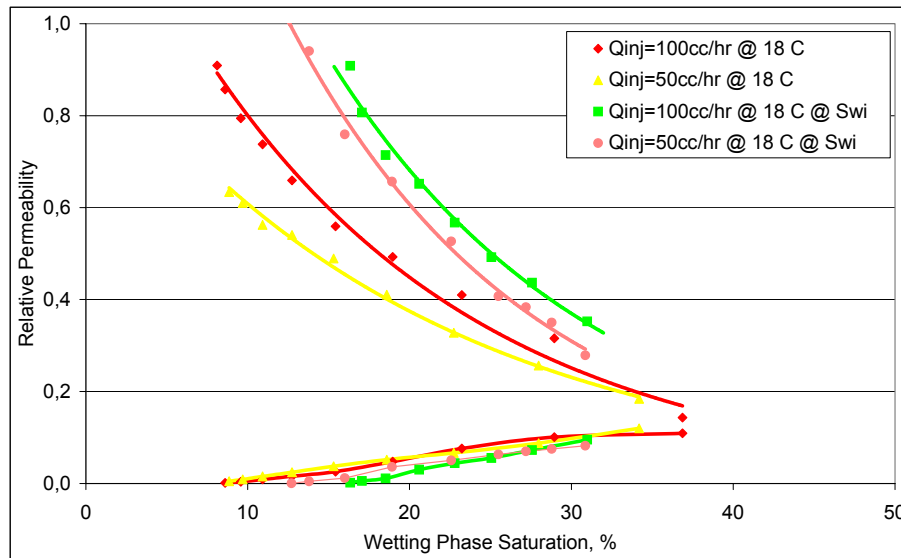


Figure 6.22: Influence of Immobile Water Saturation with Flow Rate Change on Relative Permeability at 18 °C

The effect of flow rate at higher interfacial tension (kept constant as 0.290 mN/m) on relative permeability in Figure 6.22 represents an increase in the flow velocity by a factor of about 2. A slight improvement of the relative permeability data to the non-wetting phase can be clearly observed in the figure. From the Figure 6.22, one may conclude that the wetting phase relative permeability is increased as well, but this is not that significant with respect to the experimental errors due to the pressure difference readings from the gauge

and the amount of the volume readings for produced methane and hexane during the injection stages.

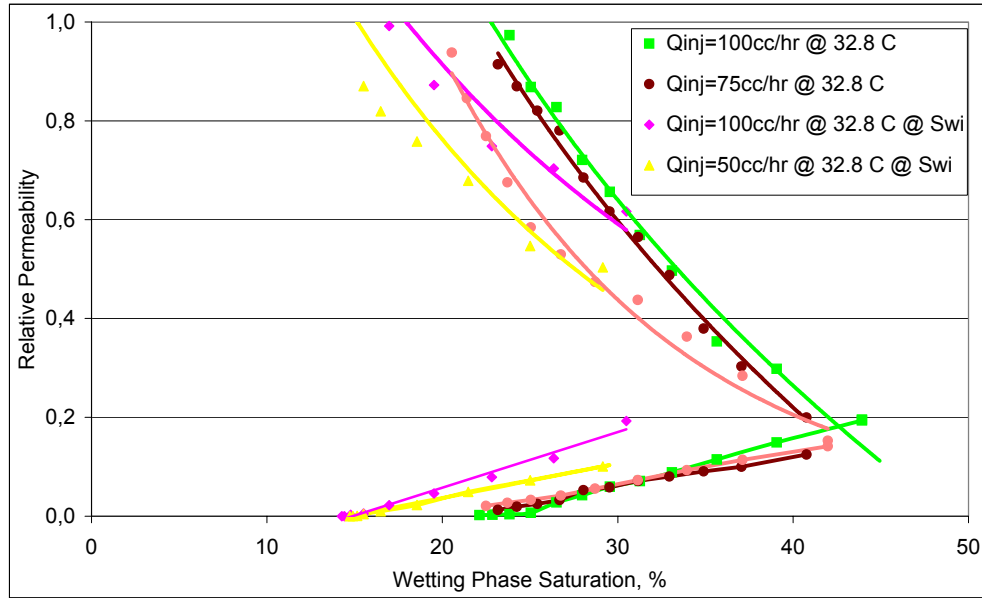


Figure 6.23: Influence of Immobile Water Saturation with Flow Rate Change on Relative Permeability at 32.8 °C

Figure 6.23 shows the comparisons of four experiments at the low interfacial tension of 0.010 mN/m, at the injection rates of 50 cc/hr and 100 cc/hr with and without immobile water saturation of 24.45 %.

The effect of flow rate on relative permeability at lower interfacial tension (kept constant as 0.010 mN/m) on relative permeability in Figure 6.23 represents an enhancement of the relative permeability data to the non-wetting phase. It can be noted that the wetting phase relative permeability increases with the increasing flow velocity at very low interfacial tensions. Also, in addition to Figure 6.23, this generalization can be verified according to the Figures 6.20 and 6.21.

6.6.2 Effect of Interfacial Tension on Relative Permeability at S_{wi}

The effect of varying the interfacial tension is summarized in Figure 6.24 that shows the results of four experiments at a flow rate of 50 cc/hr with the large interfacial tensions ranges of 0.29 mN/m and 0.010 mN/m with/out the constant immobile water saturations of 24.45 %. The interfacial tension among the phases was maintained by adjusting the applied temperature in the medium.

The influence of immobile water saturation is presented in Figures 6.24 and 6.25. All the experiments are compared to according to the conditions where flow rate kept constant and then different temperatures are applied.

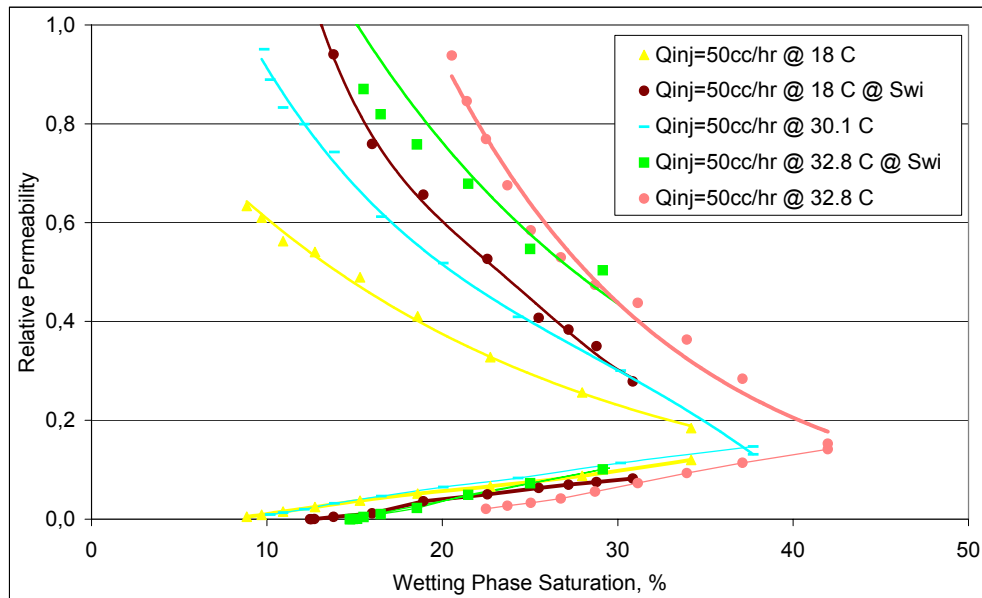


Figure 6.24: Influence of Immobile Water Saturation with Interfacial Tension Change on Relative Permeability at 50 cc/hr

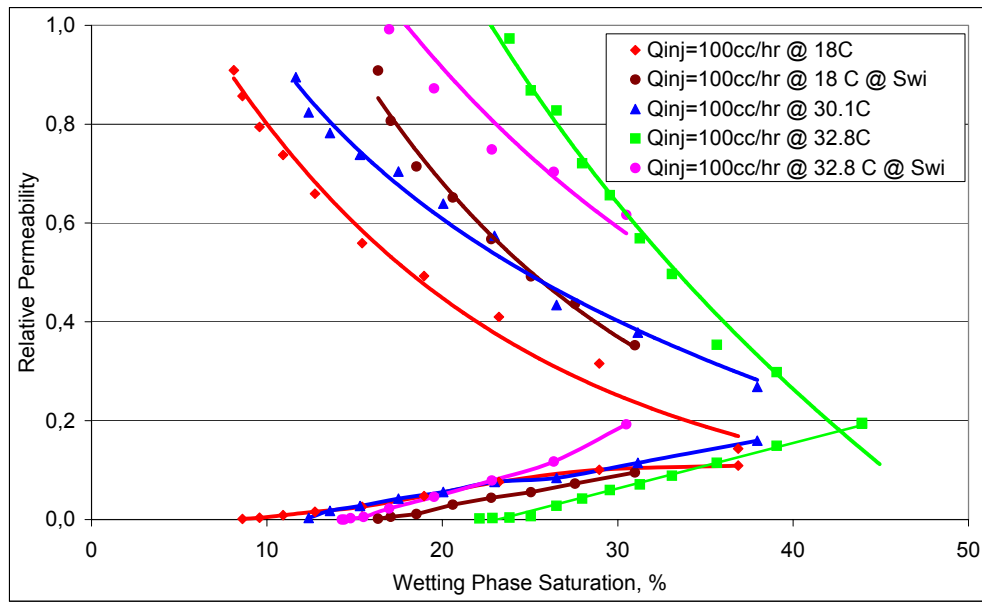


Figure 6.25: Influence of Immobile Water Saturation with Interfacial Tension Change on Relative Permeability at 100 cc/hr

The methanol was set to be insoluble in water by adding K_2CO_3 as a powder to the solution. This process [89] is explained in Appendix D in detailed for the solubility analysis of phase behavior for methanol and water fluid mixture systems.

6.7 Test Assumptions and Sources of Errors

Here in this section, we will examine the validity of the assumptions that it was used to obtain relative permeability from the measured pressure drop and produced volume data.

In the laboratory measurement methods, eight assumptions have been made. Firstly, it is assumed that the generalized Darcy equation (Eq. 5.2) is valid. This requires two concepts; one of them is (1) the validity of relative permeability concept, and the other is (2) the assumption of a negligible effect of inertial forces. Some authors have questioned the concept of relative permeability. It has been widely reviewed in literature [44] for validity. From the review it is concluded that the concept of relative permeability as used in Equation 5.2 is valid throughout this study.

Secondly, the saturation profile in the medium was approximated by the Buckley-Leverett equation. This approximation is only valid if the following items were neglected: (3) the effect of in-homogeneities in the core sample, (4) gross mass transfer between phases, (5) the compressibility of the fluids, (6) instabilities in the displacement front, and (7) the influence of capillary forces on macroscopic scale.

Assumptions (3) and (5) do not cause any problems; the procedures described in the Sections 5.2 and 6.5 in which core sample homogeneity was explained by the aid of CT Scanner. In addition, liquids are scarcely compressible.

Assumption (6) concerns the stability of the displacement front. If the viscosity of the displaced phase is lower than that of the injected phase ($\mu_{dis} < \mu_{inj}$), small perturbations of the front cannot grow. Such displacement would be stable for any injection velocity. In all conducted experiments, however, the viscosity of the methanol-rich phase is greater than that of the hexane-rich phase ($\mu_{dis} > \mu_{inj}$). This does not mean that the front is unstable. The criterion for stability of the front is refined because the experiments, the lighter hexane phase displaces the heavier phase. In this case, gravity comes into effect to keep the displacement front horizontal. Dietz (1953) [93] derived that a horizontal front remains stable as long as the injection velocity is lower than a critical velocity, defined by:

$$u_c = \frac{(\rho_{low} - \rho_{upp})gk}{\frac{\mu_{dis}}{k_{rdis}(S_s)} - \frac{\mu_{inj}}{k_{rinj}(S_s)}} \quad (6.1)$$

Where low refers to the lower phase (methanol-rich), upp refers to the upper phase (hexane-rich), dis refers to the displaced phase (methanol-rich), and inj refers to the injected phase (hexane-rich). The mobility is evaluated at the displacement front, where the saturation is equal to the shock saturation, denoted by S_s . The Dietz criterion is strict to be achieved. Hagoort (1974) [94] pointed out that a Buckley Leverett displacement front is stable as long as the mobility of the displaced fluid is greater than the overall mobility of the two phases just behind the shock:

$$\frac{1}{\mu_{dis}} > \frac{k_{rdis}(S_s)}{\mu_{dis}} + \frac{k_{rinj}(S_s)}{\mu_{inj}} \quad (6.2)$$

In all tests we conducted the mobility in the front was in the ranges of above equation. Assumption (7) concerns the deviation from the Buckley-Leverett profile due to capillary forces. The deviation is most happened to be near the end of the porous medium, where the wetting phase saturation approaches unity because the capillary forces [77, 84, 86] retain the wetting phase. Since a high wetting phase saturation implies a high resistance to non-wetting phase flow, the pressure gradient near the outlet is greater than predicted from a Buckley-Leverett profile. The deviation becomes more important towards the end of experiments when the wetting phase saturation reaches to its lowest value.

To estimate the influence of the capillary end effect, we calculate the pressure gradient in the case that the wetting phase is immobile while steady state conditions have been established. So, the effect of gravity in the calculation of the capillary end effect can be ignored.

Both the experimental procedure and processing of the raw data may give some errors in the relative permeability results. An error in the origin of time will affect the mass balance. Although this causes a systematic error in the results of a single experiment, the errors will be different for each experiment. In the section of reproducibility of measurements, it is shown that test data is acceptable, so these types of errors are not important.

Another source of error may be a gradual contamination of the fluids during the experiment, which affects the interfacial tension, viscosity and density of the liquids. In generally, impurities can cause an increase in critical temperature. [85,87,88]

The other problem was that the flow velocity was subjected to sudden peaks and dips, probably due to cavitations within the filters that were connected to pump head. Since a constant injection rate in the calculations of relative permeability and saturation were assumed, this may affect the results. But, the peaks and dips were averaged out, so that the result did not induce a systematic error.

CHAPTER 7

MATHEMATICAL MODELLING

7.1 Introduction

The gas relative permeability is a function of the interfacial tension (IFT) between the gas and condensate among other variables. For this reason, several laboratory studies [4,6,7,8,46,48,80] have been reported on the measurement of relative permeability data of gas-condensate fluids as a function of interfacial tension. These studies show a significant increase in the relative permeability of the gas as the interfacial tension between the gas and condensate decreases. The relative permeability data of the gas and condensate have often been modeled directly as an empirical function of the interfacial tension. [50] However, it has been known since at least 1947 [51] that the relative permeabilities in general actually depend on the ratio of forces on the trapped phase, which can be expressed as either a capillary number or Bond number. This has been recognized in recent years to be true for gas-condensate relative permeabilities [13,18]. The key to a gas-condensate relative permeability model is the dependence of the critical condensate saturation on the capillary number or its generalization called the trapping number. [63,64,65,69,77]

A simple three-parameter capillary trapping model is presented that shows good agreement with experimental data. This model is a generalization of the approach first presented by Delshad *et al.* [52] and then extended by Pope *et al.* [21]. We then present a general scheme for computing the gas and condensate

relative permeabilities as a function of the trapping number, with only data at low trapping numbers (high IFT) as input, and have found good agreement with the experimental data in the literature. This model, with typical parameters for gas condensates, can be used in a compositional simulation study of a single well to better understand the productivity of the field.

7.2 Mathematical Model Description

The fundamental problem with condensate buildup in the reservoir is that capillary forces can keep the condensate in the pores if the forces displacing the condensate do not exceed the capillary forces. The pressure forces in the displacing gas phase and the buoyancy force on the condensate exceed the capillary force on the condensate, the condensate saturation will be reduced and the gas relative permeability increased. Brownell and Katz (1947) [51] and others recognized early on that the residual oil saturation should be a function of the ratio of viscous to interfacial forces and defined a capillary number to capture this ratio. Then, many variations of the definition have been published, [52-55] with some of the most common ones written in terms of the velocity of the displacing fluid, which can be done by using Darcy's law to replace the pressure gradient with velocity. However, it is the force on the trapped fluid that is most fundamental and so we prefer the following definition:

$$N_c = \frac{\vec{u}\mu_d}{\sigma_{dd'}} \quad (7.1)$$

Where definitions and dimensions of each term are provided in the nomenclature. Although the distinction is not usually made, one should designate the displacing phase d' and the displaced phase d in any such definition. In some cases, buoyancy forces can contribute significantly to the

total force on the trapped phase. To quantify this effect, the Bond number was introduced and it also takes different forms in the literature [57].

$$N_{Bd} = \frac{\vec{k}g(\rho_{d'} - \rho_d)}{\sigma_{dd'}} \quad (7.2)$$

For special cases such as vertical flow, the force vectors are collinear and one can just add the scalar values of the viscous and buoyancy forces and correlate the residual oil saturation with this sum, or in some cases one force is negligible compared to the other force and just the capillary number or Bond number can be used by itself. This is the case with most laboratory studies including the recent ones by Boom et al. [18,41] and by Henderson et al. [13]. However, in general the forces on the trapped phase are not collinear in reservoir flow and the vector sum must be used. A generalization of the capillary and Bond numbers was derived by Jin [56] and called the trapping number. The trapping number for phase displaced by phase is defined as follows:

$$N_T = \frac{\vec{k}(\vec{\nabla}\Phi_{d'} + g(\rho_{d'} - \rho_d) + \vec{\nabla}D)}{\sigma_{dd'}} \quad (7.3)$$

The trapping number, N_T , (Pope et al 1998) [21] uses generalized form of the capillary, N_C and bond numbers, N_B . But, This definition does not explicitly account for the very important effects of spreading and wetting on the trapping of a residual phase. However, it has been shown to correlate very well with the residual saturations of the non-wetting, wetting, and intermediate wetting phases in a wide variety of rock types.

Similarly a dimensionless condensate number, N_K , given by the sum of capillary, N_C and bond numbers, N_B can be obtained. Note that condensate number is more sensitive to temperature changes compared to trapping number, because N_K is affected by both viscosity and density changes. Moreover, it minimizes the measurement errors resulting from the use of inaccurate pressure transducers or gauges.

$$N_{Kd} = \frac{\vec{u}\mu_d + \vec{k}g(\rho_{d'} - \rho_d)}{\sigma_{dd'}} \quad (7.4)$$

The residual saturation is newly modeled by 3 parameters that is similar to Pope et al (1998) [21] based on the trapping number as shown below:

$$S_{dr} = \min\left(S_d, S_{dr}^{high} + \frac{S_{dr}^{low} - S_{dr}^{high}}{c + a(N_K)^b}\right) \quad (7.5)$$

In the Equation 7.5, the parameters a, b and c are constants that change with formations to represent the flow of phases. Here superscripts high and low refer to residual saturations of the gas and condensate. High value of S_{dr} is high typically zeroed. The end point relative permeability data of each phase, which increases as the trapping number increases.

The next step is to correlate the endpoint relative permeability of each phase, which increases in a very predictable way as the trapping number increases and can be correlated using the following equation:

$$k_{rd}^0 = k_{rd}^{0low} + \frac{S_{d'r}^{low} - S_{d'r}^{high}}{S_{d'r}^{low} - S_{d'r}^{high}} (k_{rd}^{0high} - k_{rd}^{0low}) \quad (7.6)$$

The final step is to calculate the relative permeability of each phase d as a function of saturation. One approach to this problem is to assume a simple function such as a Corey-type relative function [52]. This requires correlating the Corey exponent with trapping number. However, not all the relative permeability data can be fit with a Corey-type model, so we have generalized our approach by using the following equation:

$$\log(k_{rd}) = \log k_{rd}^0 + \log(\bar{S}_d) + \frac{\log\left(\frac{k_{rd}}{k_{rd}^0}\right)^{low} - \log(\bar{S}_d)}{c + a(N_K)^b} \quad (7.7)$$

Where; k_{rd}^0 End point relative permeability for a given trapping number and saturation, k_{rd}^{low} and k_{rd}^{0low} k_r and end point k_r at low trapping number. Saturations are normalized as:

$$\bar{S}_d = \frac{S_d - S_{dr}}{1 - \sum_{d=1}^n S_{dr}} \quad (7.8)$$

Where n is the number of the phases present in the system, S_d is saturation and S_{dr} is residual saturation for phase d . These saturations are calculated by using the equation (7.4).

7.3 Comparison of Mathematical Model with Laboratory Tests

The proposed mathematical model is tested with the laboratory test results for two different flow rates and for three different temperatures to give a wide

range of interfacial tension values. The condensate parameters; a, b and c for condensate phases and gas phases are shown in Tables 7.1 and 7.2. The mathematical model was compared with experimental results by the parameter R2 that is the Mean Square Error to check the deviation.

Mean square error is a model to show the fitness degree of any output data to compare between experimental and model calculation values.

Using the equation 7.9 to indicate the deviation for experiment and model showed the results of fitness degree in Table 7.1 and 7.2.

$$R2 = \sum_{i=1}^N (kr_{\text{exp}_i} - kr_{\text{model}_i})^2 \quad (7.9)$$

Table 7.1: Condensate Parameters for Tests at 50 cc/hr

Test	Qinj. = 50 cc/hr @ 18 C	Qinj. = 50 cc/hr @ 30.1 C	Qinj. = 50 cc/hr @ 32.8 C
Condensate			
a	709736031.1	715596228.3	696626633.6
b	1.339251439	1.115299088	1.522623893
c	1.25405351	1.45372054	1.453589991
R2	0.009426105	0.00084069	0.000188313
Gas			
a	5.19E+00	5.19E+00	5.23E+00
b	1.58E-05	1.58E-05	1.58E-05
c	6.47E+00	1.88E+01	6.96E+02
R2	7.92E-02	1.39E-01	9.25E-02

Table 7.2: Condensate Parameters for Tests at 100 cc/hr

Test	Qinj. = 100 cc/hr @ 18 C	Qinj. = 100 cc/hr @ 30.1C	Qinj. = 100 cc/hr @ 32.8 C
Condensate			
a	899463029.8	900045915.8	899252231.2
b	1.669644575	1.647325507	1.674676
c	1.297121752	1.297515094	1.294253058
R2	0.000732321	0.000197792	0.002317348
Gas			
a	5.00E+00	1.19E+02	4.47E+02
b	1.58E-05	1.47E-03	1.40E-03
c	2.60E+01	2.20E+01	3.36E+01
R2	8.21E-02	1.30E-01	1.05E-01

Figures 7.1 and 7.2 show the computed relative permeability of gas and condensate calculated for a wide range of trapping numbers using just three parameters.

The new model results for gas k_r versus gas saturation are given in Figure 7.1 below for different condensate numbers. As the condensate number is high (between $10E-2$ and $10E-3$), gas relative permeability gas saturation has a linear relationship. For low condensate number, N_K gas relative permeability, k_{rg} versus gas, S_g is not linear.

The mean square error, the modeling the fitness degree of any output data to compare between experimental and model, has fairly good results for condensate compared to the gas relative permeability fitness analysis as shown in Table 7.1 and 7.2.

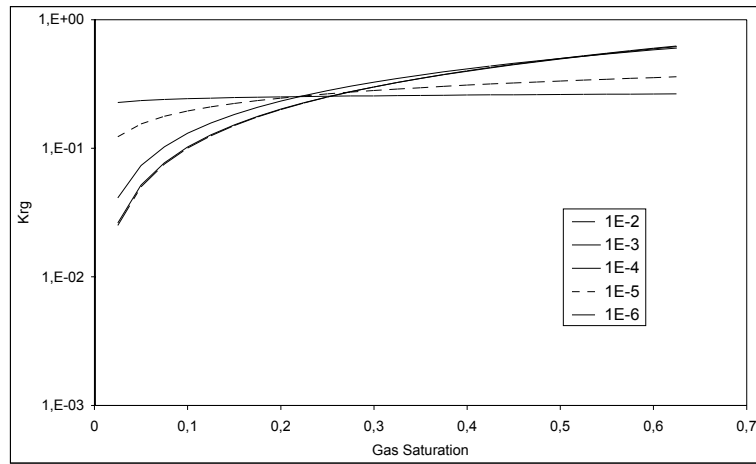


Figure 7.1: Gas Relative Permeability versus Gas Saturation.

The new model results for condensate k_r versus condensate saturation are presented below in Figure 7.2 for different condensate numbers. For high condensate numbers N_K , ($10E-2$ - $10E-3$) condensate relative permeability versus condensate saturation has a linear relationship.

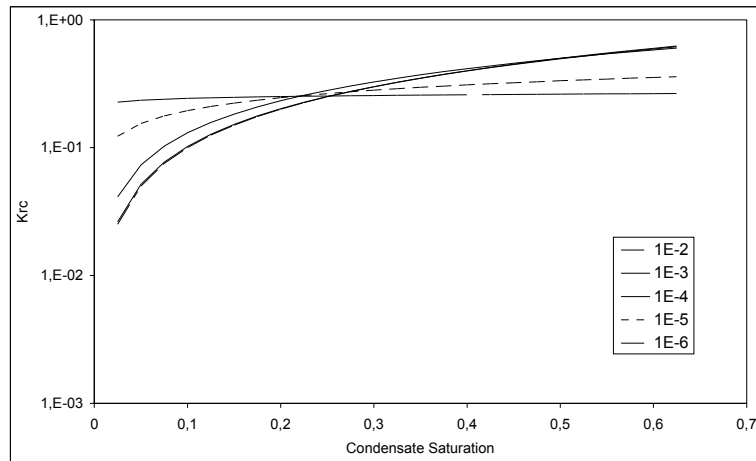


Figure 7.2: Condensate Relative Permeability versus Condensate Saturation

We show the comparisons with end point relative permeability data and experimental non-wetting phase data for various porous media. Hartman & Cullick (1994) [45] used slim tube sand pack with binary testing fluids as methane and butane; C_1/nC_4 and Henderson (1996) [13] used Berea sandstone as a porous medium, also same testing fluid as a methane and butane C_1/nC_4 in the same plot.

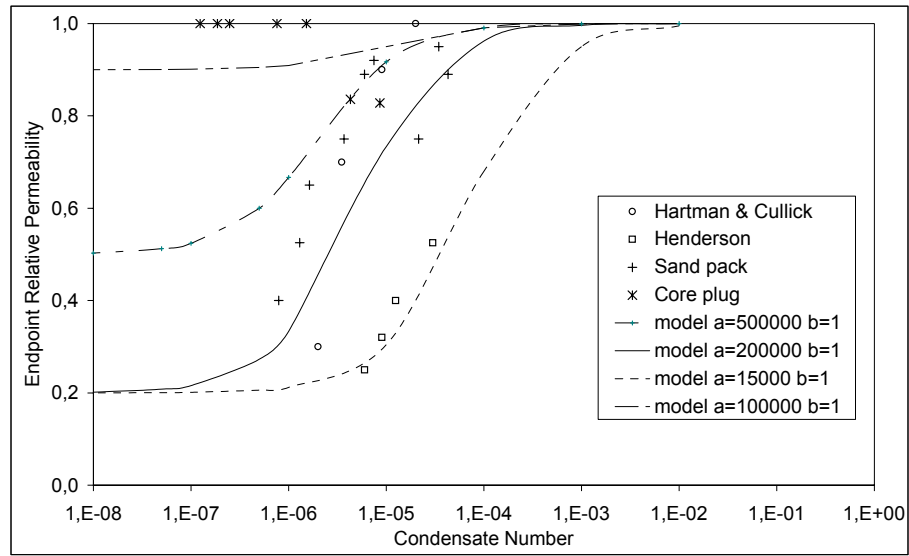


Figure 7.3: End Point Relative Permeability versus Condensate Number

Figure 7.3 shows endpoint relative permeability for various liquid phases and porous media as a function of the condensate number. The proposed model matches well with the literature test results shown in Figure 7.3 for the methane/n-butane binary mixture from both Hartman and Cullick [45], and Henderson et al [13]. The values vary significantly due to the differing rocks and for the same rock such as Berea sandstone due to differing wettability. The constant “a” changes between 500000 and 15000 and it is quite different due to use of various types of porous media of differing wettability and the

constant “b” is 1. However, the general trend of increasing endpoint relative permeability with increasing condensate number is consistent.

The effect of various condensate parameters on the wetting phase as a condensate end point relative permeability and condensate number is shown in Figure 7.4.

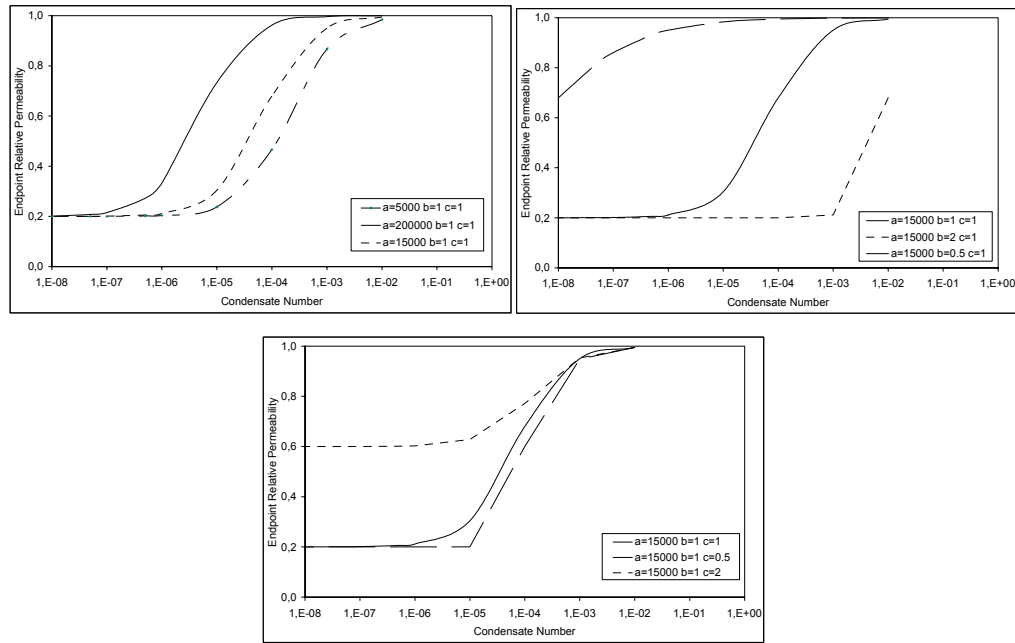


Figure 7.4: Effect of various Condensate Parameters on the End Point Relative Permeability and Condensate Number

The curves in Figure 7.4 for various condensate parameters calculated from the Equation 7.6 of the model are shown for comparison with these data. In all of these cases, the wetting phase endpoint relative permeability appears to approach 1,0 at a sufficiently high condensate number. This high condensate number value is sometimes referred to as the miscible value.

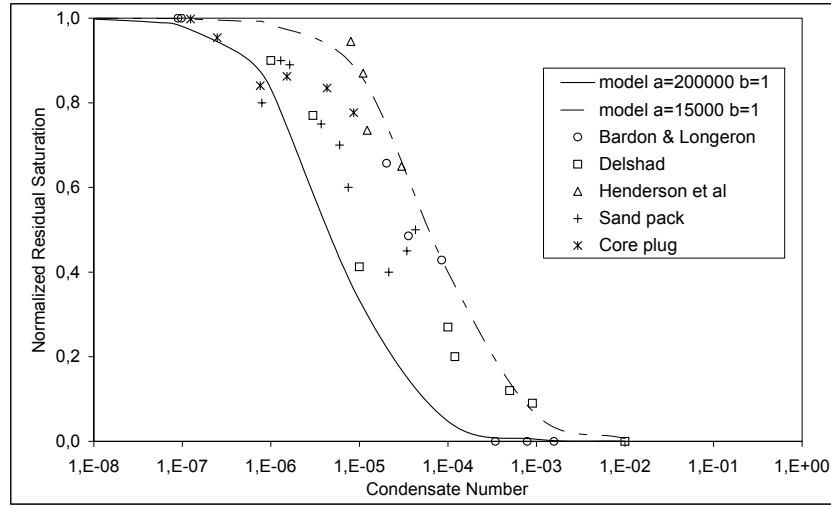


Figure 7.5: Normalized Residual Saturations versus Condensate Number

Normalized residual saturations versus condensate number data were compared with literature data in Figure 7.5. In our case, we have conducted tests on sand pack and core plug samples.

Bardon and Langeron (1980) [4] used sandstone as porous medium and C_7 -rich liquid for measurement of relative permeability curves by unsteady state injection method at $S_{wr} = 0.35$. Delshad (1990) [57]; however, run the tests at $S_{wr} = 0.40$. Henderson (1996) [13] used methane and n-butane in steady state displacement tests at the non-wetting phase residual saturation, $S_{nwr} = 0.29$. In order to compare all data saturations are normalized between 0 and 1 according to residual saturations. The constant as a porous medium property, “a” changes between 200000 and 15000 due to high wettability differences and the constant “b” is again 1. As can be seen the proposed model matches well with the literature test results.

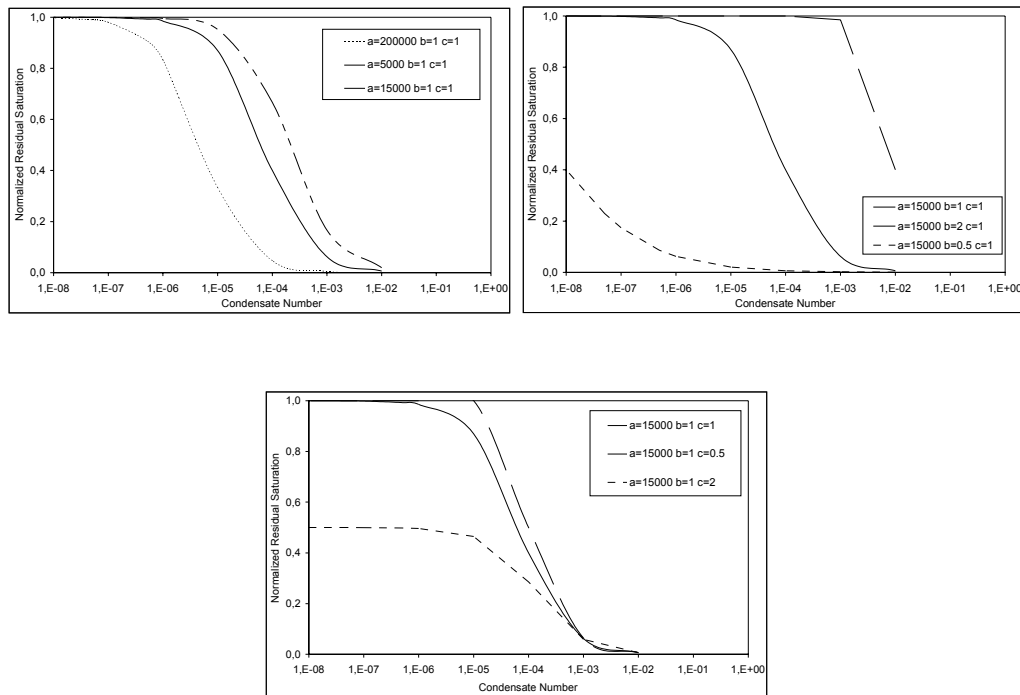


Figure 7.6: Effect of various Condensate Parameters on the Normalized Residual Saturations and Condensate Number

The mathematical model is compared with the laboratory test results for two different flow rates and for two different temperatures when the core sample was introduced with brine at immobile saturation.

The condensate three parameters; a , b and c for condensate phases and gas phases are shown in Tables 7.3 for the flow rate of 50 cc/hr and 7.4 for the flow rate of 100 cc/hr. In each table data, the interfacial tension data was changed as much as by a factor of 29. The parameter $R2$ as a mean square error to check the deviation was determined as small value, which especially good for the condensate model.

Table 7.3: Condensate Parameters at 50 cc/hr at Swi

Test	Qinj. = 50 cc/hr @ 18 C	Qinj. = 50 cc/hr @ 32.8 C
Condensate		
a	900283859.1	900841522.9
b	1.635189122	1.628045199
c	1.295937188	1.574546681
R2	7.39493E-05	0.000190342
Gas		
a	4.34E-01	1.20E+01
b	1.42E-03	2.64E-01
c	1.12E+00	6.22E-01
R2	9.76E-02	2.32E-01

Table 7.4: Condensate Parameters at 100 cc/hr at Swi

Test	Qinj. = 100 cc/hr @ 18 C	Qinj. = 100 cc/hr @ 32.8 C
Condensate		
a	900980823.5	896647248.7
b	1.613328099	1.760694671
c	1.301955288	1.290437205
R2	0.001423101	0.007702967
Gas		
a	4.13E-01	3.69E-01
b	1.42E-03	1.42E-03
c	9.98E-01	6.83E-01
R2	7.25E-02	3.56E-01

The mean square error as the fitness value for the model compared to laboratory data is very good results for condensate phase. The mean square error is in the order of about 10^{-5} for condensate, on the other hand, it is calculated as 10^{-1} or 10^{-2} for gas phase as seen in Table 7.3 and 7.4.

7.4 Discussion of the Mathematical Model and Laboratory Test Results

As pointed out above, the best starting point for understanding and modeling relative permeability data as a function of interfacial tension is the relationship between the residual saturations and trapping number (or its special cases of capillary number or Bond number when appropriate to the experimental conditions). For this reason, we first show an example of normalized residual saturations vs. condensate number in Figures 7.5. Dividing them by the low condensate number plateau values normalized the residual saturations. As seen from these data, there is a very large difference between the nonwetting and wetting phase data. A much larger condensate number is required to decrease the residual saturation for the wetting phase than for the nonwetting phase. This is typical of all of the data in the literature for all types of phases and rocks (e.g., see the review in Ref. [57]). We selected these data from the many examples in the literature to make the point that even widely different phases have similar behavior in a given rock if their wettability is the same.

The normalized wetting phase residual saturations in Figures 7.5 are presented for condensate phase. The gas data of Henderson *et al.* [13] are for the equilibrium gas in a binary mixture of methane and *n*-butane intended to represent a gas-condensate fluid. The oil data of Delshad [57] are for the equilibrium oil for a mixture of decane, brine, isobutanol, and sodium sulfonate under three-phase conditions. The wetting phase in Figures 7.5 is the aqueous and micro emulsion phases. The aqueous data of Boom *et al.* [18,41] are for the equilibrium aqueous phase in a ternary mixture of water, *n*-heptane, and isopropyl alcohol. The micro emulsion data of Delshad [57] are for the equilibrium micro emulsion. The condensate data of Henderson *et al.* [13] appear to be of intermediate wettability (between the gas and water), which emphasizes the importance of including all three phases in the experiments.

More examples of end point wetting phase relative permeability for the porous media are shown in Figures 7.4 compared with the effect of various condensate parameters. The normalized residual saturations versus condensate number for the wetting phase are shown in Figure 7.5 for various porous medium. These data emphasize the strong dependence on the rock as well as on the wettability of the phases. The overwhelming conclusion is that one must measure the residual saturations for the wetting state and rock of interest to get useful results that can be accurately applied to a particular reservoir state. In particular, if there are three phases in the reservoir such as there are with gas condensates then, to ensure the correct wetting and spreading state in the rock, three phases need to be in the laboratory core even if one of the phases such as the brine is always at residual saturation. There are too many other similar examples in the literature to review here, but many other data sets can be found in the work of Stegemeier [31], Chatzis and Morrow[58], Delshad, [57] and Filco and Sharma [59] among others. Stegemeier [31] provides an excellent theoretical treatment as well.

Next we show the comparisons with endpoint relative permeabilities using these same values of N_C . The endpoint relative permeability of the gas phase as a function of trapping number for the methane/*n*-butane binary mixture reported by both Hartman and Cullick [45] and Henderson *et al.*[13] and the endpoint relative permeability for various liquid phases and porous media as a function of the trapping number was shown [4,18,41,45]. The values vary significantly due to the differing rocks and for the same rock such as Berea sandstone due to the differing wettability. However, the general trend of increasing endpoint relative permeability with increasing trapping number is consistent and clear and agrees with that previously reported by Delshad *et al.* [52] for widely different fluids.

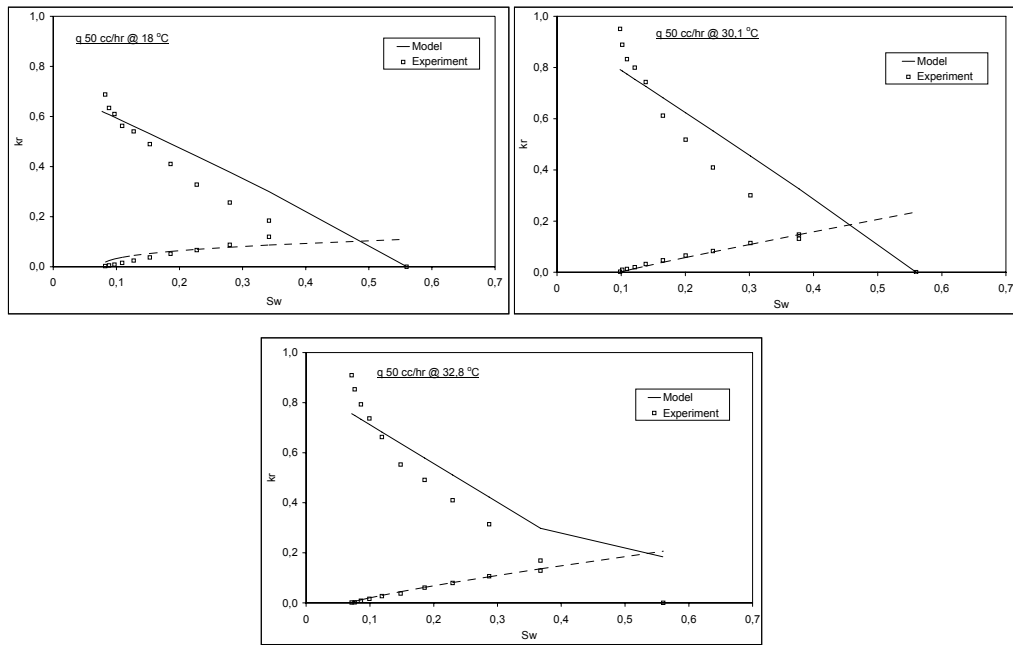


Figure 7.7: Relative Permeability Data from Mathematical Model for various IFT at 50 cc/hr

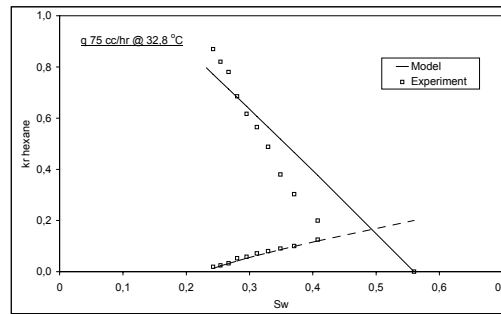


Figure 7.8: Relative Permeability Data from Mathematical Model for 75 cc/hr

Figures 7.7, 7.8 and 7.9 show the plot of relative permeability versus wetting phase saturation. In Figure 7.7, it is the case of different interfacial tension value at constant slower flow rate of 50 cc/hr. The next Figure 7.8 gives the

result of one run at the lowest interfacial tension data as 0.010mN/m at an intermediate flow rate value of 75 cc/hr.

Figure 7.9 gives the results of the proposed new mathematical model for the higher constant flow rate of 100 cc/hr with differing the interfacial tension from 0.290 to 0.010 mN/m as a big range factor of 29.

As one carefully examines the Figures 7.7, 7.8 and 7.9, it will be easily observed that the proposed model has a good match with the experiment data for the case of condensate relative permeability curves. This was also noted from the square mean error analysis.

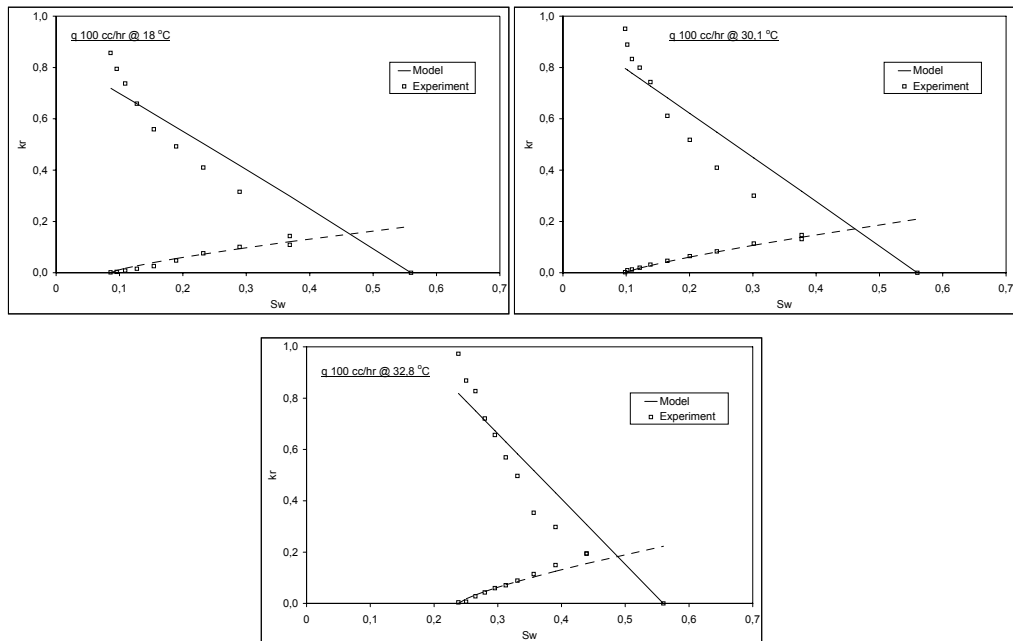


Figure 7.9: Relative Permeability Data from Mathematical Model
for various IFT at 100 cc/hr

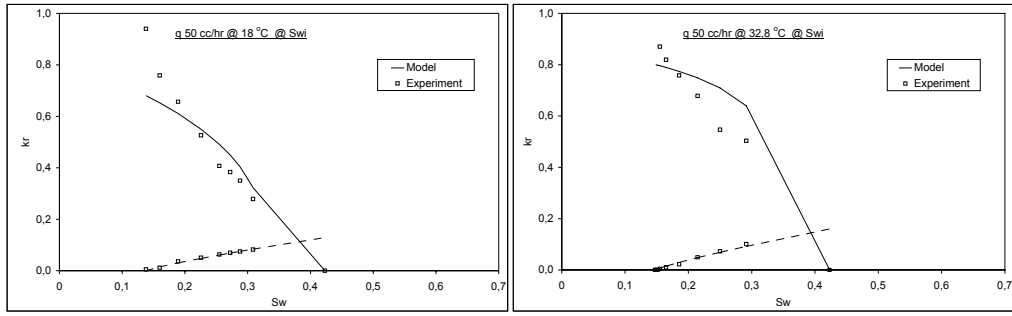


Figure 7.10: Relative Permeability Data from Mathematical Model for various IFT at 50 cc/hr at S_{wi}

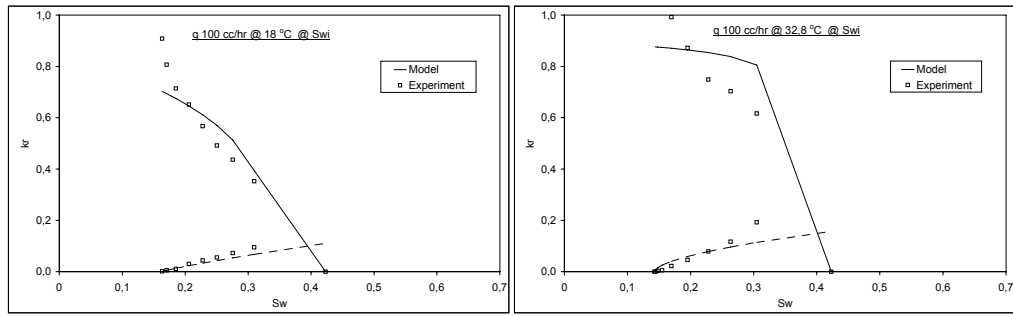


Figure 7.11: Relative Permeability Data from Mathematical Model for various IFT at 100 cc/hr at S_{wi}

Figures 7.10 and 7.11 show the plot of relative permeability versus wetting phase saturation for the case of immobile water saturation. In Figure 7.10, it is the case of two different interfacial tension values (i.e. due to the temperature sensitivity at 18 °C and 32.8 °C) at constant slower flow rate of 50 cc/hr. The curve of Figure 7.11 gives the results of the proposed new mathematical model for the higher constant flow rate of 100 cc/hr with two different the interfacial tensions ranging from 0.290 mN/m to 0.010 mN/m (i.e. at 18 °C and 32.8 °C) as a big range factor of 29.

When the Figures 7.10 and 7.11 are examined in detail, it will also be observed that the proposed model has a good match with the experiment data for the case of condensate relative permeability curves. This was also noted from the square mean error analysis shown in Tables 7.3 and 7.4.

Relative permeability to near-miscible fluids can be measured with acceptable accuracy using laboratory displacement test set-up. The laboratory test results showed that relative permeability to non-wetting phase is less enhanced by an increase in flow velocity than by a decrease in interfacial tension. In addition, the capillary number changes during the measurements. We see that at a given saturation, relative permeability is increased when the condensate number is higher. It was further found that the wetting phase relative permeability is affected at low interfacial tensions. By comparing the results of experiments conducted at more or less the same flow velocity and varying interfacial tension, we observed that the relative permeability to the wetting phase was only affected when the interfacial tension was below 0.06 mN/m. This would seem to point to a threshold interfacial tension, as was reported by Bardon and Langeron (1980) [4], Ameafule and Handy (1982) [5], Harbert (1983) [6], and Handerson (1996) [13].

We developed a mathematical model as a function of condensate number, which is the combination of capillary number and bond number to represent the gas condensate flow in a porous medium. It is a type of modeling of relative permeability data as a function of combined effects of pressure gradient, buoyancy, gravity forces and capillary forces. This requires a generalization of the classical capillary number and Bond number into a different version of trapping number that is a new model we developed as condensate number. As shown in this study, this condensate number can be used in a generalized relative permeability model to correlate gas condensate data.

CHAPTER 8

CONCLUSIONS

This thesis contains five main important field of studies. First of all, a series of laboratory displacements experiments were conducted to get the relative permeability data for representing the gas condensate reservoir behavior. These displacement experiments on the binary liquid system methanol/n-hexane showed that the relative permeability to the near-miscible phases in this system depends strongly on the interfacial tension between the phases and on the flow velocity (see Section 6.4). It was found that the relative permeability functions are curved if the interfacial tension is high and the flow velocity is low. On the other hand the relative permeability curves became as a linear at lower values of the interfacial tension and higher levels of the flow velocity.

Then, the presence of water into this binary liquid system to identify the influence of immobile water saturation in the gas condensate systems (see Section 6.5) was studied. Relative permeability curves were effected by interfacial tension and flow rate, similar to the zero water saturation case. The relative permeability curves with immobile water saturation were generated to be used in North Marmara Field in case of maintaining the same brine saturation.

A simple new three-parameter mathematical model based on condensate number; N_K for condensate system is developed and its theory for capillary trapping mechanism for condensate reservoir is presented in this study (see Chapter 7). The new proposed model is sensitive to temperature that implicitly

affects interfacial tension. The general equation for computing the gas and condensate relative permeabilities as a function of the Condensate number, N_K resulted in good agreement with the experimental data reported in the literature. This model, with typical parameters for gas condensates, can be used in a compositional simulation study to better understand the productivity of the field.

As a fourth stage of this study, the proposed new mathematical model was compared with literature data (see Chapter 7). The condensate number; N_K successfully generates the gas-condensate relative permeability data reported in literature. The developed model resulted in a good agreement with published gas-condensate relative permeability data as well as the end point relative permeability data and saturations.

Finally, the developed mathematical model was compared with the all laboratory experiments (see sections 7.3 and 7.4) by using the Mean Square Error parameter to show the goodness of fit. The model results of the condensate relative permeability curves have fairly good mean square errors compared to the gas relative permeability ones. So, the suggested mathematical model can be used to describe the condensate relative permeability behavior.

The following specific conclusions were obtained as a result of this study:

1. Methanol/n-Hexane mixture can be used as near critical binary fluid pair to represent Gas-Condensate behavior.
2. The laboratory test results show a strong dependence of relative permeability on interfacial tension and superficial velocity. There is a clear trend from curved relative permeability functions to straight lines with increasing superficial velocity and with decreasing interfacial tension.

3. These laboratory tests are supported with a new mathematical model of three-parameter condensate, N_K number which match as well with literature data.
4. The mathematical model results of the condensate relative permeability curves have fairly good mean square errors when compared to the gas relative permeability data.
5. The end point relative permeability data and residual saturations satisfactorily correlate with literature data. The most important parameter, which affects field performance, is the residual condensate saturation value.
6. Different temperatures are used to get different IFT for representing gas-condensate reservoir so that full relative permeability tables can be determined for realistic field performance prediction.
7. During the depletion stages from the reservoir, the gas condensate wells may reach to higher production flow rates (i.e. high N_K). Such cases represented in the laboratory tests that resulted in low residual wetting saturation.
8. When the phases have low interfacial tension that can be ensured by increasing the temperature, led to lower residual wetting saturation.
9. The capillary-number and condensate number dependence of relative permeability differ for the two phases. The relative permeability to the non-wetting phase is affected at lower values of the capillary number and condensate number.

CHAPTER 9

RECOMMENDATIONS

For the further work, a simulation part has to be added to this study. This study includes laboratory works for testing, mathematical model for analytical analysis and literature comparisons as a detailed comprehensive work for gas condensate analysis. Only, the simulation part for numerical analysis is missing for further research in this thesis.

REFERENCES

1. Darcy, H.P.G. (1856). Les Fontaines Publiques de la Ville de Dijon, Exposition et application des principes a suivre et des formules a employer dans les questions de distribution d'eau. Victor Dalmont, Paris.
2. Muskat, M. and Meres, M. W. (1936). The Flow of Heterogeneous Fluids through Porous Media. Physics, 7, 346-363.
3. Wyckoff, R. D. and Botset, H. G. (1936). The flow of Gas-Liquid Mixtures through Unconsolidated Sands. Physics, 7, 325-345.
4. Bardon, C. and Langeron, D.G.: "Influence of Very Low Interfacial Tensions on Relative Permeability," SPEJ (October 1980) 391; Trans., AIME, 269.
5. Ameafule, J.O. and Handy, L.L.: "The Effect of Interfacial Tensions on Relative Oil/Water Permeabilities of Consolidated Porous Media," SPEJ (June 1982) 371; Trans., AIME, 273.
6. Harbert, L.W.: "Low Interfacial Tension Relative Permeability," paper SPE 12171 presented at the 1983 SPE Annual Technical Conference and Exhibition, San Francisco, 5–8 October.
7. Asar, H. and Handy, L.L.: "Influence of Interfacial Tension on Gas/Oil Relative Permeability in a Gas-Condensate System," SPERE (February 1988) 57.

8. Haniff, M.S. and Ali, J.K.: “Relative Permeability and Low Tension Fluid Flow in Gas Condensate Systems,” paper SPE 20917 presented at the 1990 SPE Europec, The Hague, The Netherlands, 22–24 October.
9. Schechter, D.S. and Haynes, J.M.: “Relative Permeabilities of a Near-Critical Binary Fluid,” *Transp. Porous Media* (1992) 9, 241.
10. Jerauld, G.R.: “General Three-Phase Relative Permeability Model for Prudhoe Bay,” *SPERE* (November 1997) 255.
11. Morel, D.C., J-F., Morineu, Y.M., and Putz, A.G. (1992). “Mobility of Hydrocarbon Liquids in Gas Condensate Reservoirs: Interpretation of Depletion Laboratory Experiments,” paper SPE 24939 presented at the 1992 SPE Annual Technical Conference and Exhibition, Washington, DC, 4–7 October, 875-886.
12. Cahn, J.W.: “Critical Point Wetting,” *J. Chem. Phys.* (1977) 66, No. 8, 3667.
13. Henderson, G.D., Danesh, A., Tehrani, D.H., Al-Shaidi, S., and Peden, J. M. (1996). “Measurement and Correlation of Gas Condensate Relative Permeability by the Steady-State Method,” *SPEJ* (January 1996), 1(2), 191-201.
14. Delclaud, J., Rochon, J., and Nectoux, A: “Investigation of Gas/Oil Relative Permeabilities: High-Permeability Oil Reservoir Application,” paper SPE 16966 presented at the 1987 SPE Annual Technical Conference and Exhibition, Dallas, 27–30 September.

15. Kalaydjian, F.J.M., Bourbiaux, B.J., and Lombard, J.M.: “Predicting Gas Condensate Reservoir Performance: How Flow Parameters Are Altered When Approaching Production Wells,” paper SPE 36715 presented at the 1996 SPE Annual Technical Conference and Exhibition, Denver, Colorado, 6–9 October.
16. Fulcher, R.A., Ertekin, T., and Stahl, C.D.: “Effect of Capillary Number and Its Constituents on Two-Phase Relative Permeability Curves,” JPT (February 1985) 249; Trans., AIME, 279.
17. Schechter, D.S.: “Immiscible Flow Behavior in Porous Media,” PhD dissertation, U. of Bristol, United Kingdom (1988).
18. Boom, W., Wit, K., Schulte, A.M., Oedai, S., Zeelenberg, J.P.W., and Maas, J.G. (1995) “Experimental Evidence for Improved Condensate Mobility at Near-Wellbore Flow Conditions,” paper SPE 30766 presented at the 1995 SPE Annual Technical Conference and Exhibition, Dallas, 22–25 October, 667-675.
19. Teletzke, G.F., Scriven, L.E., and Davis, H. T. (1981). Patterns of Wetting Behavior in Multicomponent Systems. SPE 10112. In Proc. SPE ATCE
20. Leverett, M.C.: “Flow of Oil-Water Mixtures through Unconsolidated Sands,” Trans., AIME (TP 1223) (1939) 132, 149.
21. Pope, G. A., Wu, W., Narayanaswamy, G., Delshad, M., Sharma, M., and Wang P.: “Modeling Relative Permeability Effects in Gas Condensate Reservoirs”, paper SPE 49266 presented at the 1998 SPE Annual Technical Conference and Exhibition, New Orleans, 27–30 September.

22. Laplace, P.-S. (1806). *Traite' de Me'canique Ce'leste; Supple'ment au dixie'me livre: Sur l'Action Capillaire*. Courcier, Paris.

23. Leverett, M.C.: "Capillary Behavior in Porous Media" *Trans., AIME*, 1942, 341-358.

24. Kozeny, J. (1927). "Über kooillare Leitung des Wassers im Boden (Aufstieg, Versickerung und Anwendung auf die Bewa'sserung). *Sitzungs-Ber.Akad.Wiss., Vienna, Austria*, 136, 271-306.

25. Carman, P.C. (1937). *Fluid Flow through a Granular Bed*. *Trans. Inst. Chem. Eng., London*, 15, 150-166.

26. Reynolds, O. (1883). *An Experimental Investigation of the Circumstances which determine whether the Motion of Water shall be direct or sinuous and of the Law of Resistance in Parallel Channels*. *Phil. Trans. Roy. Soc.*, 174, 935.

27. Collins, R. (1961). *Flow of Fluids through Porous Materials*. Reinhold, New York.

28. Scheidegger, A. E. (1974). *The Physics of Flow through Porous Media*. University of Toronto Press.

29. Ergun, S. (1952). *Fluid Flow through Packed Columns*. *Chem. Eng. Progr.*, 48(2), 89-94.

30. Lefebvre du Prey, E. J. (1973). *Factors Affecting Liquid-Liquid Relative Permeabilities of a Consolidated Porous Medium*. SPE 3039. *SPEJ*, 13(1), 39-47.

31. Stegemeier, G.L.: “Oil Entrapment and Mobilization in Porous Media,” Improved Oil Recovery by Surfactant and Polymer Flooding, D.Shah and R. Schechter (eds.), Academic Press, Inc., New York City (1977) 55–91.
32. Taber, J.J.: Research on Enhanced Oil Recovery: Past Present and Future, D. Shah (ed.), Plenum Publishing Corp., New York City, 1981, 13–51.
33. Larson, R.G., Davis, H.T., and Scriven, L.E.: “Displacement of Residual Nonwetting Fluid from Porous Media,” Chem. Eng. Sci. (1981) 36, 75.
34. Peters, E.J. and Khataniar, S. (1987). The Effect of Instability on Relative Permeability Curves Obtained by the Dynamic displacement Method. SPE 14713. SPEFE, 2(4), 469-474.
35. Van der Waals, J.D. (1873). Over de Continuïteit van den Gas-en Vloeistofoestand. Ph.D. thesis, University of Leiden, the Netherlands.
36. Griffiths, R. B. and Wheeler J.C. (1970). “Critical points in multicomponent systems”, Phys.Rev.A. 2, 1047-1064
37. Wagner, O.R. and Leach, R.O.: ‘.Effect of Interfacial Tension on Oil Displacement Efficiency,’ *SPEJ* (Dec. 1966) 335-% Trans., AIIME, 237.
38. Fevang, Ø. and Whitson, C.H.: “Modeling Gas Condensate Well Deliverability,” SPERE (November 1996) 221.

39. Afidick, D., Kaczorowski, N.J., and Bette, S.: “Production Performance of a Retrograde Gas: A Case Study of the Arun Field,” paper SPE 28749 presented at the 1994 Asia Pacific Oil and Gas Conference, Melbourne, Australia, 7–10 November.
40. Barnum, R.S. “Gas Condensate Reservoir Behavior: Productivity and Recovery Reduction Due to Condensation,” paper SPE 30767 presented at the 1995 SPE Annual Technical Conference and Exhibition, Dallas, 22–25 October.
41. Boom, W., Wit, K., Zeelenberg, J.P.W., Weeda, H.C., and Maas, J.G. (1996) “On the Use of Model Experiments for Assessing Improved Gas-Condensate Mobility Under Near-Wellbore Flow Conditions,” paper SPE 36714 presented at the 1996 SPE Annual Technical Conference and Exhibition, Denver, Colorado, 6–9, October.
42. Amyx, J., Bass, D., Whiting, R., “Petroleum Reservoir Engineering”, McGraw-Hill Book Company, 1960.
43. Blom, S. M. P., Hagoort, J. and Soetekouw, D. P. N., “Relative Permeability at Near Critical Conditions,” SPE 62874 Journal, Vol. 5, No. 2, June 2000
44. Blom, S.M.P: “Relative Permeability to Near-Miscible Fluids,” PhD dissertation, Dietz Laboratory, Delft U. of Technology, The Netherlands (June 1999).
45. Hartman, K.J. and Cullick, A.S.: “Oil Recovery by Gas Displacement at Low Interfacial Tension,” J. Pet. Sci. Eng. (1994) 10, 197.

46. Chen, H.L., Monger-McClure, T.G., and Wilson, S.D.: “Determination of Relative Permeability and Recovery for North Sea Gas Condensate Reservoirs,” paper SPE 30769 presented at the 1995 SPE Annual Technical Conference and Exhibition, Dallas, 22–25 October.
47. Ali, J.K., McGauley, P.J., and Wilson, C.J.: “The Effects of High-Velocity Flow and PVT Changes Near the Wellbore on Condensate Well Performance,” paper SPE 38923 presented at the 1997 SPE Annual Technical Conference and Exhibition, San Antonio, Texas, 5–8 October.
48. Morel, D.C., Nectoux, A., and Danquigny, J.: “Experimental Determination of the Mobility of Hydrocarbon Liquids During Gas Condensate Reservoir Depletion: Three Actual Cases,” paper SPE 38922 presented at the 1997 SPE Annual Technical Conference and Exhibition, San Antonio, Texas, 5–8 October.
49. McDougall, S.R., Salino, P.A., and Sorbie, K.S.: “The Effect of Interfacial Tension Upon Gas-Oil Relative Permeability Measurements: Interpretation Using Pore-Scale Models,” paper SPE 38920 presented at the 1997 SPE Annual Technical Conference and Exhibition, San Antonio, Texas, 5–8 October.
50. Coats, K.H.: “An Equation of State Compositional Model,” *SPEJ* (1980) **20**, 363.
51. Brownell, L.E. and Katz, D.L.: “Flow of Fluids Through Porous Media—Part II,” *Chem. Eng. Prog.* (1947) **43**, No. 11, 601.
52. Delshad, M., Bhuyan D., Pope G.A., and Lake L.W.: “Effects of Capillary Number on the Residual Saturation of Three Phase Micellar

- Solution,” paper SPE 14911 presented at the 1986 SPE/DOE Symposium on Enhanced Oil Recovery, Tulsa, Oklahoma, 20–23 April.
53. Lake, L.W.: *Enhanced Oil Recovery*, Prentice–Hall, Englewood Cliffs, New Jersey (1989).
54. Jerauld, G.R.: “General Three-Phase Relative Permeability Model for Prudhoe Bay,” *SPE* (November 1997) 255.
55. Morrow, N.R. and Songkran, B.: *Surface Phenomena in Enhanced Oil Recovery*, D.O. Shah (ed.), Plenum Press, New York City (1982) 387–411.
56. Jin, M.: “A Study of Non-Aqueous Phase Liquid Characterization and Surfactant Remediation,” PhD dissertation, The U. of Texas, Austin, Texas (1995).
57. Delshad, M.: “Trapping of Micellar Fluids in Berea Sandstone,” PhD dissertation, The U. of Texas, Austin, Texas (1990).
58. Chatzis, I. and Morrow, N.R.: “Correlation of Capillary Number Relationships for Sandstones,” paper SPE 10114 presented at the 1981 Annual SPE Conference, San Antonio, Texas, 5–7 October.
59. Filco, P. and Sharma, M.M.: “Effect of Brine Salinity and Crude Oil Properties on Relative Permeabilities and Residual Saturations,” paper SPE 49320 presented at the 1998 SPE Annual Technical Conference and Exhibition, New Orleans, 27–30 September.

60. Chang, Y.-B., Pope, G.A., and Sepehrnoori, K.: “A Higher-Order Finite-Difference Compositional Simulator,” *J. Pet. Sci. Eng.* (1990) **5**, 35.
61. Wu, W., Wang, P., Delshad, M., Wang, C., Pope, G.A. and Sharma, M. “Modeling Non-Equilibrium Mass Transfer Effects for a Gas-Condensate Field,” paper SPE 39746 presented at the 1998 Asia Pacific Conference, Kuala Lumpur, 23–24, March 1998.
62. Narayanaswamy, G.: “Well Deliverability of Gas Condensate Reservoirs,” MS thesis, The U. of Texas, Austin, Texas (1998).
63. Narayanaswamy, G., Pope, G.A., and Sharma, M.M.: “Predicting Gas-Condensate Well Productivity Using Capillary Number and Non-Darcy Effects,” paper SPE 51910 presented at the 1999 SPE Reservoir Simulation Symposium, Houston, 14–17 February.
64. Blom, S.M.P. and Hagoort, J.: “The Combined Effect of Near-Critical Relative Permeability and Non-Darcy Flow on Well Impairment by Condensate Drop-Out,” paper SPE 39976 presented at the 1998 SPE Gas Technology Symposium, Calgary, 15–18 March.
65. Narayanaswamy, G., Sharma, M.M., and Pope, G.A.: “Effect of Heterogeneity on the Non-Darcy Flow Coefficient,” *SPERE* (June 1999) 296.
66. Munkerd, P.K.: “The Effects of Interfacial Tension and Spreading on Relative Permeability in Gas Condensate Systems,” Proc., 8th European IOR Symposium (1995).

67. Coşkuner, G. (1997). Microvisual Study of Multiphase Gas Condensate Flow in Porous Media. *Transport in Porous Media*, 28, 1-18.

68. Jones, J.R. and Raghavan, R.: "Interpretation of Flowing Well Response in Gas-Condensate Wells," SPEFE (September 1988) 578; Trans., AIME, 285.

69. Rowlinson, J.S. and Widom, B.: *Molecular Theory of Capillarity*, Clarendon Press, Oxford (1982).

70. Hölscher, I.F., Scheider, G.M., and Ott, J.B.: "Liquid-Liquid Phase Equilibria of Binary Mixtures of Methanol with Hexane, Nonane and Decane at Pressures up to 150 MPa," *Fluid Phase Equilibria* (1986) 27, 153.

71. Abbas, S., Satherley, J., and Penfold, R.: "The Liquid-Liquid Coexistence Curve and the Interfacial Tension of the Methanol-n-Hexane System," *J. Chem. Soc., Faraday Trans.* (1997) 93, No. 11, 2083.

72. Hradetzky, G. and Lempe, D.A.: "Phase Equilibria in Binary and Higher Systems Methanol+Hydrocarbon(s)," *Fluid Phase Equilibria* (1991) 69, 285.

73. Derdulla, H.-J. and Rusanow, A.I.: "Untersuchung der Grenzflächenspannung in der Nähe der kritischen Lösungstemperatur," *Z. Phys. Chem. (Leipzig)* (1970) 245, 375.

74. Johnson, E.F., Bossler, D.P., and Naumann, V.O.: "Calculation of Relative Permeability from Displacement Experiments," Trans., AIME (1959) 216.

75. Marle, C.M.: *Multiphase Flow in Porous Media*, Technip, Paris, France (1981).
76. Wygal, R.J.: “Construction of Models that Simulate Oil Reservoirs,” SPEJ (December 1963) 281; Trans., AIME, 228.
77. Blom, S.M.P. and Hagoort, J.: “How To Include the Capillary Number in Gas Condensate Relative Permeability Functions?,” paper SPE 49268 prepared for presentation at the 1998 Annual Technical Conference and Exhibition, New Orleans, 27–30 October.
78. Blom, S.M.P. and Hagoort, J.: “The Combined Effect of Near-Critical Relative Permeability and Non-Darcy Flow on Well Impairment by Condensate Drop-Out,” SPERE (October 1998) 1, No. 5, 421.
79. Henderson, G.D., Danesh, A., Tehrani, D.H., Al-Shaidi, S., and Peden, J.M.: “The Effect of Velocity and Interfacial Tension on Relative Permeability of Gas Condensate Fluids in the Wellbore Region,” J. Pet. Sci. Eng. (1997) 17, 265.
80. Peng, D.-Y. and Robinson, D.B.: “A New Two-Constant Equation of State,” Ind. Eng. Chem. Fundam. (1976) 15, No. 1, 59.
81. Lee, A.L., Gonzalez, M.H., and Eakin, B.E.: “The Viscosity of Natural Gases,” JPT (August 1966) 997; Trans., AIME, 237.
82. Lohrenz, J., Bray, B.G., and Clark, C.R.: “Calculating Viscosities of Reservoir Fluids from their Compositions,” JPT (October 1964) 1171; Trans., AIME, 231.

83. Cornelisse, P.M.W.: “The Gradient Theory Applied, Simultaneous Modeling of Interfacial Tension and Phase Behaviour,” PhD dissertation, Laboratory of Applied Thermodynamics and Phase Equilibria, Delft U. of Technology, The Netherlands (1997).
84. Melrose, J.C. and Brandner, C.F.: “Role of Capillary Forces in Determining Microscopic Displacement Efficiency for Oil recovery by Waterflooding,” J. Cdn. Pet. Tech. (1974) 13, No. 4, 54.
85. Ehrlich, R., Hasiba, H.H., and Raimondi, P.: “Alkaline Waterflooding for Wettability Alteration—Evaluating a Potential Field Application,” JPT (December 1974) 1335.
86. Moore, T.F. and Slobod, R.L.: “The Effect of Viscosity and Capillarity on the Displacement of Oil by Water,” Producer’s Monthly(1956) 20, No. 10, 20.
87. Saffman, P.G. and Taylor, G.: “The Penetration of a Fluid into a Porous Medium or Hele-Shaw Cell Containing a More Viscous Liquid,” Proc. R. Soc. London, Ser. A (1958) 245, 312.
88. Foster, W.R.: “A Low Tension Waterflooding Process,” JPT (February 1973) 205; Trans., AIME, 255.
89. University of Regensburg Institute for Organic Chemistry, http://www.uni-regensburg.de/Fakultaeten/nat_Fak_IV/Organische_Chemie/Didaktik/Keusch/D-Traffic-lights.htm, last accessed date August 2005.

90. Huijgens, R.J.M. (1994). The influence of Interfacial Tension on Nitrogen Flooding. Ph.D. thesis, Dietz Laboratory, Delft University of Technology, the Netherlands.
91. Brinkman, H.C. (1948). Calculations on the Flow of Heterogeneous Mixtures through Porous Media. Appl. Sci. Res., A1, 333-346.
92. Welge, H. (1952). A Simplified Method for Computing Oil Recovery by Gas or Water Drive. Trans. AIME TP 3309, 195, 91-98.
93. Dietz, D.N. (1953). A Theoretical Approach to the Problem of Encroaching and Bypassing Edge Water. Proc. Kon. A cad. Wet. (Amsterdam), Ser. B, 56 (1), 83-92.
94. Hagoort, J. (1974). Displacement Stability of Water Drives in Water-wet Connate Water Bearing Reservoirs. SPE 4268. SPEJ, 14 (1), 63-74.
95. Lombard, J.M., Longeron, D.G., and Kalaydjian, F.J.M., (1999), Influence of Connate Water and Condensate Saturation on Inertial Effects in Gas/Condensate Reservoirs. SPE 65430, SPE Journal 5 (3), September 2000, 301-308
96. Kokal, S., Al-Dokhi, M., and Sayegh, S. (2003), Phase Behavior of a Gas-Condensate/Water System. SPE 87307, SPE Reservoir Evaluation and Engineering, December 2003, 412-419.
97. Çınar, Y., and Orr, M. F. (2005), Measurement of Three-Phase Relative Permeability with IFT Variation, SPE Reservoir Evaluation and Engineering, February 2005, 33-42.

98. Bond, W. N. and Newton, d.A. (1928), Bubbles, Drops, and Stokes' Law. Phil. Mag. (7), 5(31), 794-800.
99. Williams, J. K. and Dawe A. R. (1989), Near-Critical Condensate Fluid Behavior in Porous Media – A Modeling Approach, SPE 17137 SPE Reservoir Engineering, May 1989, 221 – 228.

APPENDIX A

MEASURED DATA ON THE FLUID SYSTEM

In this appendix, the details of the measurements that conducted on the methanol/hexane fluid system that is used in the experimental part of this study are presented. The physical and chemical properties of the fluid system were measured as a function of the temperature as expressed in °C and dynamic viscosity as expressed in centipoises, cp. Density and viscosity measurements were conducted at TPAO Research Center, Production Technology Unit facilities.

The results of the density and viscosity measurements for hexane and methanol phase are listed in Table A.1 and Table A.2, respectively.

Table A.1: Measured Density and Viscosity Data for Hexane

Temperature	Hexane Density	Kinematic Viscosity	Hexane Dynamic Viscosity
C	gr/cc	cst	cp
5	0.6782	0.553	0.375
10	0.6764	0.536	0.363
15	0.6732	0.527	0.355
20	0.6705	0.515	0.345
25	0.6653	0.509	0.339
30	0.6697	0.508	0.340
33	0.6792	0.586	0.398

Table A.2: Measured Density and Viscosity Data for Methanol

Temperature	Methanol Density	Kinematic Viscosity	Methanol Dynamic Viscosity
C	gr/cc	cst	cp
5	0.7519	0.835	0.628
10	0.7479	0.772	0.577
15	0.7412	0.734	0.544
20	0.7323	0.693	0.507
25	0.7252	0.651	0.472
30	0.7091	0.615	0.436
33	0.6898	0.581	0.401

The interfacial tension data between the methanol-rich phase and the hexane rich phase obtained by the pendant drop technique are presented in Table A.3.

Table A.3: Measured Interfacial Tension for Methanol/Hexane

Temperature	Interfacial Tension
C	mN/m
10	0.4833
15.0	0.3620
18.0	0.2950
25.5	0.1520
30.0	0.0595
33.2	0.0035

APPENDIX B

MEASURED DATA OF THE FLOOD TESTS

In this appendix, the measured raw data for the relative permeability runs are presented in a tabular form with respect to time. The first 7 test runs, given in Table B.1 through B.7, were conducted without water saturation at 3 different flow rates as 50 cc/hr, 75 cc/hr and 100 cc/hr. These tests are also conducted on 3 different temperatures to get a wide range of interfacial tension data. In the 4 of the 11 tables, the effect of immobile water saturation is presented at the end in Tables B.8 through B.11.

Table B.1: Laboratory Measured Test Data for 100 cc/hr at 32.8 °C

Time	Pressure	Produced Methanol	Total Produced Methanol	Produced Hexane	Injected Hexane	fw
sec.	psi	cc	cc	cc	PV	
112	9.40	1.85	1.85	0.30	0.15	13.95
174	9.30	1.25	3.10	0.45	0.24	26.47
247	9.20	0.75	3.85	0.80	0.33	51.61
337	9.05	0.65	4.50	1.15	0.46	63.89
420	8.80	0.40	4.90	1.45	0.57	78.38
530	8.40	0.35	5.25	2.10	0.72	85.71
643	8.10	0.35	5.60	2.40	0.87	87.27
810	7.80	0.30	5.90	3.75	1.10	92.59
1050	7.50	0.30	6.20	5.95	1.42	95.20
1470	7.00	0.30	6.50	10.20	1.99	97.14
2305	6.50	0.20	6.70	21.10	3.12	99.06
3584	6.20	0.20	6.90	35.20	4.85	99.44
8960	5.80	0.10	7.00	149.50	12.13	99.93
12276	5.60	0.05	7.05	92.10	16.62	99.95
14140	5.50	0.03	7.08	202.00	19.14	99.99

Table B.2: Laboratory Measured Test Data for 50 cc/hr at 32.8 °C

Time	Pressure	Produced Methanol	Total Produced Methanol	Produced Hexane	Injected Hexane	fw
sec.	psi	cc	cc	cc	PV	
180	6.30	2.25	2.25	0.05	0.12	2.17
257	6.20	1.25	3.50	0.27	0.17	17.76
312	6.05	0.75	4.25	0.35	0.21	31.82
375	5.90	0.55	4.80	0.50	0.25	47.62
440	5.70	0.60	5.40	0.60	0.30	50.00
535	5.40	0.40	5.80	0.90	0.36	69.23
627	5.10	0.40	6.20	0.92	0.42	69.70
747	4.70	0.30	6.50	1.22	0.51	80.26
897	4.40	0.25	6.75	1.65	0.61	86.84
1077	4.10	0.25	7.00	2.10	0.73	89.36
1325	3.80	0.20	7.20	2.95	0.90	93.65
1581	3.60	0.15	7.35	3.20	1.07	95.52
1980	3.40	0.15	7.50	5.50	1.34	97.35
2717	3.20	0.15	7.65	10.00	1.84	98.52
5550	3.10	0.15	7.80	39.00	3.76	99.62
7914	3.05	0.11	7.91	32.00	5.36	99.66
14250	3.00	0.03	7.94	88.00	9.65	99.97

Table B.3: Laboratory Measured Test Data for 100 cc/hr at 30.1 °C

Time	Pressure	Produced Methanol	Total Produced Methanol	Produced Hexane	Injected Hexane	fw
sec.	psi	cc	cc	cc	PV	
125	10.70	2.85	2.85	0.40	0.17	12.31
198	10.20	1.70	4.55	0.70	0.27	29.17
259	9.90	1.10	5.65	0.80	0.35	42.11
355	9.60	0.80	6.45	1.40	0.48	63.64
474	9.20	0.65	7.10	2.20	0.64	77.19
700	8.60	0.55	7.65	4.35	0.95	88.78
920	8.30	0.50	8.15	4.50	1.25	90.00
1116	7.90	0.40	8.55	4.00	1.51	90.91
1267	7.50	0.30	8.85	3.10	1.72	91.18
1400	7.30	0.20	9.05	2.80	1.90	93.33
1770	6.90	0.10	9.15	8.00	2.40	98.77
3020	6.40	0.06	9.21	39.90	4.09	99.85
11000	6.00	0.02	9.23	220.00	14.89	99.99

Table B.4: Laboratory Measured Test Data for 50 cc/hr at 30.1 °C

Time	Pressure	Produced Methanol	Total Produced Methanol	Produced Hexane	Injected Hexane	fw
sec.	psi	cc	cc	cc	PV	
225	6.30	2.90	2.90	0.30	0.15	9.38
448	6.10	1.70	4.60	0.75	0.30	30.61
610	5.90	1.40	6.00	1.21	0.41	46.36
785	5.80	1.00	7.00	1.75	0.53	63.64
1010	5.60	0.75	7.75	2.75	0.68	78.57
1275	5.30	0.70	8.45	3.62	0.86	83.80
1530	5.20	0.40	8.85	4.15	1.04	91.21
1770	4.95	0.30	9.15	4.00	1.20	93.02
2040	4.75	0.20	9.35	4.50	1.38	95.74
2307	4.50	0.10	9.45	4.50	1.56	97.83
2628	4.20	0.04	9.49	5.40	1.78	99.26
3350	3.90	0.02	9.51	12.00	2.27	99.83
4750	3.50	0.01	9.52	22.00	3.22	99.95
10165	3.20	0.01	9.53	74.99	6.88	99.99

Table B.5: Laboratory Measured Test Data for 100 cc/hr at 18 °C

Time	Pressure	Produced Methanol	Total Produced Methanol	Produced Hexane	Injected Hexane	fw
sec.	psi	cc	cc	cc	PV	
160	14.80	3.00	3.00	0.35	4.44	10.45
395	14.40	1.85	4.85	1.55	10.97	45.59
680	13.40	1.40	6.25	3.85	18.89	73.33
900	12.50	0.95	7.20	3.60	25.00	79.12
1110	11.50	0.80	8.00	3.80	30.83	82.61
1350	10.50	0.65	8.65	4.50	37.50	87.38
1740	9.50	0.45	9.10	7.80	48.33	94.55
2150	8.80	0.30	9.40	8.50	59.72	96.59
2650	8.00	0.25	9.65	10.15	73.61	97.60
3320	7.20	0.15	9.80	13.20	92.22	98.88
4050	6.70	0.05	9.85	14.20	112.50	99.65
5575	6.40	0.02	9.87	42.30	154.86	99.95
14400	6.30	0.01	9.88	245.20	400.00	100.00

Table B.6: Laboratory Measured Test Data for 75 cc/hr at 32.8 °C

Time	Pressure	Produced Methanol	Total Produced Methanol	Produced Hexane	Injected Hexane	fw
sec.	psi	cc	cc	cc	PV	
140	11.30	2.60	2.60	0.07	2.92	2.62
178	11.00	1.05	3.65	0.30	3.71	22.22
217	10.60	0.47	4.12	0.45	4.52	48.91
270	10.10	0.42	4.54	0.73	5.63	63.48
337	9.80	0.38	4.92	1.15	7.02	75.16
419	9.50	0.35	5.27	1.58	8.73	81.87
527	9.20	0.32	5.59	2.20	10.98	87.30
648	8.90	0.29	5.88	2.65	13.50	90.14
792	8.30	0.27	6.15	3.35	16.50	92.54
990	7.80	0.25	6.40	4.55	20.63	94.79
1247	7.10	0.23	6.63	5.70	25.98	96.12
1600	6.60	0.21	6.84	7.65	33.33	97.33
2050	6.10	0.20	7.04	9.90	42.71	98.02
2650	5.50	0.15	7.19	12.10	55.21	98.78
3585	5.00	0.13	7.32	19.75	74.69	99.35
7110	4.80	0.10	7.42	72.90	148.13	99.86
10100	4.60	0.05	7.47	59.95	210.42	99.92

Table B.7: Laboratory Measured Test Data for 50 cc/hr at 18 °C

Time	Pressure	Produced Methanol	Total Produced Methanol	Produced Hexane	Injected Hexane	fw
sec.	psi	cc	cc	cc	PV	
250	6.50	3.80	3.80	0.05	3.47	1.30
355	6.30	1.35	5.15	0.63	4.93	31.82
486	6.10	1.20	6.35	1.06	6.75	46.90
600	5.90	0.95	7.30	1.14	8.33	54.55
705	5.70	0.75	8.05	1.27	9.79	62.87
802	5.50	0.60	8.65	1.35	11.14	69.23
930	5.20	0.45	9.10	1.86	12.92	80.52
1080	5.00	0.30	9.40	2.18	15.00	87.90
1230	4.80	0.20	9.60	2.27	17.08	91.90
1620	4.50	0.15	9.75	5.75	22.50	97.46
2400	4.00	0.10	9.85	11.09	33.33	99.11
3170	3.70	0.05	9.90	10.60	44.03	99.53
5500	3.20	0.03	9.93	28.30	76.39	99.89
8500	3.10	0.02	9.95	38.20	118.06	99.95
11450	3.00	0.01	9.96	50.00	159.03	99.98

In the rest of this appendix, the measured test data for the relative permeability runs are presented in a tabular form with respect to time as a second. The four more test runs conducted with water saturation at 2 different flow rates as 50 cc/hr and 100 cc/hr are given in Table B.8 and Table B.9. These tests were also conducted on 2 different temperatures with the larger range of interfacial tension data to show the effect of immobile water saturation and presented in Table B.10 and B.11. In the 4 of the 11 tables, the effect of immobile water saturation on pressure, injected hexane, hexane fractions, produced methanol and hexane phases was presented as a function of time at the end in Tables B.8 through B.11.

Table B.8: Laboratory Measured Test Data for 50 cc/hr at 18 °C for Swi

Time	Pressure	Produced Methanol	Total Produced Methanol	Produced Hexane	Injected Hexane	fw
sec.	psi	cc	cc	cc	PV	
225	7.00	2.10	2.10	0.80	0.15	27.59
350	6.95	0.50	2.60	0.85	0.24	62.96
450	6.92	0.35	2.95	0.85	0.30	70.83
590	6.90	0.30	3.25	1.30	0.40	81.25
800	6.83	0.40	3.65	2.05	0.54	83.67
1150	6.80	0.80	4.45	4.40	0.78	84.62
1670	5.80	0.70	5.15	6.95	1.13	90.85
2250	4.95	0.50	5.65	7.65	1.52	93.87
3260	4.20	0.40	6.05	14.00	2.21	97.22
4800	3.90	0.05	6.10	21.50	3.25	99.77
11760	3.50	0.02	6.12	97.00	7.96	99.98
21400	3.40	0.01	6.13	132.00	14.48	99.99

Table B.9: Laboratory Measured Test Data for 100 cc/hr at 18 °C for Swi

Time	Pressure	Produced Methanol	Total Produced Methanol	Produced Hexane	Injected Hexane	fw
sec.	psi	cc	cc	cc	PV	
116	14.00	1.90	1.90	1.20	3.22	38.71
210	13.80	0.85	2.75	1.60	5.83	65.31
290	13.50	0.55	3.3	1.65	8.06	75.00
400	13.20	0.48	3.78	2.50	11.11	83.89
520	12.80	0.45	4.23	3.05	14.44	87.14
700	12.30	0.45	4.68	5.05	19.44	91.82
900	11.50	0.40	5.08	5.75	25.00	93.50
1150	10.20	0.20	5.28	7.20	31.94	97.30
1790	8.60	0.10	5.38	17.85	49.72	99.44
3750	7.80	0.10	5.48	54.00	104.17	99.82
6500	7.60	0.05	5.53	76.50	180.56	99.93
14400	7.55	0.01	5.54	219.00	400.00	100.00

Table B.10: Laboratory Measured Test Data for 100 cc/hr at 32.8 °C for Swi

Time	Pressure	Produced Methanol	Total Produced Methanol	Produced Hexane	Injected Hexane	fw
sec.	psi	cc	cc	cc	PV	
121	10.80	1.95	1.95	0.45	3.36	18.75
155	10.70	0.95	2.9	0.85	4.31	47.22
285	10.50	0.75	3.65	3.05	7.92	80.26
450	9.80	0.70	4.35	4.00	12.50	85.11
648	8.85	0.65	5	5.05	18.00	88.60
875	8.00	0.40	5.4	6.05	24.31	93.80
1185	7.50	0.20	5.6	8.00	32.92	97.56
1520	7.00	0.10	5.7	9.50	42.22	98.96
3000	6.80	0.05	5.75	41.00	83.33	99.88
12000	6.70	0.01	5.76	250.00	333.33	100.00

Table B.11: Laboratory Measured Test Data for 50 cc/hr at 32.8 °C for Swi

Time	Pressure	Produced Methanol	Total Produced Methanol	Produced Hexane	Injected Hexane	fw
sec.	psi	cc.	cc.	cc.	PV	
220	6.90	2.25	2.25	0.80	3.06	26.23
440	6.85	0.90	3.15	2.55	6.11	73.91
715	6.75	0.80	3.95	3.35	9.93	80.72
980	6.40	0.65	4.60	3.65	13.61	84.88
1335	5.80	0.55	5.15	5.10	18.54	90.27
1790	5.10	0.30	5.45	6.25	24.86	95.42
2550	4.50	0.10	5.55	10.40	35.42	99.05
3800	4.00	0.05	5.60	17.30	52.78	99.71
5000	3.60	0.05	5.65	16.60	69.44	99.70
11500	3.50	0.01	5.66	90.30	159.72	99.99

APPENDIX C

RESULTS OF THE RELATIVE PERMEABILITY TESTS

In this appendix, the test results of relative permeability runs are presented in a tabular form. The first 7 test runs were conducted without water saturation at 3 different flow rates as 50 cc/hr, 75 cc/hr and 100 cc/hr. These tests are also conducted on 3 different temperatures to get the wide range of interfacial tension data. In the rest of the test tables, the effect of immobile water saturation was presented.

Table C.1: Result of Relative Permeability Test for 100 cc/hr at 32.8 °C

Snw (%)	Sw (%)	kr-hex	kr-meth	kr-h/kr-m
44.01	55.99	0.000	1.000	0.000
56.07	43.93	0.195	0.193	1.010
60.94	39.06	0.298	0.149	2.000
64.35	35.65	0.353	0.115	3.083
66.91	33.09	0.497	0.089	5.584
68.74	31.26	0.569	0.071	8.013
70.44	29.56	0.656	0.060	11.013
72.03	27.97	0.721	0.042	17.159
73.49	26.51	0.827	0.028	30.003
74.95	25.05	0.869	0.007	124.964
76.17	23.83	0.973	0.004	249.535

Table C.2: Result of Relative Permeability Test for 50 cc/hr at 32.8 °C

Snw (%)	Sw (%)	kr-hex	kr-meth	kr-h/kr-m
44.01	55.99	0.000	1.000	0.000
58.02	41.98	0.153	0.141	1.080
62.89	37.11	0.284	0.114	2.488
66.06	33.94	0.363	0.093	3.895
68.86	31.14	0.438	0.073	5.997
71.30	28.70	0.474	0.056	8.464
73.25	26.75	0.529	0.042	12.595
74.95	25.05	0.584	0.033	17.697
76.29	23.71	0.674	0.027	24.963
77.51	22.49	0.769	0.021	36.619
78.61	21.39	0.845	0.018	46.944
79.46	20.54	0.938	0.013	72.154

Table C.3: Result of Relative Permeability Test for 100 cc/hr at 30.1 °C

Snw (%) -hex	Sw (%) -meth	kr-hex	kr-meth	kr-h/kr-m
44.01	55.99	0.000	1.000	0.000
62.04	37.96	0.269	0.160	1.683
68.86	31.14	0.378	0.115	3.296
73.49	26.51	0.434	0.084	5.164
77.02	22.98	0.574	0.076	7.551
79.95	20.05	0.639	0.056	11.500
82.50	17.50	0.704	0.043	16.558
84.70	15.30	0.738	0.027	27.102
86.40	13.60	0.782	0.018	44.361
87.62	12.38	0.824	0.003	254.683
88.35	11.65	0.895	0.001	813.727

Table C.4: Result of Relative Permeability Test for 50 cc/hr at 30.1 °C

Snw (%)	Sw (%)	kr-hex	kr-meth	kr-h/kr-m
44.01	55.99	0.000	1.000	0.000
62.28	37.72	0.131	0.147	0.890
69.83	30.17	0.301	0.114	2.640
75.68	24.32	0.409	0.083	4.930
79.95	20.05	0.518	0.065	7.980
83.48	16.52	0.612	0.047	13.120
86.16	13.84	0.743	0.032	23.290
87.87	12.13	0.799	0.020	40.210
89.08	10.92	0.833	0.013	64.560
89.81	10.19	0.889	0.010	92.590
90.16	9.84	0.951	0.002	513.250

Table C.5: Result of Relative Permeability Test for 100 cc/hr at 18 °C

Snw (%)	Sw (%)	kr-hex	kr-meth	kr-h/kr-m
44.01	55.99	0.000	1.000	0.000
63.13	36.87	0.143	0.109	1.315
71.05	28.95	0.316	0.101	3.130
76.78	23.22	0.410	0.076	5.396
81.04	18.96	0.493	0.048	10.359
84.58	15.42	0.559	0.026	21.677
87.26	12.74	0.659	0.016	42.462
89.08	10.92	0.738	0.009	84.918
90.42	9.58	0.795	0.004	222.844
91.40	8.60	0.857	0.001	750.000
91.89	8.11	0.909	0.0003	3030.287

Table C.6: Result of Relative Permeability Test for 75 cc/hr at 32.8 °C

Snw (%)	Sw (%)	kr-hex	kr-meth	kr-h/kr-m
44.01	55.99	0.000	1.000	0.000
59.23	40.77	0.200	0.125	1.600
62.94	37.06	0.303	0.100	3.034
65.11	34.89	0.380	0.090	4.199
67.06	32.94	0.488	0.080	6.090
68.84	31.16	0.565	0.071	7.904
70.47	29.53	0.617	0.058	10.577
71.95	28.05	0.685	0.053	12.988
73.32	26.68	0.780	0.032	24.062
74.59	25.41	0.820	0.025	33.036
75.76	24.24	0.870	0.019	45.345
76.83	23.17	0.914	0.013	71.215

Table C.7: Result of Relative Permeability Test for 50 cc/hr at 18 °C

Snw (%)	Snw (%)	kr-hex	kr-meth	kr-h/kr-m
44.01	55.99	0.000	1.000	0.00
65.81	34.19	0.184	0.120	1.538
72.03	27.97	0.257	0.088	2.931
77.27	22.73	0.328	0.066	4.932
81.41	18.59	0.410	0.052	7.907
84.70	15.30	0.489	0.037	13.092
87.26	12.74	0.541	0.025	22.029
89.08	10.92	0.562	0.015	36.475
90.30	9.70	0.610	0.009	70.097
91.15	8.85	0.634	0.005	127.350
91.76	8.24	0.688	0.003	250.018
92.13	7.87	0.720	0.002	360.000
92.32	7.68	0.734	0.001	599.847
92.45	7.55	0.795	0.0003	2648.413

Four more tests conducted with water saturation at 2 different flow rates as 50 cc/hr and 100 cc/hr were given in Table C.8 and Table C.9. These tests were also conducted on 2 different temperatures with the larger range of interfacial tension data to show the effect of immobile water saturation, and presented in Table C.10 and C.11.

Table C.8: Result of Relative Permeability Test for 100 cc/hr at 18 °C at Swi

Snw (%)	Sw (%)	kr-hex	kr-meth	kr-h/kr-m
33.24	42.31	0.000	1.000	0.000
44.57	30.98	0.352	0.095	3.695
47.98	27.57	0.437	0.073	5.980
50.49	25.06	0.492	0.055	8.892
52.76	22.79	0.567	0.044	12.853
54.95	20.60	0.652	0.030	21.677
57.02	18.53	0.714	0.011	64.565
58.48	17.07	0.807	0.005	161.400
59.22	16.33	0.909	0.002	539.216

Table C.9: Result of Relative Permeability Test for 50 cc/hr at 18 °C at Swi

Snw (%)	Sw (%)	kr-hex	kr-meth	kr-h/kr-m
33.24	42.31	0.000	1.000	0.000
44.69	30.86	0.279	0.082	3.388
46.76	28.79	0.350	0.075	4.677
48.35	27.20	0.383	0.070	5.495
50.05	25.50	0.407	0.063	6.457
52.98	22.57	0.527	0.050	10.471
56.63	18.92	0.656	0.036	18.197
59.56	15.99	0.759	0.012	64.565
61.75	13.80	0.940	0.005	188.044

Table C.10: Result of Relative Permeability Test for 100 cc/hr at 32.8 °C at Swi

Snw (%)	Sw (%)	kr-hex	kr-meth	kr-h/kr-m
33.24	42.31	0.000	1.000	0.000
45.06	30.49	0.617	0.193	3.195
49.20	26.35	0.703	0.117	6.009
52.73	22.82	0.749	0.079	9.479
56.02	19.53	0.872	0.046	18.965
58.58	16.97	0.992	0.022	45.091

Table C.11: Result of Relative Permeability Test for 50 cc/hr at 32.8 °C at Swi

Snw (%)	Snw (%)	kr-hex	kr-meth	kr-h/kr-m
33.24	42.31	0.000	1.000	0.00
46.40	29.15	0.503	0.101	4.984
50.54	25.01	0.547	0.073	7.491
54.07	21.48	0.679	0.049	13.850
57.00	18.55	0.758	0.022	33.729
59.07	16.48	0.819	0.010	80.910
60.04	15.51	0.870	0.004	217.569

APPENDIX D

METHANOL SOLUBILITY IN WATER

For the last four core flood tests, hexane was injected phase at immobile water saturation for methanol/hexane equilibrium. In fact, methanol is assumed to be miscible when it is mixed with water. Here in this appendix, a way to make miscible fluids as immiscible is summarized [89].

Chemicals

:

Methanol
Toluene
methyl red
Sudan III
 $\text{CuSO}_4 \cdot 5 \text{H}_2\text{O}$
 K_2CO_3
 $\text{K}_2\text{Cr}_2\text{O}_7$

Apparatus and glass wares:

magnetic stirrer
magnetic stirring bar
stirring bar remover
gas washing bottle 250 mL (without head), fitted with a stopper
3 beakers 100 mL
powder funnel
glass stirring rod

Safety precautions:

Potassium dichromate: Hexavalent chromium compounds are generally more toxic than trivalent chromium compounds. May be fatal if absorbed through the skin, if swallowed or inhaled. Contains chromium (VI), a known cancer hazard. Allergen. Skin eye and respiratory irritant. May act as a sensitizer.



Methanol may be a reproductive hazard. Ingestion may be fatal. Risk of very serious, irreversible damage if swallowed. Exposure may cause eye, kidney, heart and liver damage. Chronic or substantial acute exposure may cause serious eye damage, including blindness.

Piperidine is a poison. May be fatal if inhaled or swallowed. Severe irritant.



Methanol and toluene are highly flammable.

Safety glasses and gloves must be worn. Good ventilation required.

Experimental procedure:

A gas washing bottle is filled with 60 mL of methanol / H₂O (1:1). Using a powder funnel 40 g of K₂CO₃ are added to the aqueous solution. Residual salt particles clinging to the wall of the gas-washing bottle are removed by shaking the bottle. The mixture is stirred, until the two phases have separated. The aqueous phase turns blue upon addition of a spatula tip full of CuSO₄ · 5 H₂O. After a few crystals of K₂Cr₂O₇ are added the color turns green (mixed color).

The alcoholic layer turns yellow when it is mixed with a spatula tip full of methyl red.

The yellow-green two-phases system is over layered with 60 mL of a solution of Sudan III (a spatula tip full) in 60 mL of toluene.

Results:

When the stoppered bottle is shaken the three layers temporarily mix, yielding a different color (i.e. blue, yellow and blue combine to make brownish). When stop moving the bottle the three liquids separate again. The colors of three dissolved compounds are visible again.

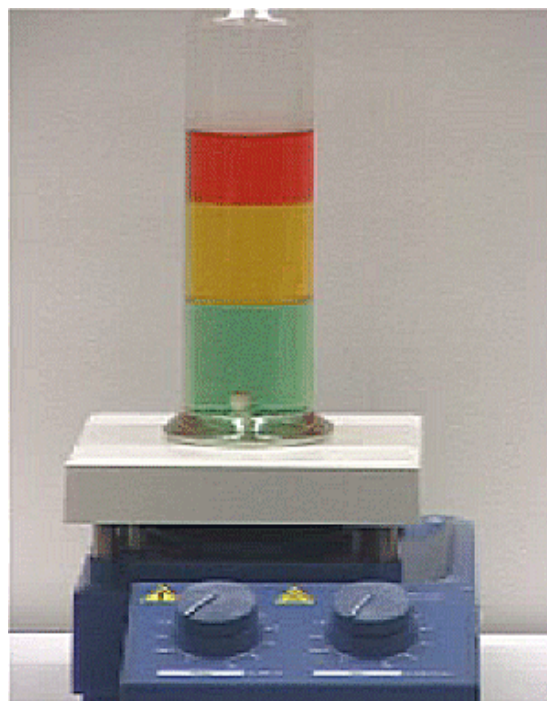


Figure C.1: Phase Segregation

Discussion:

- Substances that have similar polarities will be soluble in each other ("likes dissolve likes"). Water and methanol are miscible in all proportions but the two liquids are made immiscible by the addition of potassium carbonate. The weak intermolecular forces (i.e. hydrogen bonds) between methanol molecules and water are disrupted by the hydration of the ions. The process of salting out allows the separation of an organic phase from an aqueous phase.
- Toluene is non-polar. The methanol and water molecules respectively attract only one another, while ignoring the non-polar liquid.
- The result is that the three liquids are immiscible.

APPENDIX E

CURRICULUM VITAE

PERSONAL INFORMATION

Surname, Name : Çalışgan, Hüseyin
Nationality : Turkish (TC)
Date and Place of Birth : 08 December 1964, Ankara
Marital Status : Married and has 2 daughters
Phone : +90 312 322 4986
Email : hcalisgan@yahoo.com

EDUCATION

<u>Degree</u>	<u>Institution</u>	<u>Year of Graduation</u>
PhD	METU Petroleum and Natural Gas Engineering	2005
MS	USC Petroleum and Natural Gas Engineering	1990
BS	METU Petroleum and Natural Gas Engineering	1986
High School	Tapu Kadastro Meslek Lisesi, Ankara	1982

WORK EXPERIENCE

<u>Year</u>	<u>Place</u>	<u>Enrollment</u>
2004 – Present	TPAO Research Center	Engineer
2000 – 2004	TPIC Crude Oil Trade	Coordinator
1991 – 2000	TPAO Research Center	Engineer
1991 – 2000	University of Southern California	Research Assistant
1991 – 2000	University of Southern California	Computer Operator
1982 – 1982	Tapu ve Kadastro Genel Müdürlüğü	Officer

PUBLICATIONS AND PRESENTATIONS

1. **Çalışgan, H.**, Ershaghi, I., Chang, J. and Shikari, Y.: “An Approach to Estimate Average Reservoir Pressure in Gas Storage Reservoirs”, **Türkiye 10. Petrol Kongresi**, 11-15 Nisan, 1994, Bildiriler, 1-10.
2. Naz, H., Yoldemir, O., Alaygut, D., Bülbül M. ve **Çalışgan, H.** : “Kuzey Üst Yurt Basenindeki Petrol ve Doğal Sahalarından Alınan Karot Örneklerinin Petrografisi ve Rezervuar Özellikleri”, **Türkiye 10. Petrol Kongresi**, 11-15 Nisan, 1994, Bildiriler, s 4.
3. **Çalışgan, H.** : “Limiting Factors of Fundamental Core Analysis by Steady and Unsteady-state Measurement in Lab: Non-darcy Flow and Confining Pressure”, **12. International Petroleum Congress and Exhibition of Turkey**, Ankara, 12-15 October 1998, Proceedings, p 259-272.
4. **Çalışgan, H.**, Alpay, E., Karabakal, U., Demir, M. ve Sayılı S.: “ A Laboratory Study of Silivanka Sinan Heavy Oil Recovery by Immiscible CO₂ Injection” , **12. International Petroleum Congress and Exhibition of Turkey**, Ankara, 12-15 October 1998, Proceedings, p 418-434.
5. **Çalışgan, H.**, Demiral, B. ve Akın, S.: “Modelling of Gas Condensate Relative Permeability”, **15. International Petroleum Congress and Exhibition of Turkey**, Ankara, 11-13 May 2005, Proceedings, p 418-434.